Regeneration of retinal neurons from Müller glia in adult mice

Nikolas L Jorstad

A dissertation

submitted in partial fulfillment of the

requirements for the degree of

Doctor of Philosophy

University of Washington

2019

Reading Committee:

Thomas A. Reh, Chair

Christopher Dirk Keene

James Hurley

Program Authorized to Offer Degree:

Pathology

University of Washington

Abstract

Regeneration of retinal neurons from Müller glia in adult mice

Nikolas L Jorstad

Chair of the Supervisory Committee:

Professor Thomas A. Reh

Department of Biological Structure

There are many diseases that result in the death of specific neuron populations in the retina, resulting in blindness. Currently, few options exist for the treatment of blinding diseases, and the options that are available can be invasive and only have modest efficacy. Various non-mammalian organisms have the natural ability to regenerate their retinal neurons following injury. The proneural transcription factor, Ascl1, has been shown to be necessary and sufficient to initiate the regenerative process in these species, specifically in the retinal Müller glia. After Ascl1 induction, the Müller glia proliferate, migrate, and differentiate into all subtypes of retinal neurons and even integrate into the retinal circuitry, fully restoring function to the animal. I have identified a method for stimulating the regeneration of specific neuron subtypes in mammals by overexpressing Ascl1 in the Müller glia of adult mice. These Müller glial-derived neurons resemble nascent retinal neurons at the morphological, protein, RNA, and epigenetic levels.

Additionally, the newly generated neurons integrate into the existing retinal circuitry and response to light stimuli similar to nascent neurons. In this dissertation, I will discuss how we achieved retinal regeneration in adult mice and studies that were performed to further improve and characterize the Müller glia-derived neurons.

Table of Contents

Chapter 1: Introduction ***1***

Overview **2**

Cell types and organization of the retina **4**

Photoreceptors 7

Interneurons and ganglion cells 11

Müller glia 14

Retinal regeneration in zebrafish **15**

Retinal regeneration from MG in vitro in mice **19**

Retinal regeneration from MG in vivo in young mice **23**

Chapter 2: Stimulation of functional neuronal regeneration from Müller glia in adult mice. ***28***

INTRODUCTION **29**

RESULTS **29**

Conversion of MG into neurons by Ascl1 and TSA in vivo in adult mice 31

MG-derived neurons form synaptic specializations 36

ANT treatment enables epigenetic changes and expression of neuronal genes in MG 41

DISCUSSION **53**

Chapter 3: STAT pathway activation limits the Ascl1-mediated chromatin remodeling required for neural regeneration from Müller glia in adult mouse retina. ***55***

INTRODUCTION **56**

RESULTS: **58**

STAT pathway inhibition improves MG-derived neurogenesis in vivo 58
ANTSi treated MG-derived neurons make synaptic connections with existing circuitry 62
Single-cell RNA-seq on reprogrammed Müller glia 64
ChIP-seq for Ascl1 in P0 mouse retinal progenitors and reprogrammed Müller glia 68
Id genes are dysregulated in the presence of Ascl1 74
DISCUSSION 76
Chapter 4: Promoting proliferation and neurogenesis of diverse cell types from Müller glia. 79
INTRODUCTION 80
RESULTS 81
Mitogens in combination with Ascl1 increase MG proliferation 81
Retinal regeneration from MG in additional neuronal damage models 93
Atoh1 in combination with Ascl1 expression promotes generation of diverse cell types and increases reprogramming efficiency 102
Atoh1 and Ascl1 overexpression 104
DISCUSSION 114
Chapter 5: Discussion 119
Summary of results 120
Reprogramming MG to diverse neuronal types 128
Validating reprogramming factors in non-transgenic animals 130
Glial-based reprogramming in the CNS 132
Considerations in MG reprogramming 135

Clinical implications of this work **138**

Chapter 6: Materials and Methods ***141***

Injections **142**

Immunohistochemistry (IHC) **143**

Microscopy and Cell Counts **144**

Western Blotting (WB) **144**

Fluorescence activated cell sorting (FACS) **146**

Single-cell mRNA-sequencing (10x Genomics) **147**

Single-cell mRNA-sequencing (Fluidigm) **147**

Assay for Transposase-Accessible Chromatin (ATAC)-sequencing **148**

Chromatin Immunoprecipitation (ChIP) **150**

DNase I Hypersensititivy-Sequencing (DNase-Seq) **153**

Primary Cell Culture **153**

Electrophysiology **154**

Serial Block-Face Scanning Electron Microscopy (SBFSEM) **155**

Quantitative reverse transcription PCR (RT-qPCR) **156**

Statistics **157**

Animals **157**

References ***159***

Table of Figures

Figure 1.1 Cajal's hand-drawn illustrations of retinal neuron morphologies 5

Figure 1.2 Retinal cell types and their development..... 7

Figure 1.3 Transcription factor network for rod and cone development 11

Figure 1.4 Ascl1 ChIP-PCR from P0 developing retina and Ascl1-infected MG cultures 20

Figure 1.5 ChIP-PCR for histone modifications in P0 developing retina, WT MG, GFP-infected MG, and Ascl1-infected MG 22

Figure 1.6 Retinal regeneration in young mice..... 25

Figure 1.7 DNaseI-seq from cultured MG and whole retina from P0, P7, and adult mice 27

Figure 2.1: Conversion of MG into neurons by Ascl1 and TSA in vivo in adult mice 30

Figure 2.2: Animal age and numbers used in study..... 32

Figure 2.3: TSA increases histone acetylation..... 33

Figure 2.4: Neurogenesis and proliferation from Ascl1-expressing MG 35

Figure 2.5: MG-derived neurons form synaptic specializations in IPL..... 37

Figure 2.6: MG-derived neurons form synaptic connections with retinal circuitry 38

Figure 2.7: MG-derived GFP+ cells exhibit larger and faster visual responses than normal non-GFP MG..... 40

Figure 2.8: MG-derived GFP+ cells exhibit diverse morphologies..... 41

Figure 2.9: FACS purification of GFP+ cells 43

Figure 2.10: Table summary of all FACS-purified retinas 44

Figure 2.11: ANT treatment enables epigenetic changes and expression of neuronal genes in MG 45

Figure 2.12: ANT treatment results in MG-derived bipolar/amacrine-like cell cluster 47

Figure 2.13: Epigenetic modifications at Ascl1-binding sites 49
Figure 2.14: FACS-purified ANT-treated cells show increased neuronal gene expression and Otx2 binding 52
Figure 3.1: STAT pathway inhibition increases number of Müller glial-derived neurons 60
Figure 3.2: STAT inhibitor SH-4-54 inhibits pSTAT3 in MG 61
Figure 3.3: ANTSi-treated MG-derived neurons integrate into existing retinal circuits 63
Figure 3.4: ANTSi treatment results in more MG-derived neurons by scRNA-seq 66
Figure 3.5: Pseudotime analysis of scRNA-seq datasets 68
Figure 3.6: Ascl1 ChIP-seq from Ascl1-overexpressing MG and P0 retinal progenitors 71
Figure 3.7: Ascl1-overexpression results in dysregulated STAT-target genes 75
Figure 3.8: Stat pathway is transiently activated during NMDA damage 76
Figure 4.1: Proliferation of P15 MG in explant culture 82
Figure 4.2: Quantification of EdU+ MG in Ascl1 background and C57BL/6 background explants 84
Figure 4.3: Proliferation of adult P60+ MG in explant culture with mitogens 86
Figure 4.4: Quantification of adult P60+ MG in explant culture with mitogens 87
Figure 4.5: Proliferation of adult P60+ MG in explant culture with mitogens ± TSA (whole mount) 89
Figure 4.6: Proliferation of adult MG in vivo with mitogens 92
Figure 4.7: Light damage as injury model in MG reprogramming 96
Figure 4.8: P23H as damage model in MG reprogramming 99
Figure 4.9: Atoh1 and Ascl1 overexpression in adult mice 106

Figure 4.10: Atoh1 and Ascl1-overexpressing cells in adult mice stain for a subset of amacrine markers..... 108
Figure 4.11: Atoh1 and Ascl1-overexpressing cells in adult mice do not express mature amacrine, bipolar, or ganglion cell markers..... 109
Figure 4.12: Atoh1 and Ascl1-overexpressing cells in adult mouse brain 112

Acknowledgements

First, I would like to thank my advisor, Dr. Thomas A. Reh, for his exceptional mentorship over the last 4 and a half years. Tom truly helped me develop independent thinking, make connections between diverse fields of biology, and helped me develop logical and critical thinking to test hypotheses with numerous data modalities. His support and genuine excitement for testing new hypotheses helped me to succeed in graduate school and I cannot thank him enough. I also would like to thank every single member of the Reh lab and Bermingham-McDonogh lab present between 2015 and 2019. You all helped me understand different molecular biology techniques, gave critical insights and feedback into my findings, and allowed me to practice my mentoring skills by teaching you what I had expertise in. Truly, thank you all. I would like to thank my supervisory committee for their feedback, direction, and support. Lastly, I would like to thank my wife, Reeti Diwan, for encouraging me through the last 5 years.

Chapter 1:

Introduction

Overview

Humans are afflicted with numerous blinding diseases and currently have very few treatment options. Additionally, the treatment options that do exist consist of invasive prosthetic devices or drugs to slow disease progression and only have modest efficacy in restoring or preserving vision. Humans are a highly visual species and have constructed a modern society that relies more on vision than any other sense. When individuals are faced with a blinding disease, they lose the ability to interact with many of the technologies and creations that were made to make life more accessible and beautiful. This includes the ability to drive a car, fly an airplane, analyze complex spreadsheets of data, or appreciate visual art. If new neurons could be made in patients with blinding diseases like retinitis pigmentosa, macular degeneration, glaucoma, or central retinal artery occlusion, it is possible that restoration of the sense of sight will follow. Each of these diseases results in the loss of specific types of neurons within the retina, so finding ways to make new populations of these lost neuron types is the major hurdle to overcome. I have structured my dissertation as five main chapters, which will first introduce the field of retinal regeneration, and then describe my contributions to the field over the last several years.

In this chapter, I present an overview of what the retina is, what cell types it is comprised of, and how these cell types work together to make a functional unit. I will also discuss how the retina develops and what factors are important for generating specific subtypes of neurons during development. In the second half of this chapter, I provide a literature review of key studies that led to the mouse model I used throughout my dissertation work. This includes an overview of the

teleost fish's natural ability to regenerate retinal neurons after injury and how our lab has implemented some of the mechanistic knowledge from fish into a mouse model.

In Chapter 2, I present results showing the generation of new retinal neurons in a mature mammal for the first time. Although a major milestone in the field of retinal regeneration, the modest efficiency of neurogenesis and the limited diversity of regenerated neuron subtypes I observed led me to investigate additional factors that might improve on these points. In Chapter 3, I show how additional factors limit retinal regeneration in mice and from that knowledge developed a method that doubled reprogramming efficiency. In Chapter 4, I highlight several unpublished studies I performed to expand the total number and diversity of regenerated neurons and propose some ideas for future lines of research. Chapter 5 discusses how my dissertation work fits into the fields of retinal regeneration and regenerative neuroscience as a whole, and what the implications of this work are for blinding and neurodegenerative diseases.

As previously stated, this chapter serves to introduce the reader to the retina and also highlights the historical studies that have led to my dissertation work. Additional literature reviews of specific molecular pathways and phenomena are present throughout Chapters 2-5 and will be introduced at appropriate times as they relate to the work. Rather than provide an exhaustive list of everything that is known about the retina, I have chosen to focus this chapter on specific factors and studies that are necessary for comprehending the data presented in my results.

Cell types and organization of the retina

The mammalian retina is a projection of the anterior central nervous system (CNS) that resides at the back of the eye and enables the sense of sight. It is a thin neural sheet comprised of 6 major subclasses of neurons that work in concert to capture photons from our environment, filter this information, and transduce the signal back to the brain via the optic nerve. The retina is arguably the most highly characterized and understood region of the CNS and serves as a readily accessible model system for all neuroscience.

The complexity of diverse cell types in the retina and how they inform function was first characterized and theorized by Cajal in the late 19th century. Through his beautiful illustrations, the circuitry and highly ordered synaptic relationships between neuron subtypes can still be appreciated over 100 years later (Figure 1.1)[1]. The 6 major classes of neurons in the retina are the photoreceptors (rods and cones), horizontal cells, bipolar cells, amacrine cells, and ganglion cells. With the exception of rods, diversity exists within each of these major subclasses as well. Significant effort has been made to characterize the total number of different retinal neuron subtypes based on gene expression, morphology, and function with emerging new technologies like single-cell RNA-sequencing, serial block-face scanning electron microscopy, and whole-cell patch clamp recording, respectively (all discussed in later chapters). To date, around 40 ganglion cell subtypes, 33 amacrine cell subtypes, 14 bipolar cell subtypes, 2 horizontal cell subtypes, and 3 cone subtypes have been described[2-7]. It is expected that combinatorial approaches leveraging various technologies will reveal an estimated 100 different neuron subtypes in the mammalian retina[8]. In addition to the retinal neurons, the retina contains several glial cell types, such as astrocytes, microglia, and Müller glia. Müller glia will be the predominant cell type discussed

throughout this body of work and are notably the only glial cell derived from a common progenitor cell to the retinal neurons.

The retina is a highly ordered and laminated structure, with each of the various cell types residing in specific layers (Figure 1.2A). The rod and cone photoreceptors are located at the backmost region of the retina in what is called the outer nuclear layer (ONL). The photoreceptors synapse onto interneurons in a neuropil called the outer plexiform layer (OPL), which is absent of cell bodies and is comprised entirely of neuronal and glial processes. The interneurons (horizontal, bipolar, and amacrine cells), as well as the Müller glial cell bodies are located in the middle layer of the retina, which is known as the inner nuclear layer (INL). The interneurons synapse onto each other and ganglion cells in a second stratified neuropil called the inner plexiform layer (IPL). The last layer of the retina is known as the ganglion cell layer (GCL), which hosts the ganglion cell bodies as well as astrocytes.

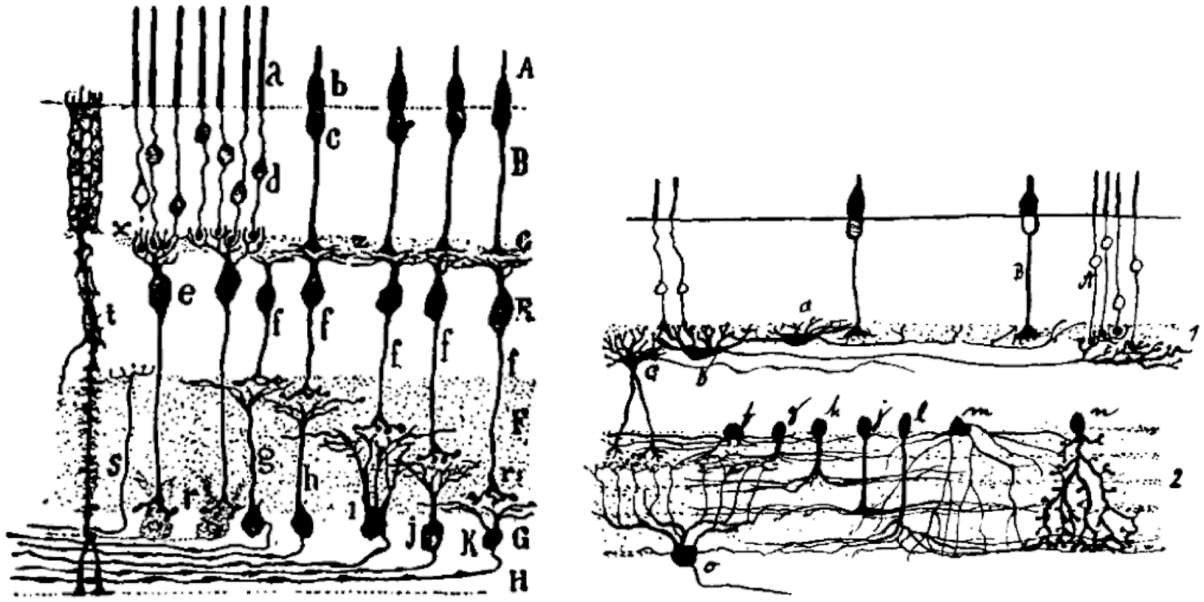

Figure 1.1 Cajal's hand-drawn illustrations of retinal neuron morphologies**.**

Broadly speaking, the photoreceptors are responsible for detecting photons and turning this light energy into a chemical signal. The photoreceptors then send the signal to bipolar

interneurons, which in turn synapse onto ganglion cells, whose axons project to the brain. The amacrine and horizontal cells are inhibitory neurons that add additional complexity to the light responses of the excitatory pathway cells. .

After the retina has been specified during embryogenesis, the multipotent retinal progenitor cells (RPCs) begin to differentiate and populate the retina with the 6 various neuronal types and Müller glia. Numerous birth dating studies tracking clones from labelled RPCs have unveiled a highly conserved sequence of cell type generation that holds true for many vertebrates, including mice and humans (Figure 1.2). In brief, there are two major waves of differentiation that occur, with ganglion cells being the first terminally differentiated neuronal type born in the retina, followed closely by cones, horizontal cells, and amacrine cells. In the second wave, bipolar cells, rods, and lastly Müller glia are born. All cell types of the retina are present at birth in humans, however, in mice the second wave of differentiation occurs postnatally (Figure 1.2)[9].

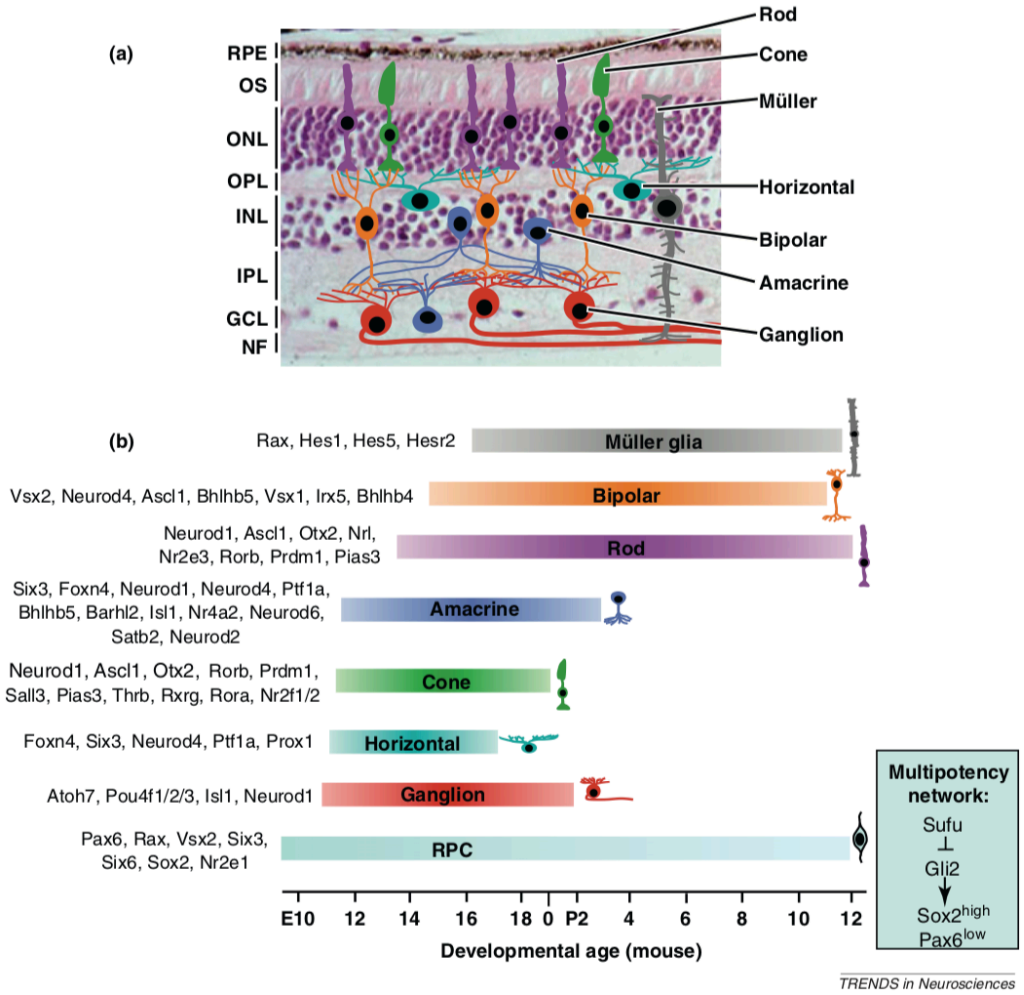

Figure 1.2 Retinal cell types and their development**. a**, Cartoon of retinal neuron subtypes overlaid on hematoxylin and eosin stain of retina to visualize their organization. Left labels show retinal layers; retinal pigmented epithelium (RPE), outer segments of photoreceptors (OS), outer nuclear layer (ONL), outer plexiform layer (OPL), inner nuclear layer (INL), inner plexiform layer (IPL), ganglion cell layer (GCL), and nerve fiber layer (NF). **b**, Diagram showing age range at which a given retinal cell type is born in mouse. Transcription factors that have effects on development of specific cell types during development are shown at the left.

Photoreceptors

Rod photoreceptors, (or rods) are the most abundant cell type found in the retina and make up around 90% of the retinal neurons in rodents[10]; rods are the primary source of night vision. In humans, rods are excluded from the most central region, called the macula.. Every rod

contains a light-sensitive pigment called rhodopsin, which is responsible for detecting light. In fact, rods are capable of detecting a single photon of light and allow humans to see individual stars in the night sky. In most mammals, rods synapse onto a rod bipolar cell, which synapses onto an amacrine cell that modulates this signal and an amacrine cell that transfers the rod output into the circuitry that processes the cone derived information[11-15]. It is this cross talk and modulation by the amacrine cells that causes our night vision to change to color/high-acuity vision when the lights are turned on in a dark room.

The second type of photoreceptor is the cone. Cones are generally present in the mammalian retina at a ratio of 1 cone per 20 rods. Unlike rods, the cone photoreceptors express different opsins, which define a particular cone's functional type. Each opsin that a cone expresses corresponds to the detection of a particular wavelength on the light spectrum. Humans have three types of cones, known as short, medium, and long wavelength cones (S, M, L cones, respectively). The S cone expresses an opsin that allows the detection of blue light (~420-440 nm), the M cone expresses an opsin that allows the detection of green light (~535-545 nm), and the L cone expresses an opsin that allows the detection of red light (~564-580 nm)[16]. Like a TV or computer monitor display that uses output of blue, green, and red pixels, the human brain uses an array of S, M, and L cones as input to enable the perception of colors from our environment. In humans, cones are densely packed at the center of the retina in the macula. Within the oval-shaped 5-6 mm diameter macula is a specialized pit-shaped region known as the fovea centralis, which is only 1-2 mm in diameter[17]. This small cone-dense region of the retina is responsible for our high-acuity daytime vision. A single cone may synapse onto numerous cone bipolar interneurons, and similarly, a cone bipolar interneuron may receive input from a number of cones within its reach. A cone bipolar cell may then synapse directly onto ganglion cells or onto

amacrine cells in the IPL for modulation of the signal. Additionally, cones may synapse onto horizontal cells in the OPL and receive feedback inhibition from horizontal cells to further modulate the signal[18,19].

During development, numerous transcription factors have been shown to regulate the photoreceptor network. Specifically, seven critical transcription factors (CRX, NRL, NR2E3, OTX2, RORβ, RXRg, and TRβ2) have been shown to act in concert and pattern RPCs to become either L/M cones, S cones, or rods (reviewed by Swaroop)[20]. Previous work in conditional Otx2 knockout mice has shown that eliminating Otx2 in RPCs results in the loss of rod, cone, bipolar, and horizontal cell lineages, demonstrating its importance for the generation of these cell types[21,22]. In adult retinas, Otx2 remains highly expressed in both bipolar cells and photoreceptors. Otx2 has been shown to be a direct target gene of Ascl1, which will be discussed in detail in later chapters. These and other studies have shown that Otx2 expression precedes the other critical photoreceptor transcription factors and that Otx2 drives Crx expression. Crx is expressed specifically in photoreceptors and bipolar cells, and Crx-deficient mice have been shown to develop photoreceptors, but lack expression of terminal phototransduction genes, suggesting that Crx is necessary for the expression of downstream photoreceptor genes but is not required for rod verses cone specification[23]. Nrl has convincingly been shown to specify the rod lineage by interacting with CRX to induce expression of rod-specific genes[24,25]. Nrl knockout mice have no rods and instead have an overabundance of S cones; and conversely, Nrl overexpression in the developing retina results in an overabundance of rods being generated at the expense of cones[26,27]. These studies highlight the importance of Nrl for instructing the rod verses cone fate. Nr2e3 is a direct downstream Nrl target gene that serves dual roles in specifying the rod fate[28]. First, it acts as a transcriptional repressor at various cone genes; and

secondly, it works in concert with Crx and Nrl to form an activation complex that induces rod gene expression[29-32]. RORβ knockout mice show several interesting photoreceptor phenotypes and highlight the importance of this factor in the development of rods and cones[33]. When RORβ is knocked out, mice fail to express Nrl and consequently lack rods. These mice also have an overabundance of S cones (similar to the Nrl knockout mice), which suggests that RORβ is an upstream regulator of Nrl. Interestingly, RORβ has also been shown to be critical for the induction of S opsin in cones and is believed to work with Crx as a co-activator[34]. The five factors above are necessary to specify whether a RPC becomes a rod or a cone, but once a cell has been specified to the cone lineage, TRβ2 patterns the type of cone it will become. Mice lacking TRβ2 fail to express M opsin and are instead restricted to the S cone fate[35]. TRβ2 is known to bind to the more active form of thyroid hormone (T3) with high affinity to activate gene expression. The S verses L/M cone fate can be selected for based on the abundance or absence of T3 in developing retina in mice and humans[35,36]. Taken together, these key transcription factors comprise the major regulatory components of photoreceptor specification and serve as a reference roadmap for normal photoreceptor-genesis (Figure 1.3)[20].

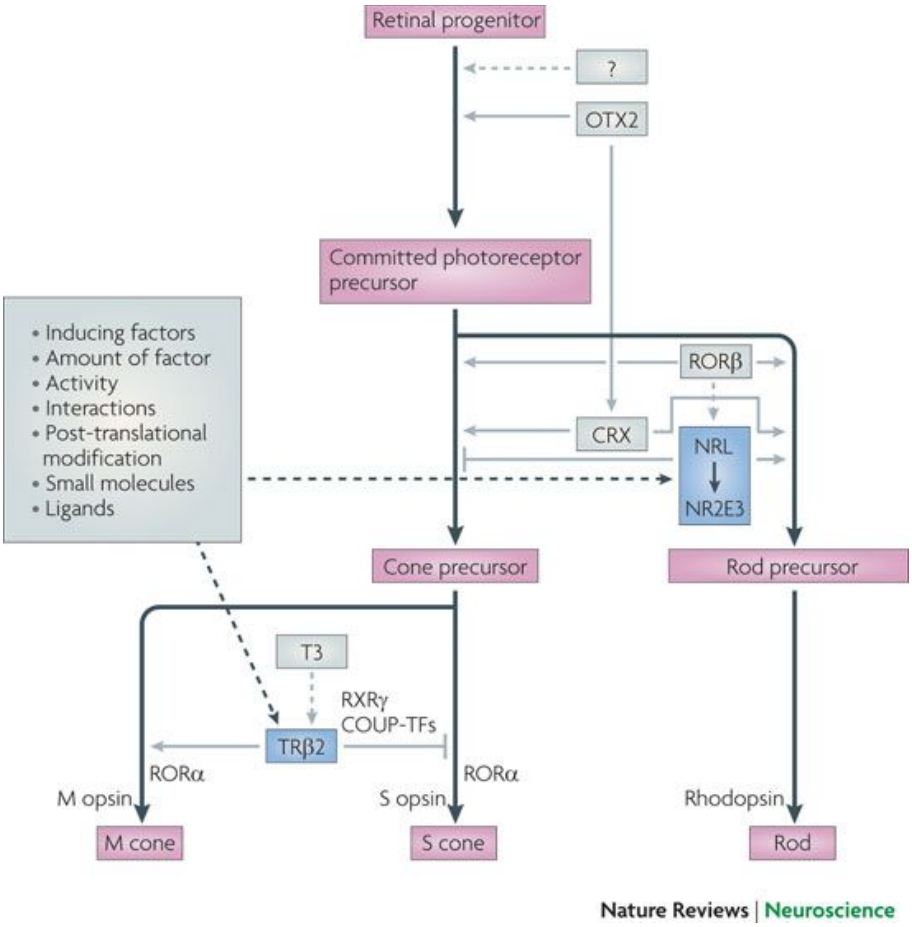

Figure 1.3 Transcription factor network for rod and cone development.

Interneurons and ganglion cells

Bipolar cells are bistratified interneurons that receive synaptic input from photoreceptors in the OPL and transmit the signal to amacrine and ganglion cells in the IPL. The two major bipolar cell subtypes are the rod bipolar cell and the cone bipolar cell, which are named for their source of synaptic input. In humans, only a single rod bipolar cell type has been identified, whereas a dozen or so cone bipolar cell types exist. The rod bipolar cells and a subset of the cone bipolar cells are classified as 'ON' bipolar cells and the remaining subtypes of cone bipolar cells are classified as 'OFF'. In dark conditions, the photoreceptors release glutamate, which will hyperpolarize (inhibit) the ON bipolar cells and depolarize (excite) the OFF bipolar cells.

Conversely, in lighted conditions, the phototransduction cascade of photoreceptors results in less glutamate release, enabling the ON bipolar cells to depolarize and causing the OFF bipolar cells to hyperpolarize[37,38].

Horizontal cells reside in the INL and in most mammals two distinct subtypes exist. Horizontal cells provide inhibitory feedback onto both cones and rods in the OPL and act as a source of gain control, similar to a volume knob, for the retina. Horizontal cells have wide arbors that spread long distances, so when a field of photoreceptors in one region detect light (or a bright white area), the horizontal cells can reduce photoreceptor input from the fields that are not detecting as bright a stimulus. This "center-surround" phenomenon allows humans to detect edges of objects and visualize environments that have variable illuminance[39-41].

Amacrine cells also reside in the INL and are one of the most diverse retinal neuron types, with over 30 unique subtypes having been identified. Their morphologies and functions vary widely, but broadly speaking, they are the horizontal cell equivalent of the IPL and most serve an inhibitory interneuron role of modulating bipolar to ganglion cell signals. Like horizontal cells, the amacrine cells can have long reaching arbors that modulate bipolar cell output in distant regions. One of their primary functions is to regulate the vertical communication of signal transduction by creating functional domains within a particular ganglion cell receptive field. Most of the various subtypes are classified as either GABA- or glycineric based on their released neurotransmitter; however, a subset (around 15%) do not release GABA or glycine[6].

Ganglion cells constitute the last major class of retinal neuron and are the most diverse, with over 40 subtypes having been identified. The ganglion cells are the only retinal neurons that generate action potentials and the sole source of retinal output to the brain. Ganglion cells send

their axons, which comprise the optic nerve, to the lateral geniculate nucleus, superior colliculus, and hypothalamus in the brain. Ganglion cells received their synaptic inputs from bipolar and amacrine cells in the IPL, with some types of amacrine cells directly synapsing onto the ganglion cell body[42].

The transcription factor networks that specify retinal interneurons and ganglion cells are less well understood than the robust photoreceptor networks that have been described. This is likely due to massive diversity of specified subtypes that are patterned during development. Figure 1.2 highlights some of the critical transcription factors that are required for the differentiation of these various cell types[9]. Bipolar cells are specified from RPCs by transcription factors Otx2 and Vsx1[43]. Vsx2 expression has been shown to bias RPCs towards a smaller distinct subset of bipolar cells and the MG fate[44]. Bipolar and cholinergic amacrine cell lineages have been shown to be controlled in part by Isl1 expression[45]. Additionally, Bhlhb5 has been shown to specify the cone bipolar subtypes as well as some amacrine cells[46]. Prdm1 is sufficient to drive RPCs towards photoreceptors at the expense of bipolar cells[47]. A critical factor for ganglion cell specification in vertebrates is Atoh7[48]. Atoh7 is transiently expressed just prior to the differentiation of RPCs and when knocked out, mice fail to generate ganglion cells, suggesting that Atoh7 is critical for their development[49]. Atoh7 also directly regulates the expression of Brn3, an important transcription factor for establishing subtypes of ganglion cells that remain on in the mature neurons[50]. There are dozens of other transcription and extrinsic factors, including growth factors, Wnt signaling, Shh signaling, and retinoic acid signaling, that have been implicated in the development of specific retinal neuron populations; however, for the purposes of my dissertation work, the factors mentioned above are sufficient for inferring retinal neuron types.

Müller glia

The most important retinal cell type for my dissertation research is the Müller glia (MG). The MG have a cell body that resides in the INL and processes that span across the entire thickness of the retina, forming the inner and outer limiting membranes with their end feet at the edges of the GCL and ONL, respectively. MG make up between 1-3% of all retinal cell types and are the only retinal glial cell type that shares a common progenitor cell with the retinal neurons[51]. They were first characterized and described by Heinrich Müller in 1851 and were so named Müller glia after their discoverer. Their primary role is to maintain the structural integrity of the retina and to provide trophic support for neurons by regulating potassium and neurotransmitter levels.

MG development relies heavily on transcription factors Hes1 and Hes5[52]. Studies of Hes1 null mice show that all six neuronal cell types develop normally in the retina, but MG are not generated[53]. Similarly, Hes5 null mice develop retinal neurons normally and have a significant reduction (about 40%) in the number of MG that are generated[54]. These studies demonstrate the importance of Hes genes for patterning RPCs to a MG cell fate instead of becoming retinal neurons. Additional early factors during development, such as Stat signaling components and Notch pathway proteins have been shown to play an important role in gliogenesis as well. The primary takeaways from this section are that MG and retinal neurons are derived from the same RPCs, and that various transcription factors instruct the RPCs towards specific lineages.

Now that the reader has a strong knowledge of the various cell types in the retina, in the next section of this chapter I will discuss prior studies that laid the foundation for my dissertation work and demonstrated the unique ability of MG to regenerate retinal neurons. These

key studies, along with my results described in Chapters 2-4, suggest that mammalian MG could one day soon be reprogrammed into new retinal neurons for the treatment of various retinal diseases.

Retinal regeneration in zebrafish

Zebrafish have emerged as a powerful model organism to study developmental biology and regeneration. It has been known for over 100 years that non-mammalian vertebrates, like fish, can regenerate tissues and organs, including parts of the eye, much better than mammals. Müller glia in zebrafish initially respond to retinal injury in a manner similar to mammals by undergoing a gliotic response in which they activate glial fibrillary acidic protein (Gfap) and vimentin[55]. Unlike the mammal, however, this gliotic response in zebrafish is transient and is closely followed by a reprogramming event where the MG change and become similar to a retinal stem/progenitor cell[56]. This transient switch from a gliotic response to a reprogramming event has been well characterized and serves as a benchmark for the therapeutic potential of MG in mammalian retinal regeneration. The studies in zebrafish have highlighted numerous biological mechanisms and reprogramming factors that are critical for the regenerative process, which may show promise for translation to mammalian regeneration models. In this section, I will review the teleost fish literature that has led to our current line of investigation for promoting retinal regeneration in mice.

Unlike many other vertebrate species, fish continue to grow throughout the duration of their life. This holds true for the fish retinas as well, with continued proliferation and differentiation of retinal neurons occurring throughout their life. Notably, this continued growth

only occurs at the peripheral edges of the retina in a region known as the neuroepithelial germinal zone or the ciliary marginal zone (CMZ)[57-59]. In young postnatal chick, there is limited retinal neurogenesis at the CMZ, and in mammals there is strong evidence showing a complete lack of a CMZ altogether[60]. This phenomenon is important to understand when studying regeneration in teleost fish because it helps to identify the source cell of retinal regeneration.

Some of the first evidence that teleost fish could regenerate their retinal neurons was presented in 1948 when Roger Sperry demonstrated their ability to regenerated the optic nerve following transection[61]. Decades later, other models of retinal damage, such as the ATPase inhibitor ouabain, were shown to induce regeneration of retinal neurons in goldfish[62,63]. These studies noted that the regenerating cells did not originate in the CMZ, and instead were found to proliferate within the central retina in the INL. These and similar studies led the field to believe that a second stem cell niche existed in the INL, which was responsible for this damage-induced neurogenesis (later to be called regeneration)[64]. The source of regenerating retinal neurons in avian models was initially identified as the MG[65]. These findings motivated researchers studying teleost fish to test for this source as well. Unfortunately, there were no appropriate genetic tools for lineage tracing in the goldfish to confirm or refute this hypothesis. A few years later, Fausett and Goldman performed similar damage paradigms in zebrafish with a fluorescent GFP reporter being driven by the Alpha1 tubulin (Tuba1a) promoter[66]. Tuba1a is normally expressed in new born neurons and neural progenitor cells. Shortly after retinal injury, they found that *Tuba1a*-GFP expression was colocalized with MG staining as well as BrdU-labelling. At later timepoints, these GFP+ BrdU+ cells colocalized with staining for amacrine and ganglion cell markers, providing the first evidence that this second stem cell niche in the INL were actually the MG. A year later, this work was supported by a transgenic lineage tracing study using the MG-specific

Gfap promoter to drive GFP expression. GFP+ MG were seen to proliferate, migrate, and differentiate into GFP+ retinal neurons following high-intensity light damage[67].

Shortly after identifying MG as the source cell for teleost retinal regeneration, numerous studies were performed to characterize changes in gene expression that followed injury[68,69]. Two critical studies combined MG-specific GFP reporter lines with FACS-purification to successfully isolate MG and MG-derived progenitor cells at several key timepoints during the regenerative process[70,71]. These studies generated rich microarray data that provide insights into the molecular mechanisms of MG reprogramming in teleost fish and have been mined for potential regenerative candidate genes ever since. During this same period as the gene expression studies, Fausett and Goldman were determined identify factors that regulate early reprogramming events in the MG after damage. They decided to systematically make deletions in the promoter of their *Tuba1a*-GFP reporter zebrafish to identify what promoter elements were necessary for Tuba1a expression[72]. They successfully identified a 109 bp region in the Tuba1a promoter that was necessary for GFP induction in MG after injury. Using radiolabeled oligonucleotide probes, they identified a canonical E-box motif (CATGTG) was present in this 109 bp region, suggesting a basic helix-loop-helix (bHLH) transcription factor was likely responsible for the induction of Tuba1a expression.

Work from Dr. Reh's group a few years earlier showed that the developmental proneural bHLH transcription factor Achaete-scute homolog 1, or Ascl1 (also called Hash1, Ash1, Mash1, Ascl1a, and Cash1), was expressed in MG after injury in postnatal chick[65]. Additionally, one the previously mentioned gene expression microarray datasets showed that Ascl1 is induced during regeneration in zebrafish[68]. This evidence led Fausett and Goldman to hypothesize that Ascl1 might be the bHLH that drives Tuba1a expression and potentially the regenerative process. They

performed in situation hybridizations for Ascl1 expression at various time points and found it to be colocalized with GFP+ MG as early as 4 hours post-injury. A gel electrophoretic mobility shift assay was unsuccessful in showing a direct interaction of Ascl1 with the Tuba1a promoter; however, a luciferase reporter assay driven by either the nascent or mutated Tuba1a promoter in HEK293T cells showed that Ascl1 increased induction of the reporter with the nascent promoter. To further characterize Ascl1's role in regeneration, morpholino oligonucleotides (MOs) targeting Ascl1 were electroporated into adult zebrafish retinas to knock down Ascl1 expression. In damaged retinas, there was almost no *Tuba1a*-GFP expressed in the MOs treated retinas, whereas robust expression was seen in the control. Additionally, BrdU-labelling showed that at 10 days post-injury there was a striking decrease in the number of proliferating MG in the MOs treated verses control retinas, suggesting that Ascl1 is a necessary factor to initiate the regenerative process in MG.

While numerous other studies were conducted to explore the regulation of Ascl1 and its target genes, and what effects these factors have on the dedifferentiation, proliferation, migration, and differentiation of MG to neurons (reviewed in detail by Gorsuch and Hyde[73]), the studies mentioned above serve as the core justification for introducing Ascl1 into mature mammalian MG to promote regeneration. The teleost studies identified MG as the source stem cell for retinal regeneration, demonstrated the correlation of Ascl1 induction with early reprogramming events, and showed convincingly that Ascl1 was necessary for dedifferentiation and proliferation of MG following retinal injury. In the subsequent chapters of this text, additional studies from avian and teleost regeneration models will be discussed in detail as it relates to our findings in mice. This includes highlighting the importance of Wnt and Stat3 signaling during MG reprogramming.

Retinal regeneration from MG in vitro in mice

Unlike zebrafish, mammalian MG fail to upregulate Ascl1 following retinal injury. Instead, the mammalian MG upregulate genes such as Gfap and undergo reactive gliosis in response to damage, similar to astrocytes in the brain. To determine if Ascl1 overexpression could convey regenerative potential to mammalian MG, as is seen in non-mammalian species, a former graduate student in the Reh lab, Dr. Julia Pollak, decided to introduce an Ascl1 lentivirus into mature dissociated mouse MG cultures[74].

MG from postnatal day 12 (P12) mice were cultured in Neurobasal media with 10% FBS, N2, and EGF for one week. After the cultures had grown to confluency, cells were passaged to eliminate any residual neurons, and then infected with a GFP or Ascl1-GFP lentivirus. Lentiviral particles were added to the medium for 3-6 hours followed by media replacement to wash out excess virus. By 4 days post-infection (dpi), robust proliferation was observed by EdU-labelling. Additionally, at 4 dpi high levels of Ascl1 mRNA was seen by qPCR and over 85% of the MG had detectable levels of Ascl1 protein in the Ascl1-GFP treated cells.

To determine if overexpressed Ascl1 was correctly binding to its previously described appropriate target genes[75,76], *Pollak et al* performed Ascl1 chromatin immunoprecipitation (ChIP)-PCR. As a positive control, P0 retinas were used to establish the developmental levels of Ascl1 binding at target genes. P0 retinas and Ascl1-infected P12 MG cultures were dissociated and fixed, then Ascl1-bound chromatin was immunoprecipitated using anti-Ascl1 magnetic beads. After chromatin shearing, qPCR for Dll1, Dll3, Hes5, Hes6, and Mfng was performed and showed significant enrichment at these target gene promoters over developmental levels (Figure

1.4). This data suggests that virally introduced Ascl1 does indeed function and bind at developmentally appropriate target gene promoters.

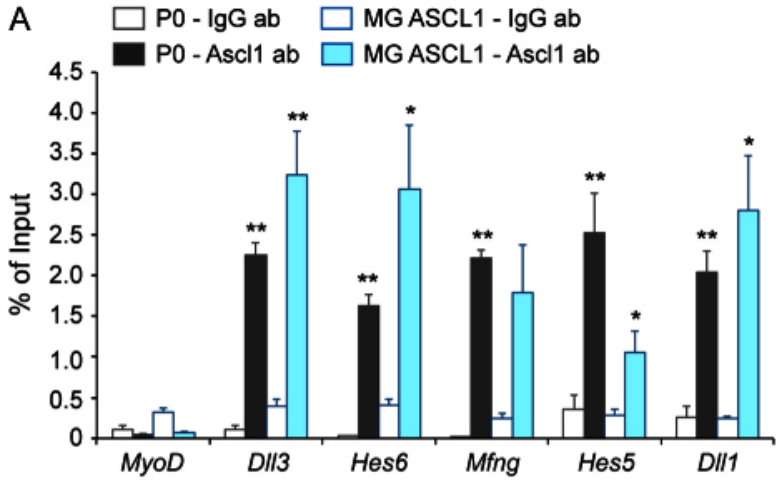

Figure 1.4 Ascl1 ChIP-PCR from P0 developing retina and Ascl1-infected MG cultures. Graph is shown as percentage of input DNA. All primers were targeted to a given gene's 5' promoter. MyoD is a negative control housekeeping gene.

Next, a gene expression microarray was performed on FACS-purified Hes5-GFP P0 progenitors, GFP-infected P12 MG cultures, and Ascl1-GFP-infected P12 MG cultures to determine if forced Ascl1 expression drives the global gene expression profile of the MG towards a retinal progenitor state. Many of Ascl1 target genes were seen to be upregulated in the Ascl1-GFP-infected cultures relative to GFP-infected cells; however, most of the genes were not expressed at the same level as was seen in P0 progenitors. Additionally, many highly expressed progenitor genes, such as Hmgb3 and Sfrp2, were not increased in the Ascl1-GFP-infected MG. These results suggested that Ascl1 may be restricted in some way from binding to a subset of progenitor genes.

To further probe the mechanism by which Ascl1 is able to induce expression of its target genes in MG, ChIP-PCR for various histone modifications was performed. Histone-3-lysine-27 (H3K27) is a residue on the histone tail that can be methylated or acetylated to regulate gene

expression. When H3K27 is methylated (H3K27me3) at gene promoters, repressed expression of that gene is observed[77,78]. Alternatively, when H3K27 is acetylated (H3K27ac) at gene promoters, increased expression of that gene is generally observed[79]. In wildtype (WT) MG, Ascl1 target genes had higher levels of the repressive H3K27me3 histone modification at their promoters, compared to P0 progenitors (Figure 1.5A). Conversely, at these same Ascl1 target promoters, the activating H3K27ac histone modification had a higher level in P0 progenitor cells than in WT MG (Figure 1.5B). To determine if Ascl1 changed the chromatin state at progenitor gene promoters in MG, H3K27ac and H3K27me3 ChIP-PCR was performed on GFP-infected and Ascl1-infected MG. Interestingly, H3K27me3 was reduced at progenitor gene promoters in the Ascl1-infected MG relative to GFP-infected MG, with a corresponding increase in the H3K27ac mark at these same promoters (Figure 1.5C and 1.5D). This data suggested that, at least in a subset of upregulated progenitor genes, Ascl1 was able to convert the chromatin from a closed methylated state to an open acetylated state.

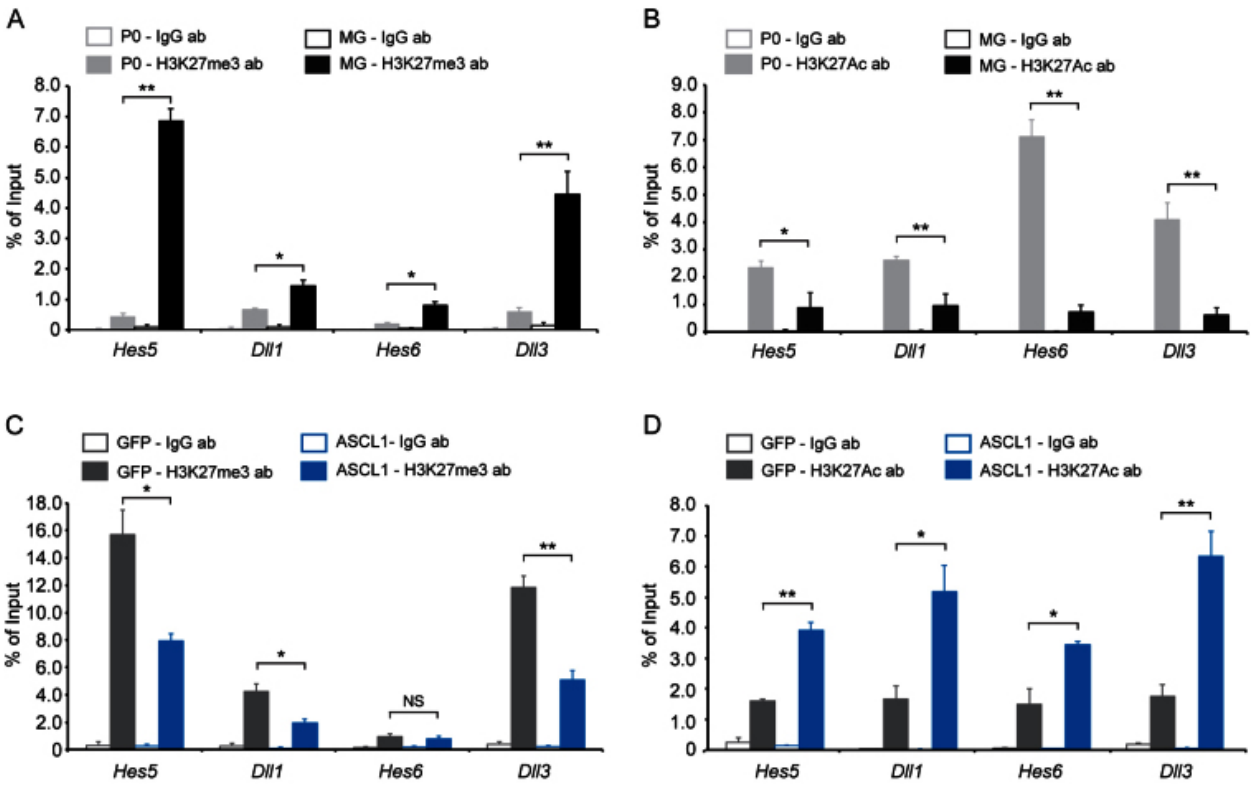

Figure 1.5 ChIP-PCR for histone modifications in P0 developing retina, WT MG, GFP-infected MG, and Ascl1-infected MG. **a**, **b**, ChIP-PCR for H3K27me3 repressive mark or H3K27ac activation mark at progenitor gene promoters in P0 developing retina and WT MG. **c**, **d**, ChIP-PCR for H3K27me3 and H3K27ac at progenitor gene promoters in GFP or Ascl1-infected MG cultures.

Additional experiments were performed in dissociated MG and retinal explant cultures that showed Ascl1-infected MG downregulated glial gene expression, and upregulated genes associated with the bipolar cell lineage, such as Otx2 and Crx. Ratiometric Ca^{2+} imaging and whole-cell electrophysiology recordings were also performed and indicated that the Ascl1-infected MG become more neuronal in their electrical properties. This study was the first to demonstrate the ability of Ascl1 to reprogram mammalian MG towards neuronal lineages. By virally introducing Ascl1 to MG, *Pollak et al* convincingly showed that Ascl1 was expressed, functional, and successfully modified the chromatin towards an open conformation at progenitor gene loci in MG. This work demonstrated the feasibility of reprogramming mammalian MG

towards neuronal cell fates and laid the foundation for future regeneration studies, including my dissertation work.

Retinal regeneration from MG in vivo in young mice

To determine whether Ascl1 was capable of stimulating regeneration from MG in vivo, Dr. Yumi Ueki created an inducible mouse model of Ascl1 expression that would be restricted specifically to the MG. Dr. Masato Nakafuku at Cincinnati Children's Hospital had previously generated a *tetO*-Ascl1-ires-GFP mouse, which overexpresses Ascl1 when a tetracycline-controlled transactivator (tTA) is present. Dr. Ueki crossed this *tetO*-Ascl1-ires-GFP mouse with a commercially available Flox-stop-*LNL*-tTA mouse, which expresses the required tTA for Ascl1 expression when its floxed stop cassette is cleaved by a Cre recombinase. To restrict Ascl1 expression specifically to the MG in the retina, a Cre recombinase driven by the Glast promoter was chosen. The gene Glast codes for a glutamate transporter that is expressed specifically in the astrocytes and MG in the retina. A previous study by *Mori et al* resulted in the generation of this mouse, which harbors a tamoxifen inducible Cre (CreERT2) in the native Glast gene loci[80]. Therefore, the *Glast*-CreER: Flox-stop-*LNL*-tTA: *tetO*-Ascl1-ires-GFP mouse that Dr. Ueki generated specifically expresses Ascl1 and GFP in MG (and some astrocytes) in the retina when tamoxifen is administered to the animal[81]. As control mice, the *Glast*-CreER: Flox-stop-*LNL*-tTA mice (lacking the *tetO*-Ascl1 cassette) were crossed with a Flox-stop-*CC*-GFP reporter line to induce a fluorescent reporter in the MG.

To first verify that the GFP control and Ascl1-GFP constructs were working as predicted, *Ueki et al* injected adult mice with tamoxifen and collected retinas 1-4 weeks later. All GFP+

cells in the CC-GFP control mice were co-labelled with Sox9 (a MG specific gene) and had canonical MG morphology with no retinal neurons being labelled by the reporter. This validated the specificity of the *Glast*-CreER and showed that there is no leakiness of the reporter. Surprisingly, in the Ascl1-GFP expressing mice, no morphological changes were observed in the MG. All the GFP+ cells were immunoreactive for Ascl1 and RT-PCR analysis showed robust expression of Ascl1; however, the transgene itself did not appear to induce a morphological change. Additionally, the MG maintained their Sox9 expression and did not express Otx2, suggesting that Ascl1 is not sufficient to induce neurogenesis or a neurogenic state in vivo as was seen in vitro.

Because MG in zebrafish normally upregulate Ascl1 following retinal injury, *Ueki et al* hypothesized that damage may be necessary to stimulate Ascl1 to induce a neurogenic state. She tested this by administering an intravitreal injection of the excitotoxin NMDA to kill ganglion and amacrine cells in adult mice after Ascl1 had been induced with tamoxifen. NMDA damage caused ~50% of the MG to reduce their Sox9 expression in the Ascl1-GFP; however, no Sox9 reduction was seen in the CC-GFP cells. Additionally, many of the MG in the Ascl1-GFP condition, but not the CC-GFP condition expressed Otx2. More mature markers of retinal neurons were not observed, even 3 weeks after NMDA injury. These results indicated that Ascl1 was not sufficient to induce neurogenesis from MG in vivo in a mature mouse.

Next, *Ueki et al* decided to test whether Ascl1 could regenerate neurons from MG in young mice following retinal injury. For these experiments, tamoxifen was administered at P12 and NMDA at P14, with retinas being collected and analyzed at P21 or P30 (Figure 1.6A). In this paradigm, Ascl1 was seen to induce regeneration of HuC/D and Pax6 positive cells with amacrine cell morphology (Figure 1.6), Otx2 and Cabp5 positive cells with bipolar cell

morphology, and Otx2 positive cells in the ONL with rod-like nuclear patterns and morphology. No neuronal morphologies or markers were present in the CC-GFP MG. This was an exciting result that showed successful regeneration from mammalian MG in vivo for the first time, but it also demonstrated that the neurogenic capacity of MG declines with age.

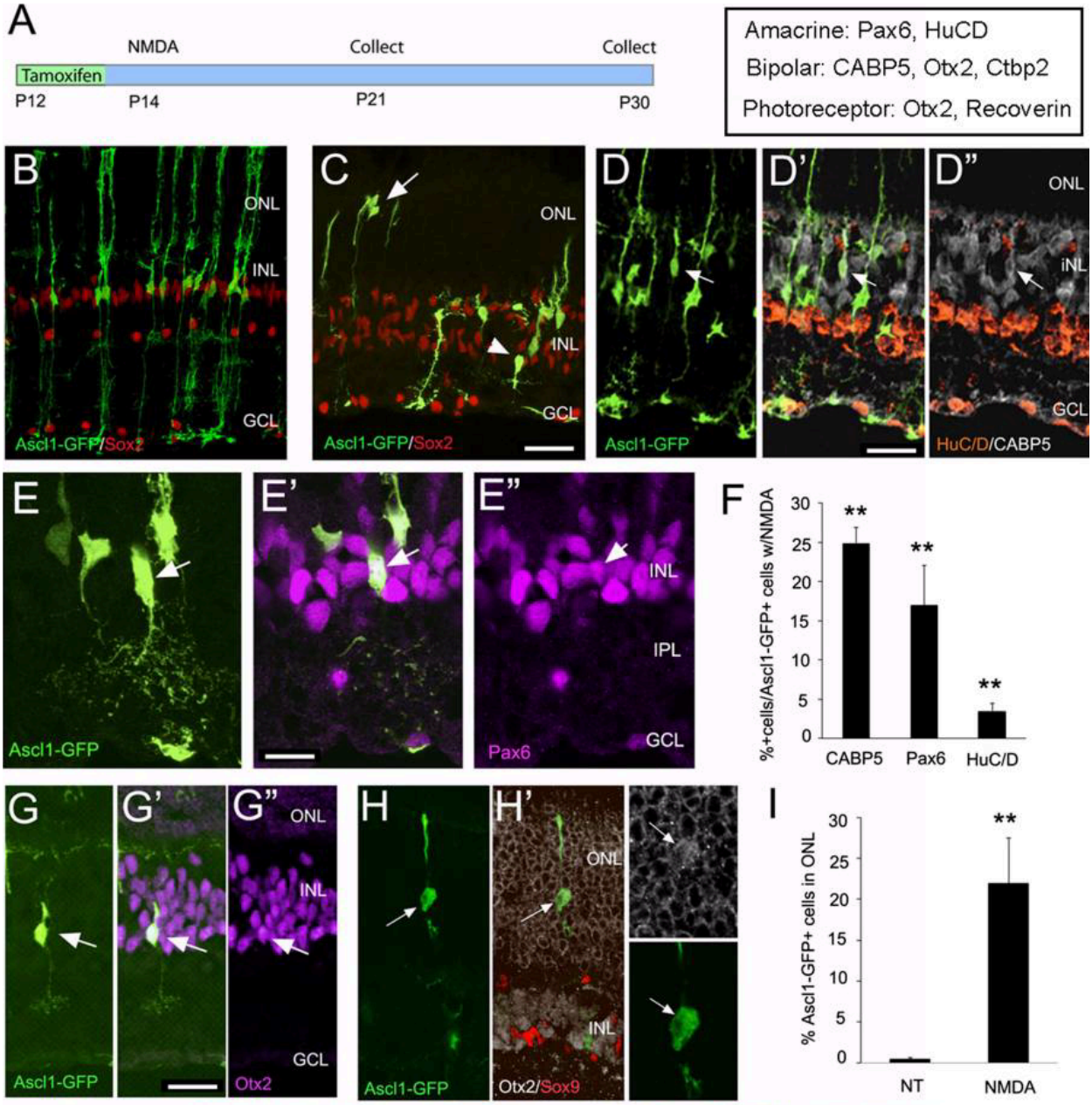

Figure 1.6 Retinal regeneration in young mice. **a**, Experimental paradigm for in vivo reprogramming of young MG to retinal neurons. Intraperitoneal injections of tamoxifen were

administered at P12 to induce Ascl1 expression, followed by intravitreal NMDA injury at P14. Retinas were collected at P21 and P30. **b**, Image of retina from Ascl1 induced retina collected at P21 without NMDA treatment stained with GFP and MG marker Sox2. **c**, Image of retina from Ascl1 induced retina collected at P21 with NMDA treatment. **d-d''**, Image of Ascl1-expressing retina treated with NMDA and stained with bipolar marker Cabp5 and amacrine marker HuC/D. **e-e''**, Zoomed image of MG-derived neuron with amacrine cell morphology stained with amacrine marker Pax6. **f**, Quantification of GFP+ cells that colocalized with neuronal markers Cabp5, Pax6, and HuC/D. **g-g''**, Images of MG-derived bipolar cell stained with bipolar marker Otx2. **h-h'**, Images of MG-derived rod with rod-like morphology in ONL and Otx2 staining. **i**, Quantification of GFP+ cells in non-treated (NT) and NMDA treated retinas.

I joined the lab near the end of this study and was fortunate to participate and co-author this study. When I joined the lab, the question I was tasked with was determining the window at which MG lose their neurogenic capacity. Dr. Ueki had successfully generated new neurons from MG at P12 with Ascl1 and NMDA damage; however, this potential was clearly lost by P30. I performed a time course experiment and found that by P16, the MG could no longer regenerate retinal neurons and instead presented with MG that resembled those of the adult Ascl1 + NMDA paradigm. We hypothesized that the MG's loss of neurogenic capacity with age may reflect changes in chromatin accessibility that occurs as cells mature. Previous evidence in zebrafish showing the importance of epigenetic changes in MG during regeneration also eluded to this potential mechanism[56].

For this reason, we decided to assess chromatin accessibility of Ascl1 target genes by performing DNaseI-seq on developing whole retina from P0, P7, and adult mice, as well as a P12 MG only sample (Figure 1.7). Surprisingly, we found that progenitor genes, such as Mfng and Dll1, that are not normally expressed in P12 WT MG have comparable levels of chromatin accessibility as P0 progenitor cells. MG clearly have chromatin accessibility at progenitor genes by P12, and Ascl1 alone is sufficient to induce their expression. Neuronal genes, however, lack chromatin accessibility at their promoters in P12 MG and are not expressed after Ascl1

induction. This suggests that chromatin accessibility may be responsible for Ascl1's ability to bind and reprogram MG to a neuronal state.

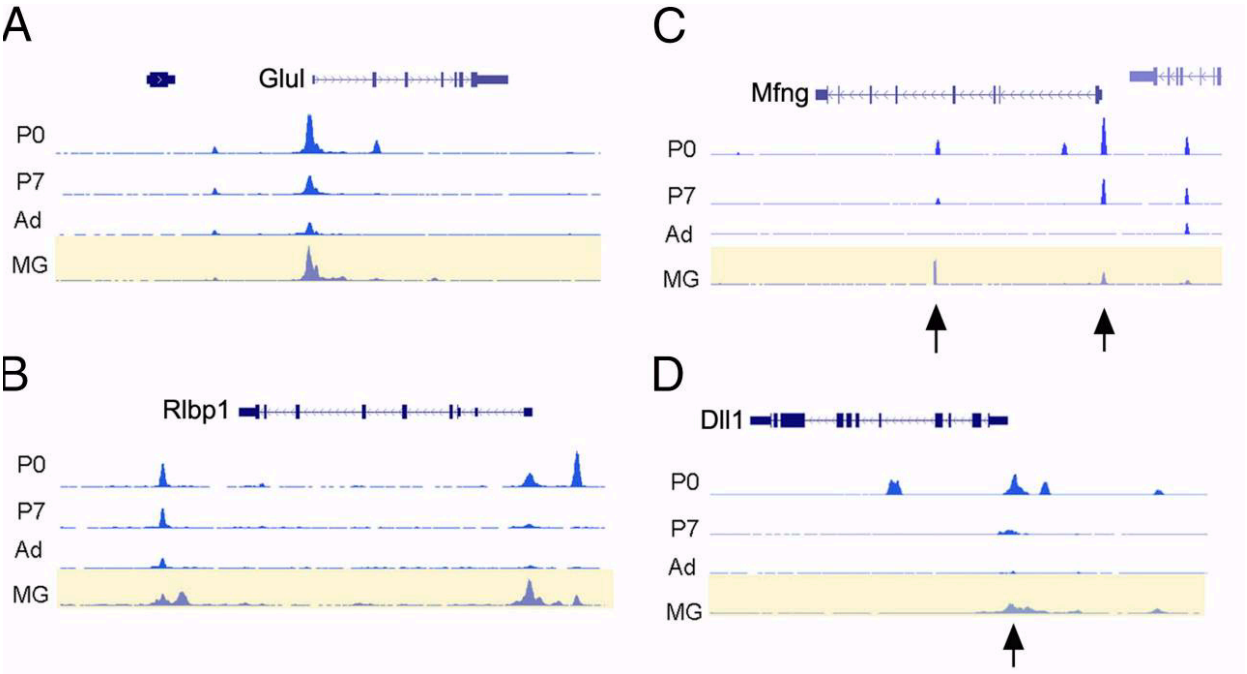

Figure 1.7 DNaseI-seq from cultured MG and whole retina from P0, P7, and adult mice. **a**, **b**, Tracks showing chromatin accessibility at promoter regions for glial genes Glul and Rlbp1, respectively. **c**, **d**, Tracks showing chromatin accessibility at promoter regions for progenitor genes Mfng and Dll1, respectively. Arrows indicate regions of DNA that are accessible in P0 RPCs and MG but not accessible in adult retina.

The findings in this study highlighted the potential for mammalian MG to be reprogrammed to retinal neurons in vivo. Ascl1 expression alone was unable to reprogram the MG into retinal neurons at any age in vivo; however, we found a developmental window (before P16), where Ascl1 expression in combination with retinal injury can stimulate the MG to become rods, amacrine cells, and bipolar cells. Lastly, we found that progenitor genes have readily accessible chromatin in WT MG but are not induced, except in the presence of Ascl1. Conversely, neuronal genes have no accessible chromatin at their promoters in MG and are not expressed in WT or Ascl1-expressing MG, suggesting a mechanism of chromatin accessibility may be responsible for their repression.

Chapter 2:

Stimulation of functional neuronal regeneration from Müller glia in adult mice.

(Text and figures modified from *Jorstad et al*, 2017)

INTRODUCTION

Many retinal diseases lead to the loss of retinal neurons and cause visual impairment. The adult mammalian retina has little capacity for regeneration. By contrast, teleost fish functionally regenerate their retina following injury, and Müller glia (MG) are the source of regenerated neurons[57,65,66,82-84]. The proneural transcription factor, Ascl1, is upregulated in MG after retinal damage[65,72] in zebrafish and is necessary for regeneration[85]. Although Ascl1 is not expressed in mammalian MG after injury[86], forced expression in mouse MG induces a neurogenic state in vitro[74] and in vivo after NMDA damage in young mice[81]. However, by postnatal day 16, mouse MG lose neurogenic capacity, despite Ascl1 overexpression[81]. Loss of neurogenic capacity in mature MG is accompanied by reduced chromatin accessibility, suggesting epigenetic factors limit regeneration. Here we show that MG-specific overexpression of Ascl1, together with a histone deacetylase inhibitor (HDACi), enables adult mice to generate neurons from MG after retinal injury. The MG-derived neurons express markers of inner retinal neurons, synapse with host retinal neurons, and respond to light. ATAC-seq shows that HDACi promotes accessibility at key gene loci in the MG, allowing more effective reprogramming. Our results thus provide a new approach for the treatment of blinding retinal diseases.

RESULTS

Expression of Ascl1 was directed to MG using mice with a tamoxifen-inducible cre-recombinase under one of two MG-specific promoters to activate a tetracycline response element driving Ascl1 (Figure 2.1a). For control animals, we used *Glast*- or *Rlbp*-CreER: Flox-stop-CC-GFP, or *Rlbp*-CreER: tdTomato mice. Adult mice (Figure 2.2) were injected with tamoxifen

before receiving either a PBS or NMDA intravitreal injection. An intravitreal injection of either DMSO or the HDACi Trichostatin-A (TSA) was then given (Figure 2.1b). TSA treatment increased H3K27ac (Figure 2.3a, b).

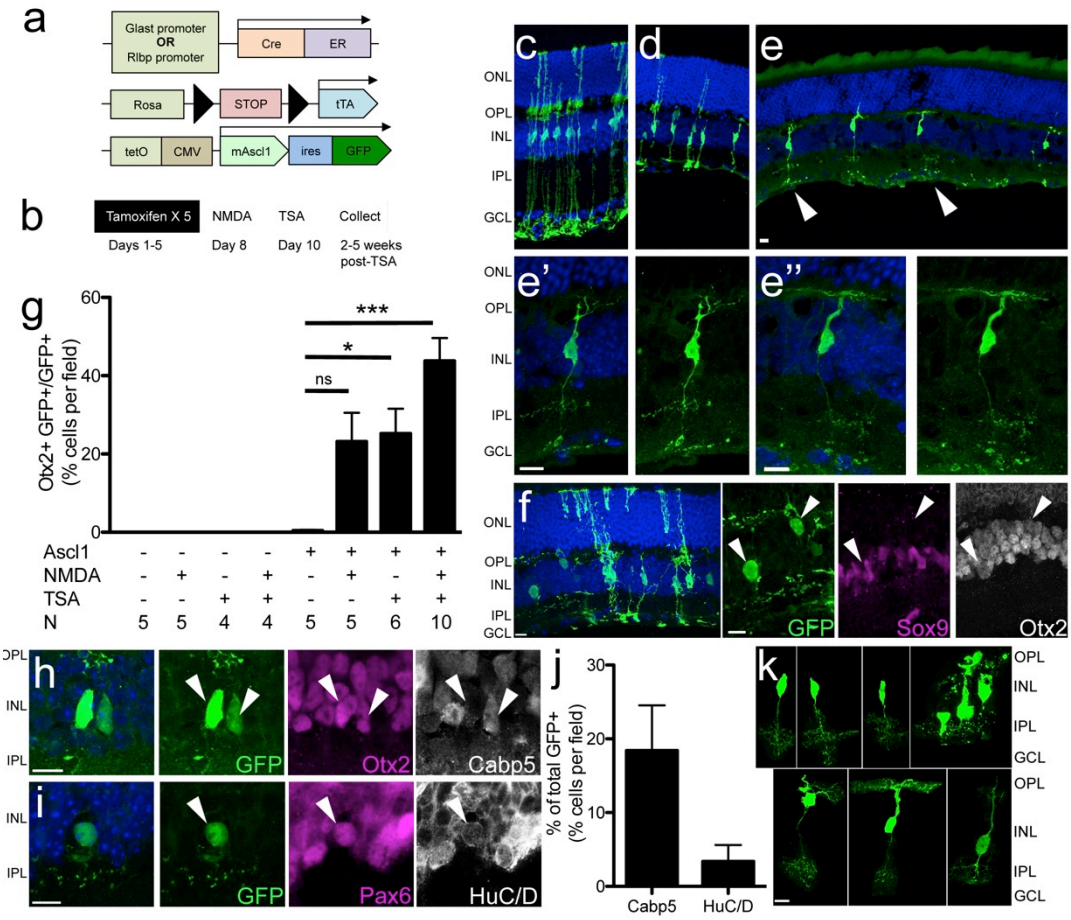

Figure 2.1: Conversion of MG into neurons by Ascl1 and TSA in vivo in adult mice. **a**, Mice strains used to express Ascl1 in MG. **b**, Paradigm for experiments. **c-e''**, Morphologies of Ascl1-overexpressing MG treated with **c** vehicle, **d** NMDA, and **e** NMDA + TSA; **e'**, **e''** higher magnification of **e** (arrows). ONL=Outer Nuclear Layer, OPL=Outer Plexiform Layer, INL=Inner Nuclear Layer, IPL=Inner Plexiform Layer, GCL=Ganglion Cell Layer. Images of cells in relative isolation chosen to highlight morphological phenotypes. **f**, Otx2+ MG-derived neurons lose Sox9 expression (arrows). **g**, Quantification of Otx2 in each condition in *Glast*-CreER animals. **P*<0.05; ****P*<0.001, One-way ANOVA with Tukey's post-test. **h**, **i**, MG-derived neurons express **h** bipolar cell-specific marker Cabp5 and **i** amacrine cell markers Pax6 and HuC/D (arrow). **j**, Quantification of Cabp5 or HuC/D in ANT-treated retinas (n = 3 mice per group). **k**, Representative images of MG-derived neuronal morphologies. All data is shown as mean ± standard error, all scale bars are 10 μm.

Conversion of MG into neurons by Ascl1 and TSA in vivo in adult mice

Ascl1-overexpressing animals treated with vehicle displayed normal retinal structure and MG morphology (Figure 2.1c). NMDA led to a loss of ganglion cells and reduction in the inner plexiform layer (IPL) thickness, though MG retained their normal morphology (Figure 2.1d). When Ascl1-overexpressing mice received TSA after NMDA, many GFP+ cells acquired a neuronal-like morphology, with processes in the outer plexiform layer (OPL) and IPL (Figure 2.1e-e''). Cells with neuronal morphology expressed neuronal markers, eg. Otx2, and lost expression of glial markers, like Sox9 (Figure 2.1f, g, Figure 2.3c, d). Otx2+ GFP+ cells with neuronal morphology were seen in both *Glast*-CreER and *Rlbp*-CreER strains and were only seen in mice that received all three factors, Ascl1, NMDA, and TSA (referred to as ANT-treated). The number of Otx2+ GFP+ cells in ANT-treated retinas did not depend on age at time of tamoxifen administration (Figure 2.3e). Many MG-derived neurons with bipolar cell-like morphology expressed the bipolar marker Cabp5 (Figure 2.1h, j, k). MG-derived neurons with an amacrine cell-like morphology were less common and often labeled with Pax6 and HuC/D (Figure 2.1i-k). We did not observe MG-derived ganglion cell or photoreceptor-specific morphology or markers Brn3, PKC, Recoverin, or Rhodopsin, in any condition (data not shown). Thus, ANT-treatment is sufficient to enable adult MG to undergo neurogenesis and give rise to retinal interneurons.

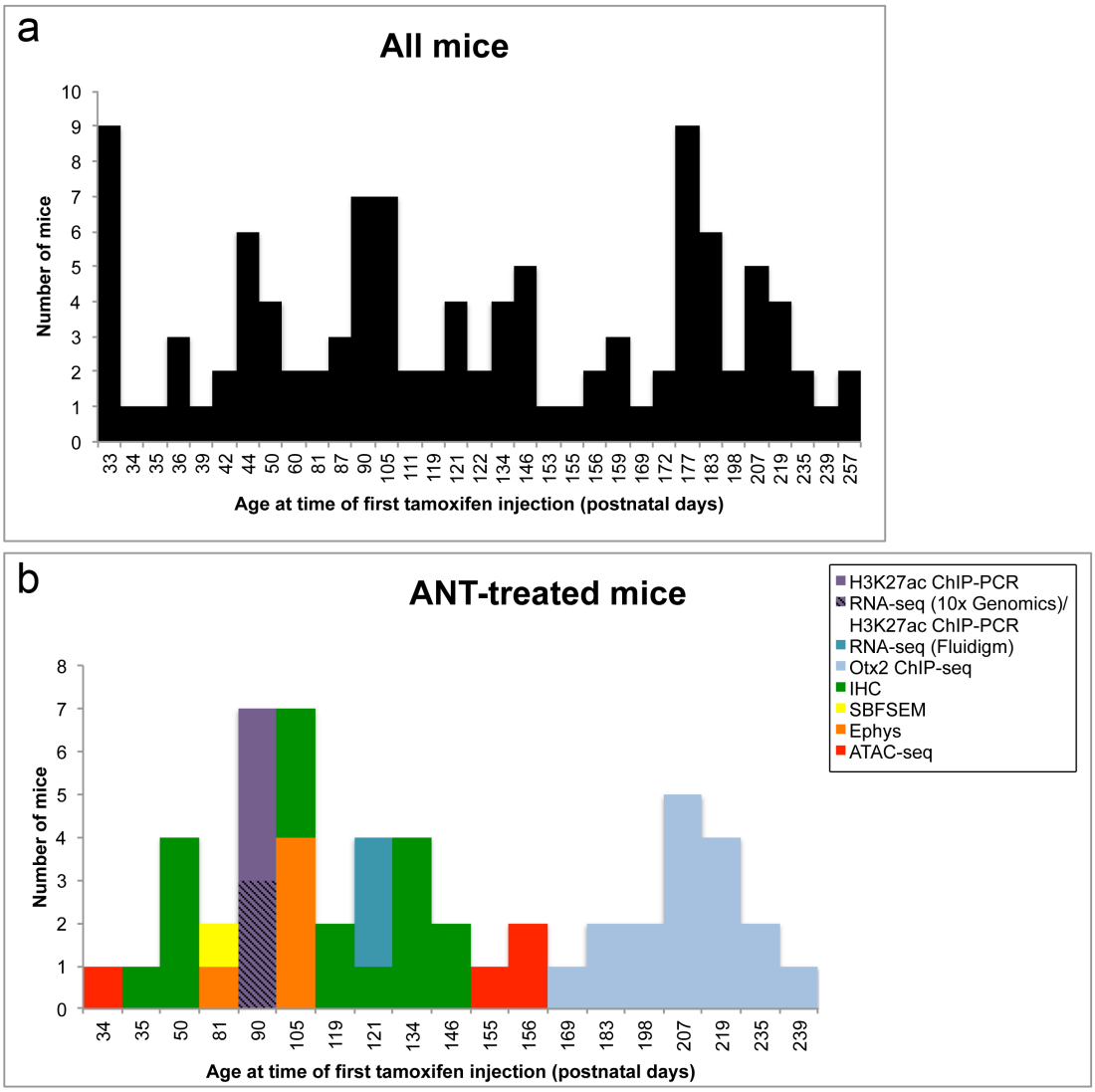

Figure 2.2: Animal age and numbers used in study. **a**, Histogram showing ages at which all *Glast*-CreER and *Rlbp*-CreER mice used for the study received their first tamoxifen injection. There were 108 *Glast*-CreER and *Rlbp*-CreER mice used for the study (122.7 ± 64.1 days, mean postnatal age ± s.d.). **b,** Histogram showing ages at which all ANT-treated mice used for the study received their first tamoxifen injection. There were 54 ANT-treated mice used for the study (136.4 ± 57.8 days, mean postnatal age ± s.d.). ANT-treated mice are classified according to experimental assay (H3K27ac ChIP-PCR, RNA-seq (10x Genomics)/H3K27ac ChIP-PCR = cells from these mice were split for both assays, RNA-seq (Fluidigm) = single-cell RNA-seq, Otx2 ChIP-seq, IHC = immunohistochemistry, SBFSEM = serial block-face scanning electron microscopy, Ephys = whole cell electrophysiology, ATAC-seq).

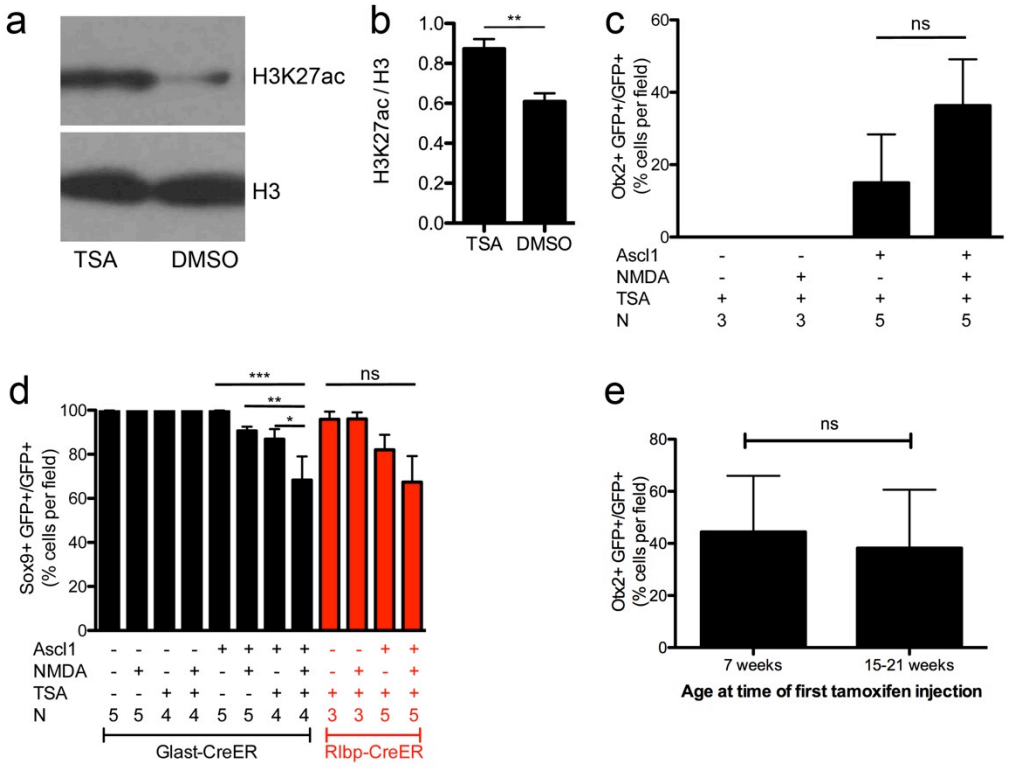

Figure 2.3: TSA increases histone acetylation. **a**, Western blot for H3K27ac and H3 24 hours after TSA or DMSO intravitreal injection. **b**, Graph shows TSA significantly increases H3K27ac relative to H3 by unpaired *t* test at ***P*=0.0033, n = 5 per group. **c**, Graph showing the percentage of GFP+ cells that express Otx2 in various conditions in *Rlbp*-CreER animals. Numbers were similar to *Glast*-CreER animals, showing no Otx2 in control mice lacking Ascl1 and ~36% of GFP+ cells expressing Otx2 when all three factors were present. Data was analyzed by One-way ANOVA with Tukey's Post-test. **d**, Graph showing the percentage of GFP+ cells that express Sox9 in various conditions in *Glast*-CreER and *Rlbp*-CreER animals. A significant reduction in the number of cells expressing Sox9 was seen by One-way ANOVA with Tukey's Post-test at **P*<0.05, ***P*<0.01, ****P*<0.001 when animals expressing Ascl1 were treated with NMDA and TSA. Data in **b-d** is shown as mean ± standard error. **e**, Graph showing the percentage of ANT-treated GFP+ cells that express Otx2 is not significantly different with age by Student's *t* test (n = 4 and 11 mice for 7 weeks and 15-21 weeks, respectively). Data in **e** is shown as mean ± standard deviation.

Some MG-derived neurons had 'hybrid' morphologies (Figure 2.4a), raising the possibility that MG undergo direct transdifferentiation into neurons. We tested this by administering EdU daily. Some MG-derived cells that expressed Otx2 also incorporated EdU; however, most MG-derived neurons were unlabeled, consistent with direct transdifferentiation

(Figure 2.4b). Ascl1 overexpression in dissociated cultures promotes MG proliferation[74]. We therefore tested whether transgenic expression of Ascl1 in vivo stimulates MG proliferation (Figure 2.4c). Ascl1 alone did not stimulate proliferation; however, when combined with mEGF, there was robust MG proliferation (Figure 2.4d-i). Thus, Ascl1 can promote either neural differentiation or proliferation of MG, depending on the presence of mitogenic factors.

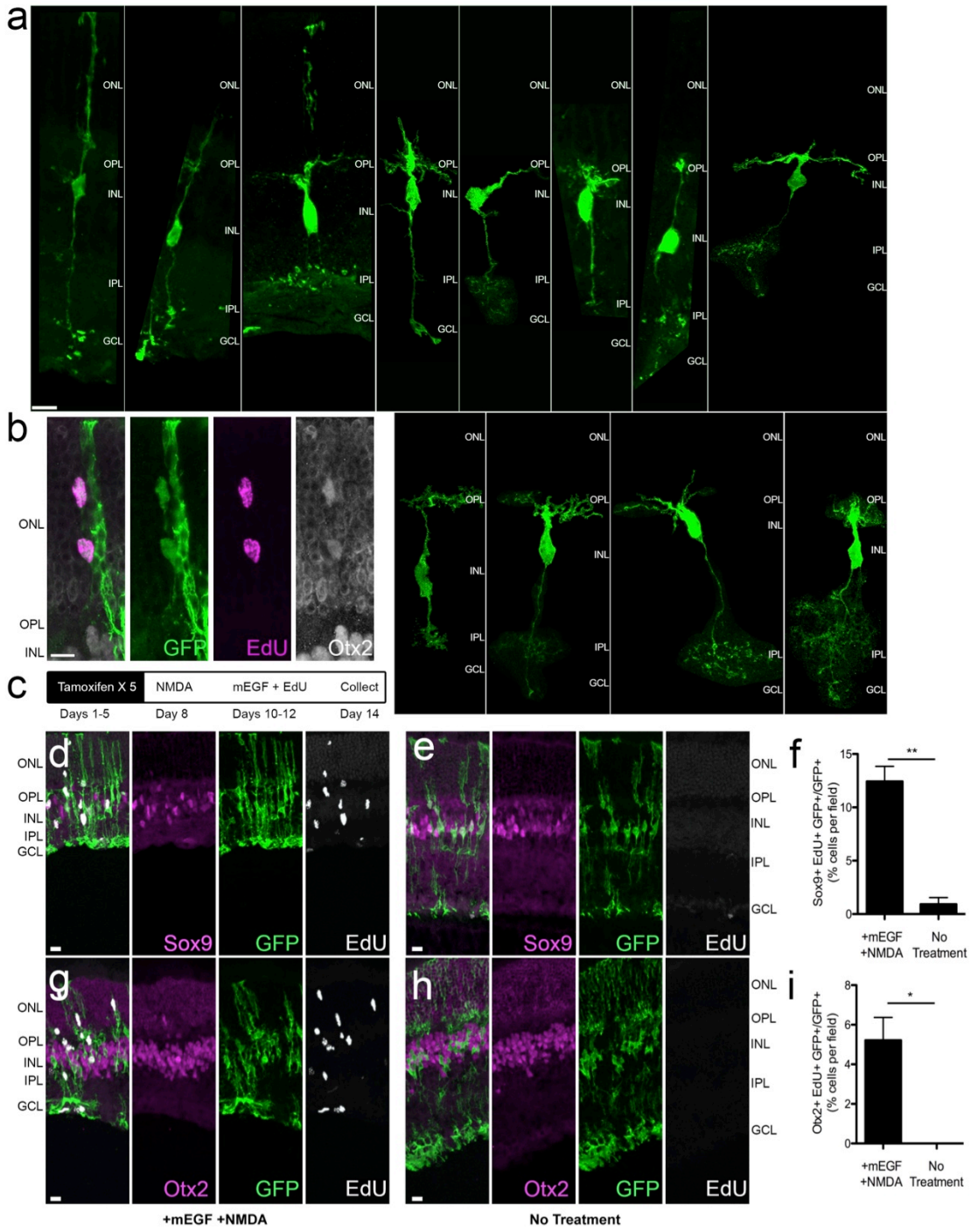

Figure 2.4: Neurogenesis and proliferation from Ascl1-expressing MG. **a**, Panel of images showing morphologies between MG and neurons. Images are from retinas that were collected 2-5 weeks post-TSA. Examples of 'hybrid' morphologies were observed at all post-TSA time points analyzed. First image of panel has normal glial morphology for comparison. **b**, Example of EdU-labeled GFP+ Otx2+ MG in ONL; cells stained with all three markers were very rare <1% of GFP+ MG (~1 cell per retinal section from 3 mice). **c**, Diagram showing experimental

treatment paradigm for proliferation analysis. **d**, Ascl1-overexpressing mice treated with mEGF and NMDA showed examples of Sox9+ EdU+ MG. **e**, Majority of MG did not label with EdU when Ascl1-overexpressing mice only received intravitreal EdU injections (No Treatment). **f**, Graph showing the percentage of GFP+ cells expressing Sox9 and that were labeled with EdU. A significant increase in Sox9+ EdU+ MG was seen when treated with NMDA and mEGF by Student's *t* test at ***P*=0.0033, n = 5 per group. **g**, Ascl1-overexpressing mice treated with mEGF and NMDA showed examples of Otx2+ EdU+ MG. **h**, Ascl1-overexpressing mice only receiving intravitreal EdU injections (No Treatment) had no MG that expressed Otx2 and labeled with EdU. **i**, Graph showing the percentage of GFP+ cells that express Otx2 and were labeled with EdU. A significant increase in Otx2+ EdU+ MG was seen when treated with NMDA and mEGF by Student's *t* test at **P*=0.0105, n = 5 per group. All data is shown as mean ± standard error, all scale bars are 10 μm.

MG-derived neurons form synaptic specializations

To determine if MG-derived neurons form synaptic connections with the host circuitry, we stained for the presynaptic ribbon marker, anti-CtBP2. We observed ribbons apposed to MG-derived neuronal processes in the OPL (Figure 2.6a-b'), and ribbons within the MG-derived neuronal processes in the IPL (Figure 2.6c-i, Figure 2.5a-g'). To view potential synaptic contacts at higher resolution, we used serial block-face scanning electron microscopy (SBFSEM) to reconstruct MG-derived cell processes (Figure 2.6j-o). We traced a process from an identified MG-derived neuron to the OPL; and found that this neuron contacted a host cone terminal in a manner similar to horizontal and bipolar cells (Figure 2.6n-o).

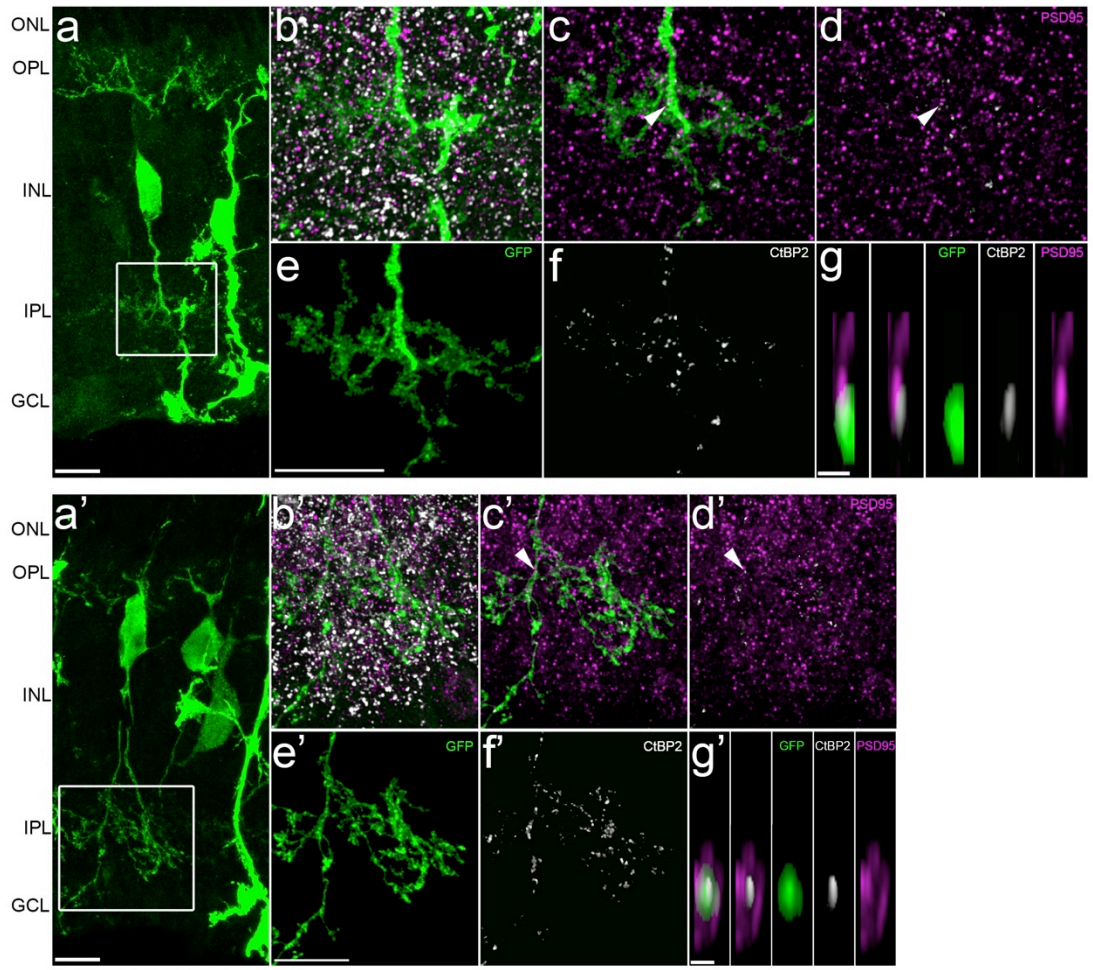

Figure 2.5: MG-derived neurons form synaptic specializations in IPL. **a-a'**, Confocal images of MG-derived bipolar-like cells with processes in IPL (scale bars, 10 μm). **b-b'**, Super-resolution Zeiss Airyscan raw images of white boxes from **a-a'** showing IPL processes stained with presynaptic ribbon marker CtBP2 (Ribeye, white) and postsynaptic marker PSD95 (magenta). **c-c'**, Images from **b-b'** masked in Amira to show presynaptic CtBP2 within GFP processes. **d-d'**, Images of masked presynaptic CtBP2 staining apposed to postsynaptic PSD95 staining. **e-e'**, Images of masks that were traced in Amira around GFP processes in IPL (scale bars, 10 μm). **f-f'**, Images of masked CtBP2 staining that is within GFP processes. **g-g'**, Images of CtBP2 apposed to PSD95 staining from **c-c'** (white arrows) rotated in XZ plane (scale bars, 1 μm). Images are from retinas that were collected 11 days post-TSA.

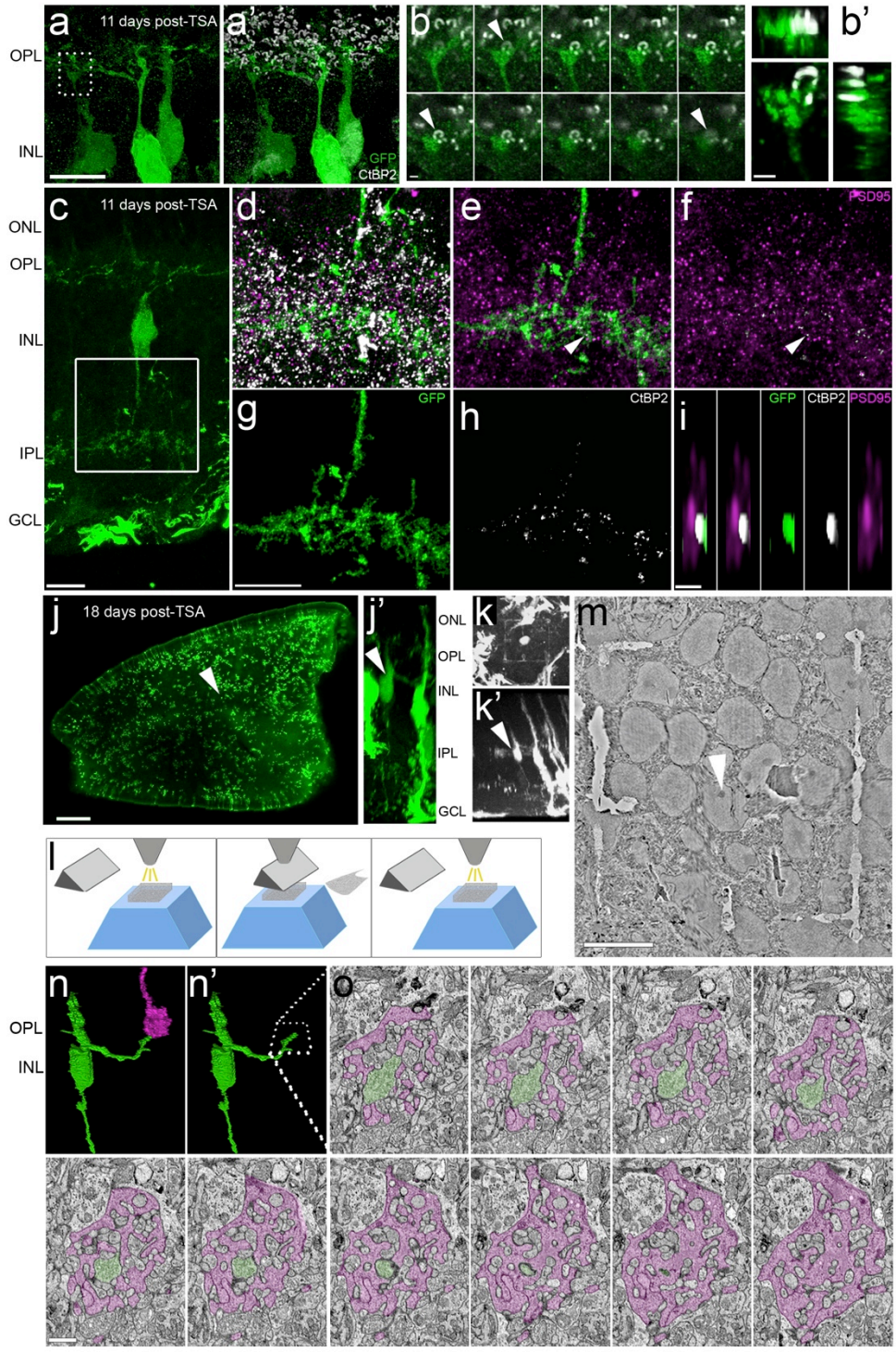

Figure 2.6: MG-derived neurons form synaptic connections with retinal circuitry. **a-a'**, Super-resolution image of MG-derived neurons. **b**, Box from **a** shows CtBP2 ribbon apposed to GFP+ process (arrows), series of 0.16 µm-thick Z-stack. **b'**, Orthogonal projection. **c**, MG-derived bipolar-like cell with processes in IPL **d-i**, Super-resolution images from **c** (box) labeled as indicated, **e-i** masked in Amira (see Methods)). **i**, Image of CtBP2 apposed to PSD95 from **e**

(arrows), XZ plane. **j**, **j'**, MG-derived neuron prior to branding (arrow). **k**, Two-photon image of branded box around MG-derived neuron. **k'**, Orthogonal projection of **k**. **l**, SBFSEM technique (see Methods). **m**, SBFSEM image of cell from **k** (arrow). **n,n'**, 3-dimensional reconstruction of cell from **k** with process (green) penetrating cone terminal (magenta). **o**, SBFSEM image series of cell from **k** color as in **n**. Scale bars are 10 μm: a,c,g,m; 1 μm: b,b',i,o; 200 μm: j.

To determine whether MG-derived cells made functional connections with host neurons, we performed whole-cell electrophysiology recordings from GFP+ and non-GFP cells. Non-GFP (i.e. normal) MG exhibited characteristic MG properties: 1) morphology, 2) hyperpolarized resting membrane potentials (V_{rest}), and 3) low input resistance[87,88] (R_{in}), suggesting that MG that do not express Ascl1 maintain relatively normal physiology in NMDA damaged retinas (Figure 2.7a, d). Recordings from GFP+ cells revealed very different physiological and morphological properties (Figure 2.7; Figure 2.8). GFP+ cells had much higher R_{in} than non-GFP MG and the V_{rest} of GFP+ cells were depolarized compared to non-GFP MG (Figure 2.7b, d). Many of the GFP+ cells had larger and faster responses to light stimulation than non-GFP MG (Figure 2.7a, b, e). Some GFP+ cells responded to light increments by depolarizing (as expected for ON-preferring cells), whereas others hyperpolarized to the same stimuli (as expected for OFF-preferring cells; Figure 2.7e). GFP+ cells exhibited diverse morphologies and electrical properties, with some cells resembling non-GFP MG and others closer to non-GFP bipolar and amacrine cells (Figure 2.7c, d, e). To further investigate the synaptic origin of visual responses in MG-derived GFP+ cells, we recorded excitatory and inhibitory synaptic currents. Seven of eight cells exhibited light-evoked excitatory input (Figure 2.7f) while four of four cells showed light-evoked inhibitory input.

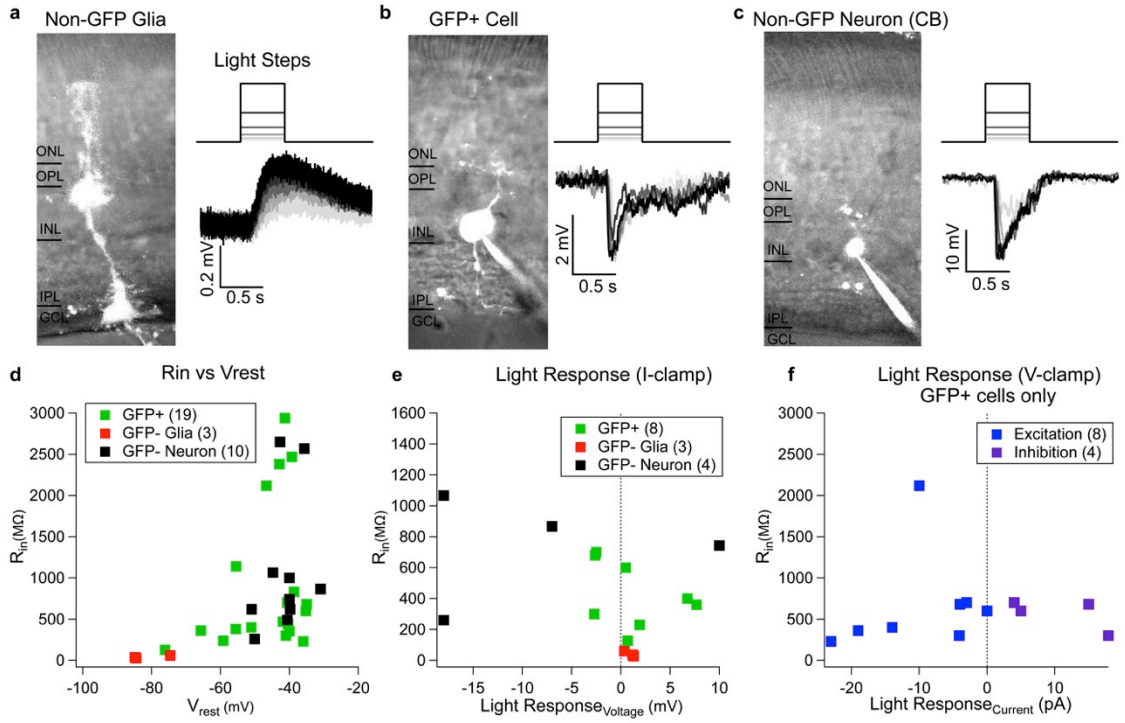

Figure 2.7: MG-derived GFP+ cells exhibit larger and faster visual responses than normal non-GFP MG. **a**, **b**, **c**, Example recordings from **a** non-GFP MG, **b** MG-derived GFP+ cell, **c** and non-GFP cone bipolar cell. Traces are visual responses to 500 ms steps in luminance, recorded in current-clamp. **d**, Population data for input resistance and resting membrane potential measurements. **e**, Population data for visual responses recorded with the current-clamp technique. **f**, Population data for light-evoked excitatory and inhibitory synaptic inputs recorded with the voltage-clamp technique. All cells recorded were from 5 ANT-treated mice. Recordings were performed at 4, 5, 10, 12, and 15 weeks post-TSA. Visual responses were found in cells regardless of post-TSA duration. **Non-GFP MG:** V_{rest} (-81 ± 6 mV), R_{in} (41 ± 17 MΩ), maximal response to light stimulation (0.95 ± 0.52 mV), n=3. **GFP+ cells:** R_{in} (871 ± 868 MΩ, n=20), V_{rest} (-46 ± 11 mV, n=19), maximal response to light stimulation (3.2 ± 2.7 mV, n=8), excitatory input (-10 ± 8 pA, n=8), inhibitory input (10 ± 7 pA, n=4). **Non-GFP neurons:** R_{in} (1088 ± 836 MΩ, n=10), V_{rest} (-42 ± 6 mV, n=10), maximal response to light stimulation (13 ± 6 mV, n=4). All responses are written mean ± standard deviation.

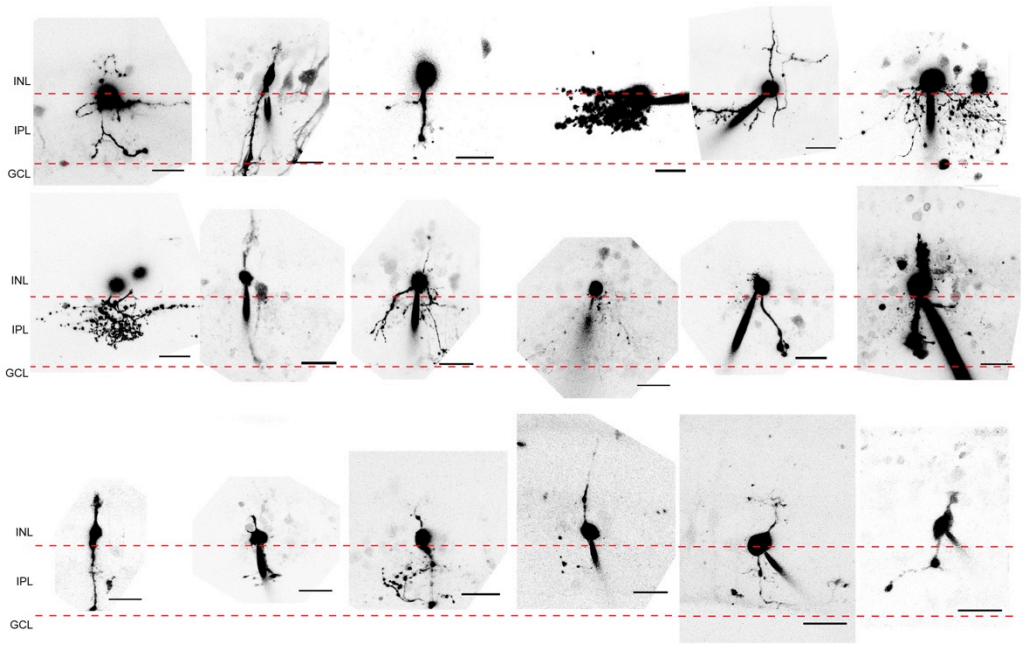

Figure 2.8: MG-derived GFP+ cells exhibit diverse morphologies. Panel of images showing 2D projections of GFP+ cells imaged post-recording (scale bars, 20 μm).

These results demonstrate that MG-derived GFP+ cells receive synaptic input. It is difficult to determine whether the MG-derived neurons contact postsynaptic partners in the IPL using electrophysiology. Therefore, we used super-resolution imaging to identify potential output synapses from MG-derived neurons. We found ribbons within MG-derived processes in the IPL that were apposed to PSD95 puncta, consistent with the MG-derived neurons forming glutamatergic synapses with amacrine or ganglion cells (Figure 2.6c-i, Figure 2.5).

ANT treatment enables epigenetic changes and expression of neuronal genes in MG

To better understand the mechanisms underlying MG reprogramming, we FACS-purified the ANT-treated and WT control cells for single-cell mRNA-seq, ATAC-seq and ChIP-seq (Figure 2.9-2.14). The single-cell mRNA-seq data was subjected to K-means clustering (Figure

2.11b, Figure 2.12). The majority of ANT-treated cells were found in two clusters; the cells in the Red cluster express bipolar and amacrine-specific genes (see Figure 2.12b), while cells in the Blue cluster express generic neural genes and progenitor genes. These cells formed separate clusters from the WT MG. The average expression for all Ascl1+ cells shows an increase in neural progenitor genes, and bipolar or amacrine cell genes compared to WT (Figure 2.11b). The ANT-treated cells also show a reduction in the expression of glial genes, when compared to WT (Figure 2.12, Figure 2.14a, b).

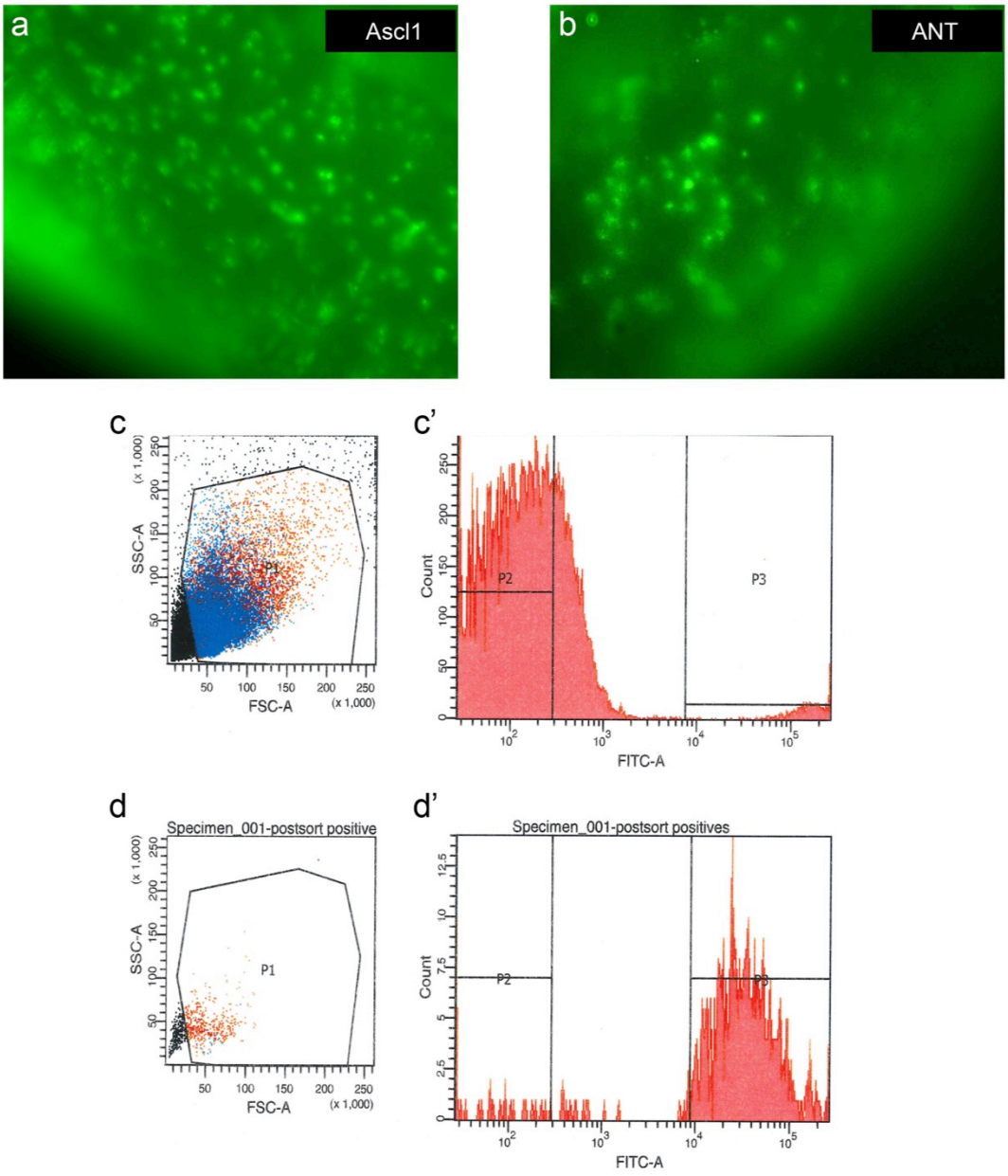

Figure 2.9: FACS purification of GFP+ cells. **a**, **b**, Live imaging of Ascl1-overexpressing retinas either **a** untreated, or **b** ANT-treated prior to dissociation and FACS purification. **c**, Representative graph shows gating (P1 gate = viable cells) for viable cells from non-viable cells and debris. **c'**, Gating P1 fraction for GFP fluorescence (P3 gate = GFP+ fraction). **d-d'**, Post-sort on P3 fraction shows majority of GFP+ cells (88.7%) are viable after sorting.

Analysis	Mouse Strain	Treatment	# retinas	# positive cells (P3)	% of total P1 cells	% of total events
Otx2 ChIP-seq	Rlbp-Ascl1	ANT	34	490,430	0.7	0.4
Otx2 ChIP-seq	Rlbp-Ascl1	Ascl1	30	692,271	1.6	0.8
H3K27ac ChIP-PCR	Glast-Ascl1	ANT	8	50,000	0.5	0.2
Single cell mRNA-seq (10x)/ H3K27ac ChIP-PCR	Glast-Ascl1	ANT	6	50,000	1.4	0.8
Single cell mRNA-seq (10x)/ H3K27ac ChIP-PCR	Rlbp-tdTomato	WT	4	125,000	5.3	1.7
Single cell mRNA-seq (Fluidigm)	Glast-Ascl1	ANT	6	18,000	0.6	0.2
Single cell mRNA-seq (Fluidigm)	Rlbp-tdTomato	WT	4	140,000	6.0	1.3
ATAC-seq	Glast-Ascl1	ANT	4	130,000	1.2	0.4
ATAC-seq	Glast-Ascl1	TSA	2	85,000	2.6	0.6
ATAC-seq	Glast-Ascl1	NMDA	4	100,000	2.3	0.6
ATAC-seq	Glast-Ascl1	Ascl1	4	85,000	0.7	0.3
ATAC-seq	Rlbp-tdTomato	WT	6	65,000	2.4	0.7

Figure 2.10: Table summary of all FACS-purified retinas.

The changes in gene expression in the ANT-treated cells were reflected in changes in DNA accessibility as shown by the ATAC-seq (Figure 2.11c, Figure 2.13a). Overall, accessibility at glial genes was reduced, and accessibility at neural genes increased. H3K27ac ChIP confirmed increased acetylation of this histone modification in the ANT-treated cells at E-box containing promoters of neural genes (Figure 2.13b). Genome-wide analysis of accessible regions in the ANT-treated cells shows significant Gene Ontology (GO) enrichment (via GREAT[89]) at genes associated with nervous system development and neuron differentiation (Figure 2.11d). The addition of TSA, or TSA and NMDA, leads to progressive increases in the number of accessible genes associated with neural development/differentiation (Figure 2.11e), suggesting that the cumulative combination of factors is most effective in reprogramming the MG epigenome.

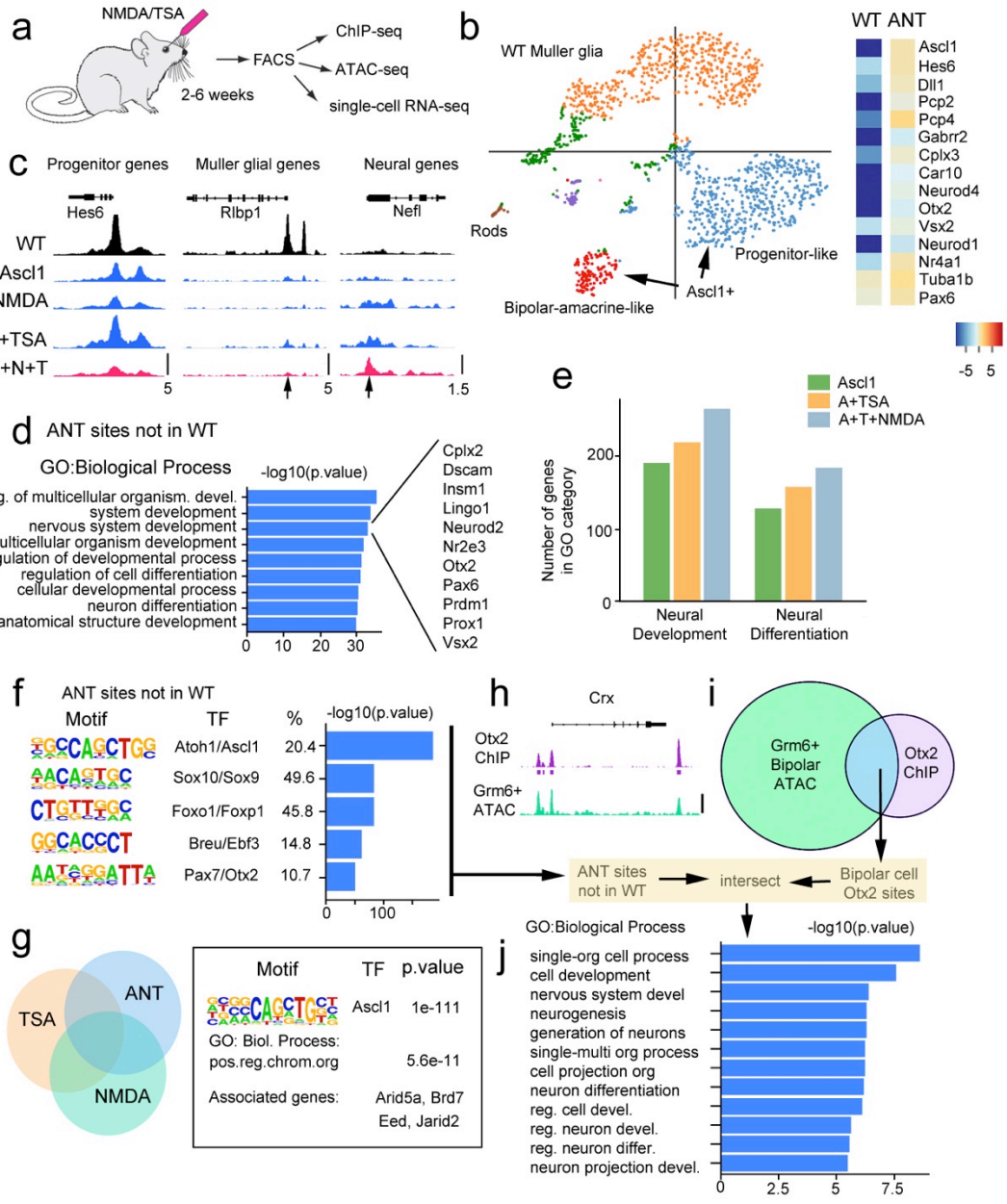

Figure 2.11: ANT treatment enables epigenetic changes and expression of neuronal genes in MG. **a**, FACS-purified MG-derived neurons subjected to genomic analyses. **b**, K-means clustering of single-cell RNA-seq from WT and ANT-treated cells shown as t-SNE plot. Heatmap showing average expression of neural genes for all Ascl1+ cells in the ANT condition (19 days post-TSA) compared with WT. **c**, ATAC-seq normalized reads shown for sample progenitor (*Hes6*), MG (*Rlbp1*) and neural (*Nefl*) genes. DNA accessibility changes with Ascl1 expression (arrows). Scale at the bottom track for each set (reads per million, RPM). ANT-treated mice 15 days post-TSA. **d**, Gene Ontology enrichment for regions of increased DNA accessibility in ANT-treated cells compared with WT. Examples of the Nervous System Development category are shown to the right. **e**, The number of genes in enriched GO categories

from MG expressing Ascl1, Ascl1 and TSA, and from ANT-treated retinas. **f**, Top 5 transcription factor motifs in peaks of ANT, but not WT; percentage of peaks with motif and enrichment score. **g**, ATAC-seq peaks for ANT vs. TSA and NMDA were compared; ANT-specific peaks analyzed for motif enrichment and Gene Ontology. Two of the top ten GO enriched Biological Processes were chromatin-remodeling genes. **h**, **i**, Otx2 ChIP-seq peaks from total retina[90], was compared with ATAC-seq from Grm6+ FACS-purified bipolar cells and the overlapping (bipolar-specific Otx2 peaks) regions intersected with the ANT peaks that were not present in the WT (scale bar = 100 CPM for Otx2-ChIP and 10 CPM for ATAC-seq). **j**, Gene Ontology enrichment for Biological Process of peaks that overlap with ANT and bipolar cell Otx2 sites showing P-value for term enrichment for neural genes.

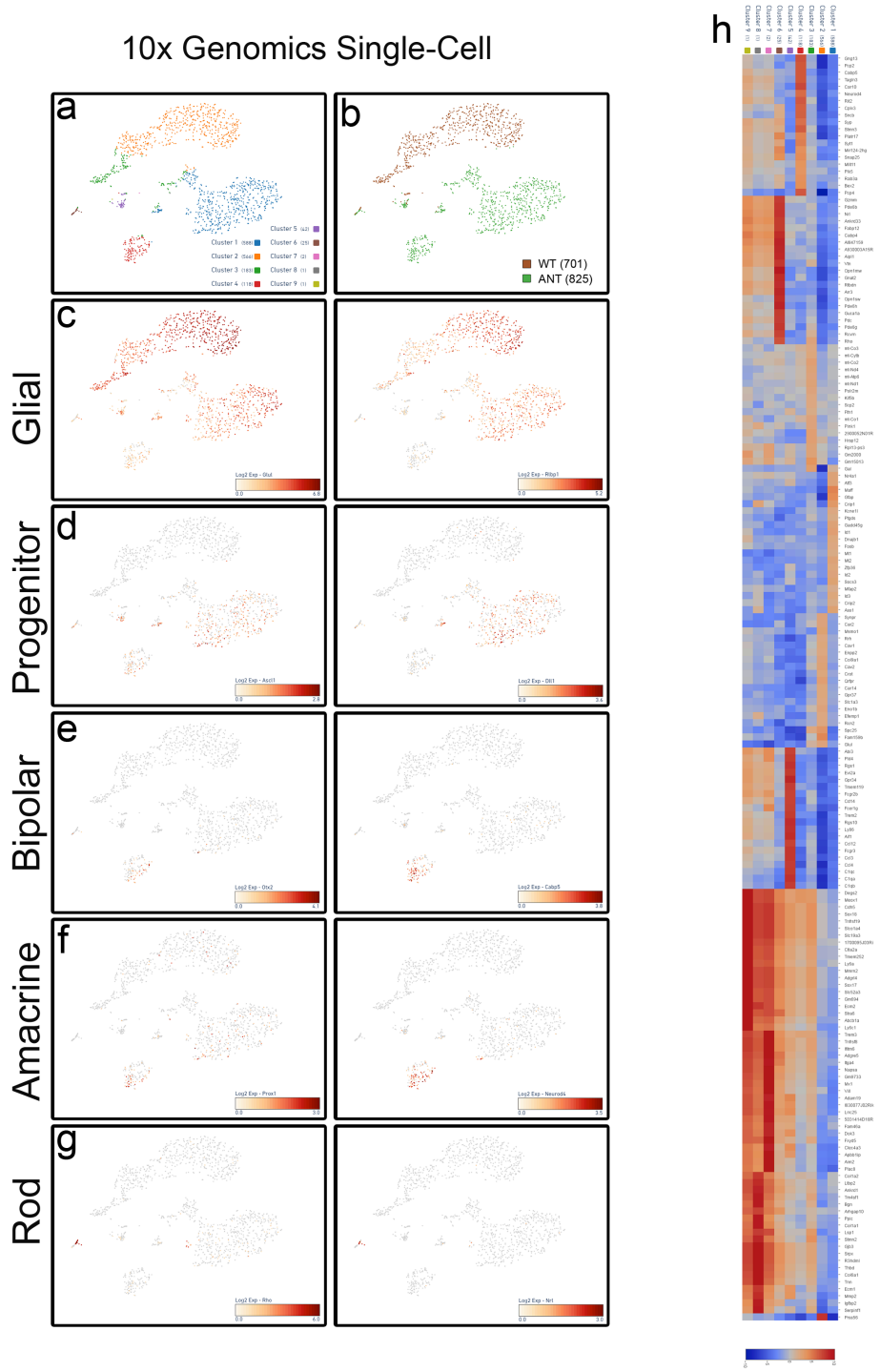

Figure 2.12: ANT treatment results in MG-derived bipolar/amacrine-like cell cluster. **a**, Principal component analyses of 10x Genomics single-cell RNA-seq from aggregate WT and ANT-treated cells showing k-means clustering. **b**, Clusters identifying WT (brown – 701 cells) and ANT-treated (green – 825 cells). **c**, Plots showing expression levels of glial genes *Glul* and *Rlbp1*. Expression of glial genes is reduced in the ANT-treated cells and further reduced in the MG-derived bipolar/amacrine-like cells. **d**, Plots showing expression levels of progenitor genes *Ascl1*

and *Dll1*. Ascl1 expression was only seen in ANT-treated cells. *Dll1* appears to be increased in the large ANT-treated cluster but decreased in the bipolar/amacrine-like cluster. **e**, Plots showing expression levels of bipolar genes *Otx2* and *Cabp5*. Both genes are enriched in the bipolar/amacrine-like cluster. **f**, Plots showing expression levels for amacrine genes *Prox1* and *Neurod4*. Both genes are enriched in the bipolar/amacrine-like cluster. **g**, Plots showing expression levels for rod genes *Rho* and *Nrl*. Rod contamination shows enrichment for both genes in small cluster. **h**, Heatmap of top 20 upregulated and differentially expressed genes for each cluster (scale, log2 fold change). Single-cell data is from retinas that were collected from ANT-treated mice 19 days post-TSA.

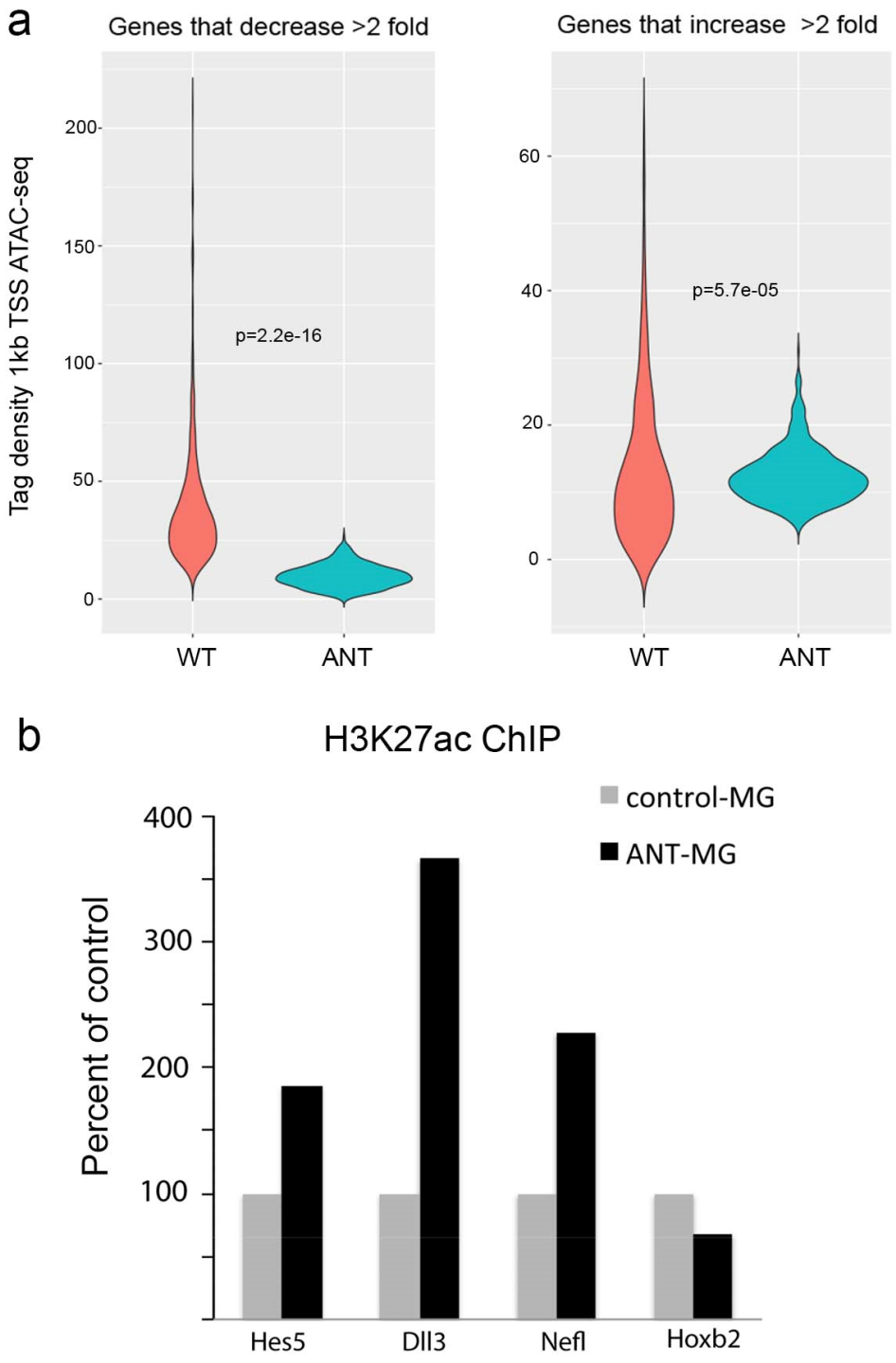

Figure 2.13: Epigenetic modifications at Ascl1-binding sites. **a**, Violin plots of ATAC-seq tag density in the region 1 kb upstream of the promoters of genes that either decrease by 2 fold or increase by 2 fold between the WT and ANT reprogrammed MG to show that the changes in gene expression are accompanied by changes in DNA accessibility during reprogramming with Ascl1, NMDA and TSA. The changes in gene expression were taken from the average of all Ascl1+ cells in the single-cell RNA-seq data from the Fluidigm data and compared with the WT

MG from the same dataset. Interestingly, many progenitor genes, like *Hes6* and *Ascl1*, show chromatin accessibility at putative cis-regulatory regions in all treatment conditions (including WT) even though these genes are not normally expressed in the mature retina. **b**, H3K27ac ChIP was carried out on FACS-purified ANT reprogrammed MG and WT MG. The data are shown as a percent of control for three neural genes that show increases in expression and a control gene (*Hoxb2*) that does not change with ANT treatment. There was a substantial increase in H3K27ac for each of the genes tested. ChIP-PCR data is from ANT-treated retinas that were collected 19 days post-TSA.

We next analyzed the accessible regions from ANT-treated cells to look for increases in DNA accessibility relative to WT MG. Ascl1 was the top-scoring motif in the ANT-unique peaks relative to WT (by HOMER), with Sox9, Foxo1, E2f3, and Otx2 also highly enriched (Figure 2.11f). When the accessible regions from the ANT-treated cells were specifically compared with those treated with only TSA or only NMDA, we found a set of peaks unique to the ANT condition. Two of the top 10 GO terms in ANT-specific peaks were associated with chromatin remodeling (Figure 2.11g), suggesting that the combination of retinal injury and TSA might promote neuronal differentiation of Ascl1-overexpressing MG by increasing the expression of genes that further facilitate epigenome reorganization.

Otx2, a transcription factor required for bipolar neurons and photoreceptors, was among the top 5 enriched motifs in an analysis of the ANT peaks (Figure 2.11f). To determine whether these were associated with cis-regulatory elements of retinal neurons, we FACS-purified bipolar cells from adult *Grm6*-tdTomato mice and carried out ATAC-seq. We compared Otx2 ChIP-seq data from whole retina[90] with the ATAC-seq from bipolar cells to generate a set of bipolar Otx2 peaks (Figure 2.11h, i). When we compare the bipolar Otx2 peaks with the newly accessible chromatin in the ANT-treated cells (peaks not in WT), we find the top categories enriched in GO (Biological Process) are in neural development and differentiation (Figure 2.11j); we do not see a similar enrichment when we intersect bipolar Otx2 peaks with the ATAC-seq peaks of normal

MG. Thus, we can conclude that reprogramming MG to neurons with Ascl1, NMDA and TSA leads to more accessible chromatin at bipolar cell Otx2 sites. ChIP-seq for Otx2 in FACS-purified ANT-treated cells further confirm that the combination of TSA and retinal injury has allowed Otx2 to bind to promoters of retinal neuron cis-regulatory regions, partly explaining the mechanism by which this combination promotes neurogenesis (Figure 2.14c-g).

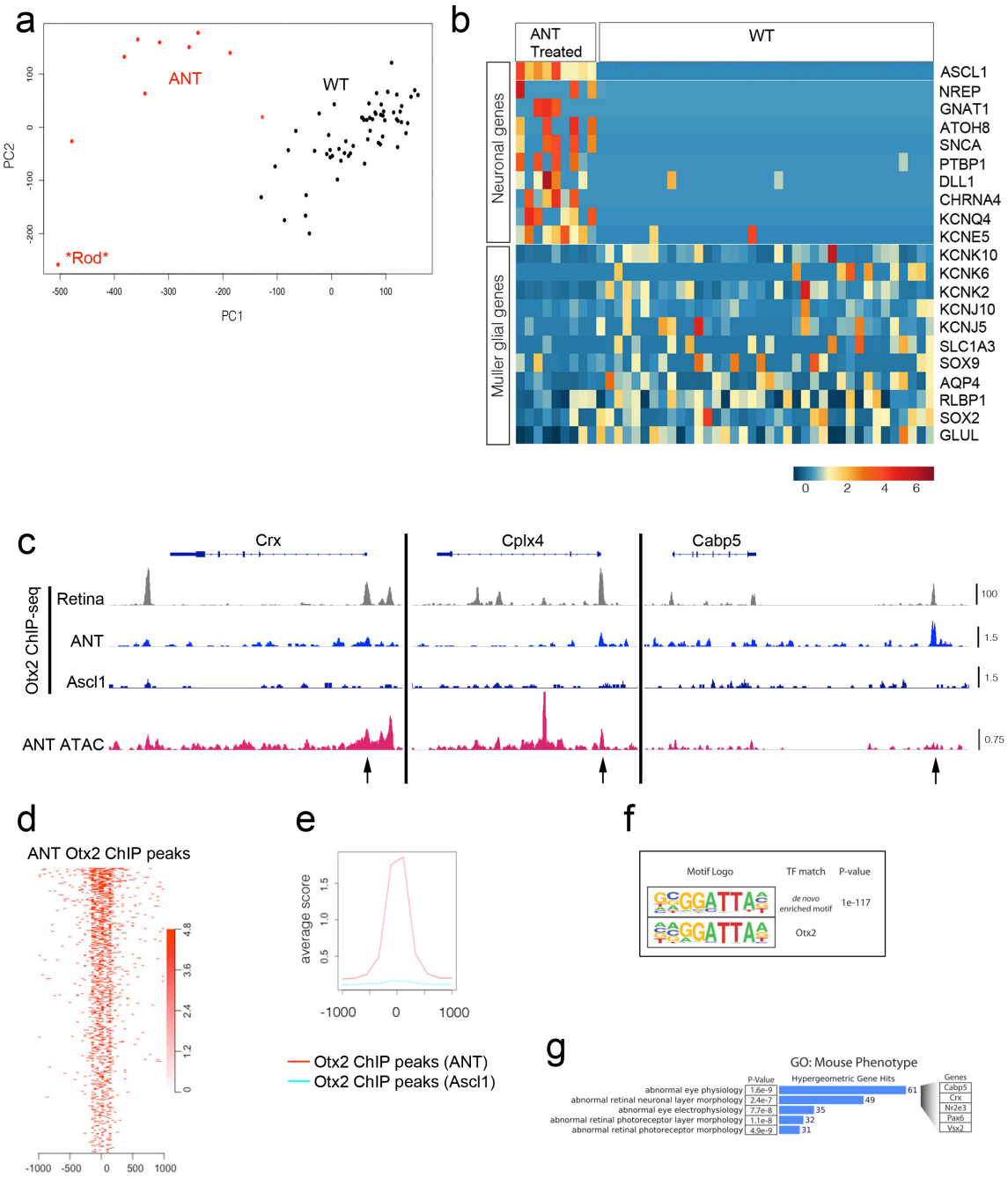

Figure 2.14: FACS-purified ANT-treated cells show increased neuronal gene expression and Otx2 binding. **a**, Principal component analysis from Fluidigm single-cell mRNA-seq showing 48 WT MG (black), 9 ANT-treated cells (red), and 1 cell that was likely a contaminating rod photoreceptor (asterisk). The ANT-treated cells formed a separate cluster from the WT MG. **b**, Heatmap showing ANT-treated MG-derived cells and WT MG. Each column is an individual

cell, with example neural and glial genes as rows. Reprogramming with ANT leads to down-regulation of glial genes and an increase in neural genes. Scale = log2CPM. ANT-treated retinas were collected 46 days post-TSA. **c**, IGV browser tracks at bipolar genes *Crx, Cplx4*, and *Cabp5* showing: Otx2 ChIP-seq from whole adult mouse retina[90] (gray), Otx2 ChIP-seq from FACS-purified ANT-treated and Ascl1 only cells (blue), and DNA accessibility from ATAC-seq of FACS-purified ANT-treated cells (red). Scale for all tracks shown to the right as RPM. Black arrows mark open chromatin in promoter regions that are bound by Otx2 in ANT-treated but not control Ascl1 cells, and are appropriate regions of binding based on a whole retina Otx2 ChIP-seq dataset. **d**, **e**, Otx2 ChIP-seq peaks from ANT-treated cells show central enrichment at Otx2 ChIP-seq sites from whole adult retina[90], but this is not present in the Otx2 ChIP-seq from MG that expressed Ascl1, but received none of the other treatments (TSA, NMDA). **f**, Top scoring transcription factor binding motif enrichment (HOMER software suite) from ANT-treated Otx2 ChIP-seq peak calls along with the closest matching transcription factor motif (TF match) and P-value for de novo motif enrichment. **g**, Gene Ontology enrichment for category, Mouse Phenotype, of peaks from **d**, showing P-value for term enrichment, the number of associated genes (blue bars), and example genes from these enriched terms (expanded at right). ChIP-seq was performed on 490,430 and 692,271-pooled cells from 17 ANT-treated *Rlbp*-Ascl1 and 15 untreated *Rlbp*-Ascl1 mice, respectively. Retinas were collected 9-18 days post-TSA.

DISCUSSION

The combination of Ascl1 overexpression and TSA causes the MG to generate new inner retinal neurons after NMDA damage. It is not clear why bipolar cells are the predominant neurons generated, since NMDA primarily causes ganglion cell and amacrine death. There is some evidence that Ascl1 biases the retinal progenitor to a bipolar fate, though studies of Ascl1+ progenitor cells show all but retinal ganglion cells are in the lineage[91]. Alternatively, the microenvironment may favor inner retinal differentiation after inner retinal damage; future studies of mice with photoreceptor injury could test this hypothesis. Nevertheless, the fact that MG-derived neurons integrate into a mature circuit suggests that factors needed to support synaptogenesis continue to be expressed into adulthood in the mammalian retina.

Our results extend the findings of similar approaches being taken in other regions of the CNS. Astrocytes and NG2 cells can be reprogrammed to neurons by expressing proneural

transcription factors in the cerebral cortical and subcortical regions[92-95]. Recordings from cortical slices and rabies-virus-based tracings indicate that these neurons are functional. Cellular reprogramming in vivo provides an unique opportunity to recruit the regenerative programs from regenerating organisms, like zebrafish, for regenerative medicine[96]. Converting the resident glial cells in the CNS to neurons by cell-specific expression of transcription factors shows the potential for this approach in the nervous system[97,98]. The results in this report demonstrate the feasibility of this approach for potential clinical translation for retinal diseases.

Chapter 3:

STAT pathway activation limits the Ascl1-mediated chromatin remodeling required for neural regeneration from Müller glia in adult mouse retina.

INTRODUCTION

Functional regeneration of retinal neurons occurs naturally in teleost fish and many amphibians[57,65,66,82-84]. In zebrafish, the Müller glia (MG) respond to a variety of injury models by generating cells that resemble multipotent progenitor cells found in the developing retina. These MG-derived progenitors have the capacity to produce all types of retinal neurons and restore visual function[99]. In amphibians and embryonic birds, the pigmented epithelial cells undergo a similar transition to retinal progenitor cells, and can regenerate a new, laminated retina[100,101].

In adult birds and mammals, functional regeneration does not occur spontaneously after retinal injury. Neurotoxic damage to retinal neurons in newly hatched chicks causes the MG to undergo the initial stages of the process that occurs in fish, but few of the MG-derived progenitors go on to make neurons and it is not known whether the few regenerated MG-derived neurons can functionally integrate into the existing retinal circuitry[65]. Injury to the mammalian retina has been studied most extensively in rodents, and as in the bird, retinal injury does not initiate a spontaneous regenerative response[86]. Attempts to stimulate MG proliferation after injury by stimulating specific signaling pathways with growth factors and small molecules have led to some evidence for new neurogenesis[102]; however, none of these treatments have been sufficient to regenerate functional neurons from MG in mice[103-105].

Recently, we have found that transgenic overexpression of the proneural bHLH Ascl1 enables MG to generate functional neurons in mice. We found that in mice up to two weeks old, Ascl1 alone can induce neurogenesis from MG after N-Methyl-D-aspartic acid (NMDA) excitotoxic damage[81]. More recently, we demonstrated that Ascl1 and the HDAC inhibitor trichostatin A (TSA) were together sufficient to induce MG to regenerate functional neurons

after retinal injury in adult mice[106]. While these studies were encouraging and demonstrated for the first time that new neurons generated in adult mice can be integrated into the mature retinal circuit, the majority of the MG in treated retinas did not undergo neurogenesis.

In the course of our analysis of single-cell RNA-seq data from the previous study, we noticed that those MG that failed to reprogram to neurons had a high level of STAT3 signaling. MG from fish, birds and mammals all respond to retinal damage by rapidly activating STAT3 signaling[107-110]. In the mouse retina, STAT3 signaling in MG is associated with reactive "gliosis"; however, in the fish retina, STAT3 is required for damage-induced MG-mediated neuronal regeneration, and JAK/STAT activation is sufficient to induce retinal regeneration in the absence of injury[107,111,112]. In the chick retina, however, experiments have suggested that STAT signaling instead may limit regeneration: inhibition of STAT3 increases the neurogenesis from MG in damaged retinas[110]. Since an increase in STAT signaling is well known to occur in glia after neuronal injury, we tested whether the injury response was potentially reducing Ascl1-mediated reprogramming. We tested this hypothesis by inhibition of STAT signaling, and found that a STAT inhibitor, in combination with our previously described treatment paradigm, doubled the efficiency of neuron regeneration in vivo. Analysis of ChIP-seq data of Ascl1-expressing MG suggests that STAT signaling may act to redirect Ascl1 to inappropriate regulatory sites in the genome, and implicate the Id1 and Id3 inhibitors of bHLH factors in this process. Our results extend previous work in fish and birds on the importance of JAK/STAT signaling in retinal regeneration. Together with the results from the non-mammalian vertebrates, it appears that an initial activation of the STAT pathway may be necessary to start the regeneration process, but sustained activation of the pathway may then become limiting.

RESULTS:

STAT pathway inhibition improves MG-derived neurogenesis in vivo

To test whether the activation of the STAT pathway in MG reduces their ability to be effectively reprogrammed by Ascl1, we inhibited this pathway in an experimental system in which Ascl1 can be targeted specifically to MG. We previously described[81,106] a MG-specific tamoxifen inducible mouse model of Ascl1-overexpression (*Glast*-CreER:Rosa-flox-stop-*LNL*-tTA:*tetO*-mAscl1-ires-GFP). Adult mice received up to five consecutive daily intraperitoneal (IP) injections of tamoxifen (1) to induce Ascl1 expression in the MG, followed by (2) an intravitreal injection of NMDA to induce degeneration of inner retinal neurons, and then (3) an intravitreal injection of either TSA or TSA and the potent STAT inhibitor, SH-4-54 (referred to as ANT and ANTSi treatment, henceforth) (Figure 3.1A). SH-4-54 successfully blocks the phosphorylation of STAT3's tyrosine 705 residue in Ascl1-overexpressing MG and was not found to be toxic at the concentrations used for this study (Figure 3.2). As previously described, ANT treatment resulted in GFP+ MG-derived neurons that expressed bipolar neuron genes Otx2 and Cabp5, in addition to many MG that failed to undergo neurogenesis (Figure 3.1B). When the STAT pathway inhibitor was co-injected with the TSA (ANTSi treatment), there was a striking increase in the number of MG-derived neurons (Figure 3.1C, 3.1D). Quantification of the mature bipolar gene Cabp5 revealed a more than two-fold increase in the number of MG-derived neurons (24 ± 5% and 52 ± 3%, n = 6 and n = 8, for ANT and ANTSi treatments, respectively; Figure 3.1E-F). All Cabp5+ GFP+ cells also expressed Otx2 and all Cabp5+ cells had neuronal morphology; however, not all Otx2+ cells expressed Cabp5 or had neuronal morphology, as previously described[106].

To determine whether the MG-derived neurons arise from mitotic proliferation or directly differentiate into neurons we intravitreally co-injected EdU with the NMDA on treatment day 8 and also with the TSA and STATi on treatment day 10 (Figure 3.1G). Additionally, we performed twice daily IP injections of EdU from treatment day 9 through 12. After collecting the retinas on treatment day 26, we found that many of the MG and MG-derived neurons were labeled with EdU (Figure 3.1H). Additionally, most of the MG-derived neurons labeled with EdU, and Cabp5, and had neuronal morphology (Figure 3.1I, orange arrows). These results show that many of the new neurons regenerated in the ANTSi condition are the result of mitotic proliferation of the MG. We found that approximately 53% of GFP+ cells in the ANTSi condition were co-labeled with EdU.

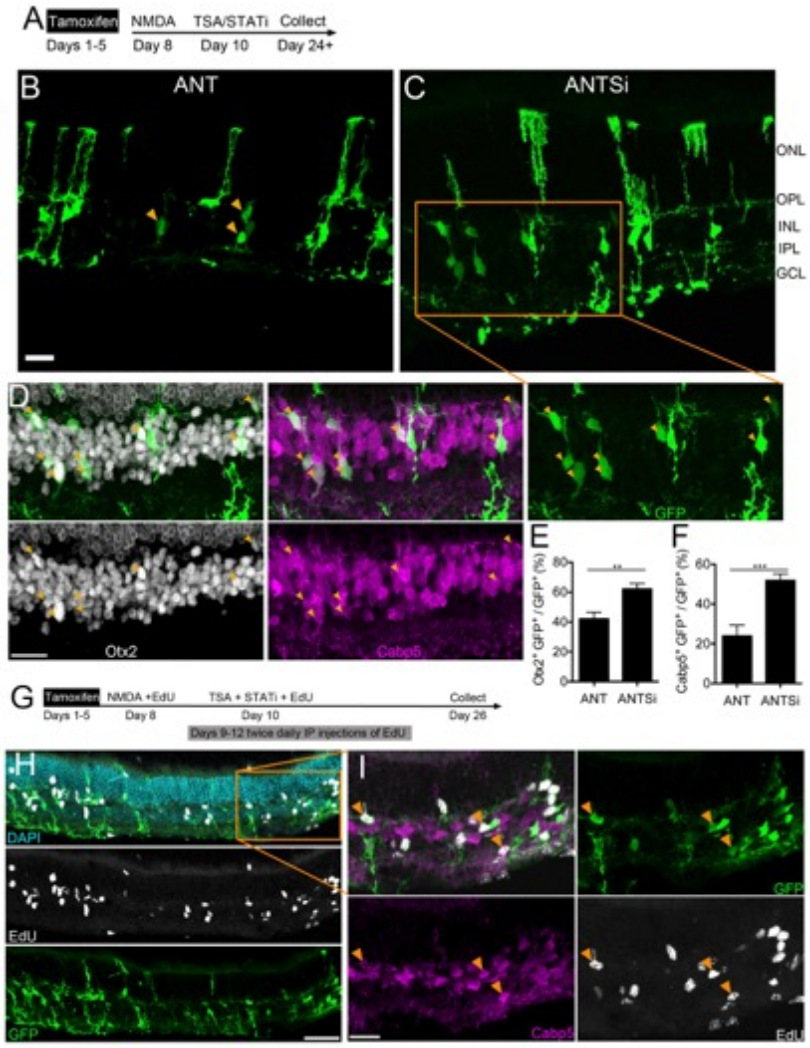

Figure 3.1: STAT pathway inhibition increases number of Müller glial-derived neurons. **A)** Experimental paradigm for increasing MG-derived regeneration efficiency. Tamoxifen is administered for up to 5 consecutive days, followed by NMDA damage a few days after tamoxifen, followed by administration of TSA and/or STAT inhibition a couple days after damage. Retinas were collected a minimum of two weeks after TSA/STATi. **B)** Representative image showing ANT-treated adult retina with MG-derived neurons. **C)** Representative image showing ANTSi-treated adult retina with increased number of MG-derived neurons. **D)** Shows enlargement of ANTSi-treated retinas from **C**. Orange arrows indicate Cabp5+ Otx2+ GFP+ cells. All images are flattened Z-stacks. Scale bars for **B-C** are 20 µm. ONL = Outer Nuclear Layer, OPL = Outer Plexiform Layer, INL = Inner Nuclear Layer, IPL = Inner Plexiform Layer, GCL = Ganglion Cell Layer. **E)** Quantification of Otx2 in ANT (n = 16) and ANTSi-treated (n = 13) retinas. **F)** Quantification of Cabp5 in ANT (n = 6) and ANTSi-treated (n = 8) retinas. ANT vs ANTSi treatments in **E** and **F** were significantly different by unpaired *t*-test at **P=0.0023 and ***P=0.0006, respectively. **G)** Experimental paradigm for testing where ANTSi-treated MG proliferate prior to neurogenesis. **H)** Representative image from proliferation experiment showing EdU and GFP colocalization. **I)** Shows enlargement of **H** and highlights GFP+ EdU+ Cabp5+ MG-derived neurons (orange arrows). Scale bars for **H-I** are 50 µm and 20 µm, respectively.

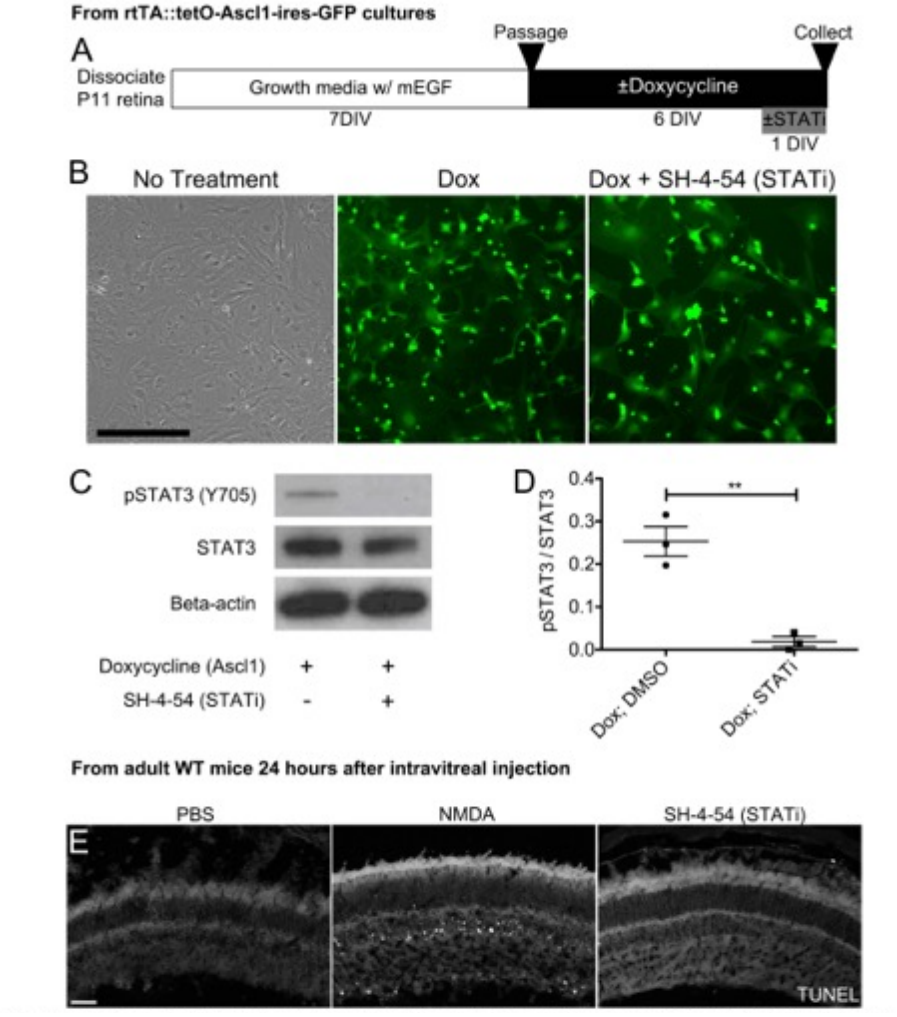

Figure 3.2: STAT inhibitor SH-4-54 inhibits pSTAT3 in MG. **A)** Experimental paradigm for analyzing STAT3 phosphorylation by western blot in MG. P11 retinas were dissociated and grown in a growth media containing mEGF for 7 DIV. MG were passaged to eliminate residual neurons and cultured in a media containing doxycycline to induce Ascl1 expression for 6 DIV. On the sixth day, the STATi SH-4-54 was added then cells were harvested 24 hours later for WB. **B)** Representative images from confluent cultures of non-treated, Dox-treated, and Dox + STATi-treated MG just before harvesting. **C)** Representative western blot for pSTAT3 (Y705), STAT3, and Beta-actin on non-treated, Dox-treated, and Dox+ STATi-treated MG cultures. **D)** Graph showing quantification of western blot bands was significantly different by One- way ANOVA with Tukey's post-test, *P < 0.05, ***P < 0.0001. **E)** Representative image of WT retinas in- jected with either PBS, NMDA, or SH-4-54 and collected 24 hours later for TUNEL staining. Scale bars for **B** and **E** are 25 and 40 μm, respectively.

ANTSi treated MG-derived neurons make synaptic connections with existing circuitry

In our previous study, we found that MG-derived neurons generated by ANT treatment express synaptic proteins, make connections with cone terminals, and successfully integrate into the existing retinal circuitry and functionally respond to light stimuli[106]. In this study, we found that similar to ANT-treated neurons, ANTSi-treated MG-derived neurons express synapse proteins Ctbp2 and Psd95. Labeling retinal sections from the ANTSi treatment group for cone blue opsin (Opn1sw) showed MG-derived neurons contacting cone photoreceptors terminals in the OPL, indicative of photoreceptor-bipolar network connections (Figure 3.3A-C).

To determine if ANTSi-treated MG-derived neurons express synaptic proteins in the correct cellular locations and form synaptic specializations with other cell types, we stained for Ctbp2 and Psd95 (Figure 3.3D-G). In the OPL, we found Psd95+ Ctbp2+ photoreceptor synapses onto MG-derived neuron processes, indicative of a photoreceptor-to-MG-derived neuron synaptic specialization. Interestingly, we also found these contacts in the ONL (Figure 3.3D-E) with photoreceptors synapsing onto the apical process of MG-derived neurons. This irregular location for photoreceptor synapse formation is likely due to the retraction of photoreceptor terminals[113]. In the IPL, we found Ctbp2 puncta within the MG-derived neuron terminals (Figure 3.3F-G). Pre-synaptic Ctbp2 within the MG-derived neurons was directly apposed to Psd95 from post-synaptic cell partners, indicative of a MG-derived neuron output onto other neurons in the IPL (Figure 3.3G). Our data suggest that MG-derived neurons make synaptic specializations with photoreceptors in the OPL and post-synaptic cells in the IPL, consistent with our previous findings that MG-derived neurons are able to make synaptic connections within the existing retinal circuitry.

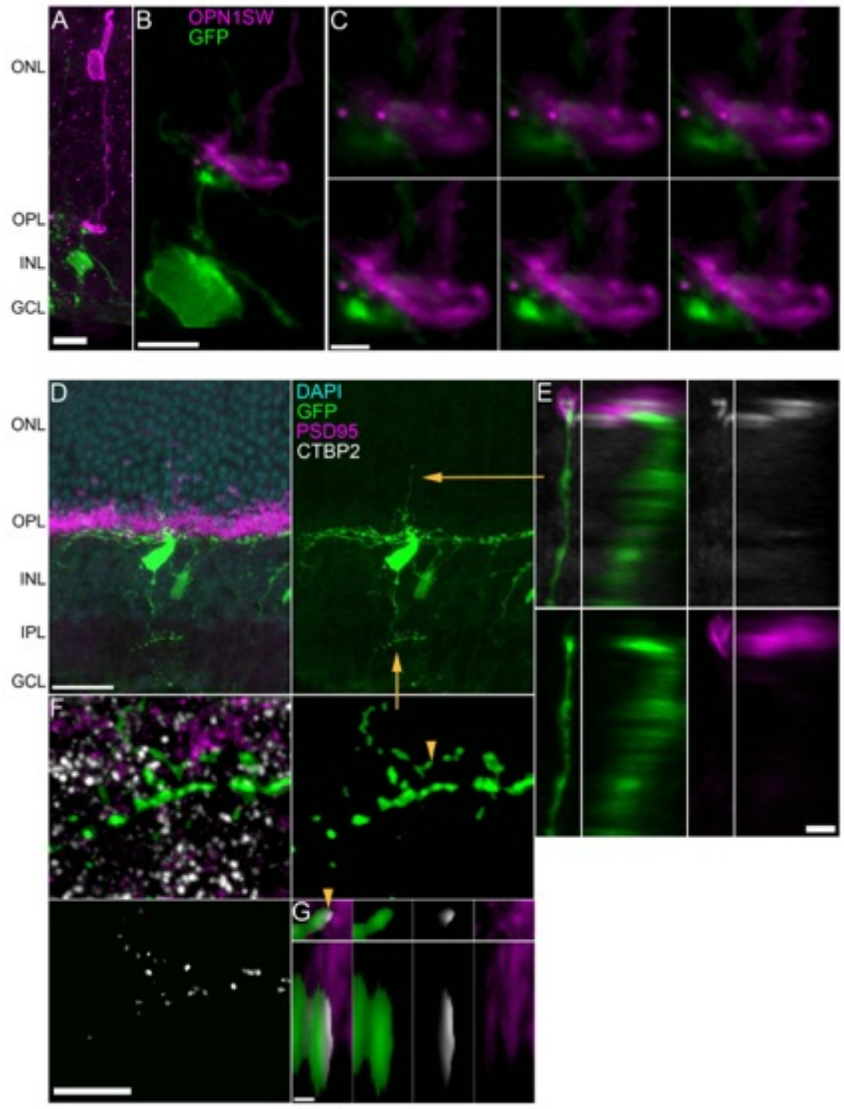

Figure 3.3: ANTSi-treated MG-derived neurons integrate into existing retinal circuits. **A and B)** Example images of MG-derived neuron (green) contacting cone photoreceptors (magenta) in the OPL, scale bars are 10 µm and 5 µm, respectively. **C)** Enlargement of **B** showing 0.18 µm z-stack steps of the MG-derived neurons making contact with cone pedicle, scale bar is 2 µm. **D)** Example image of MG-derived neuron with neuronal process in OPL and IPL, scale bar is 20 µm. **E)** Enlargement of yellow arrow from **D** showing a Psd95+ Ctbp2+ photoreceptor synapse onto an apical MG-derived neuronal process in ONL. Left image sets show XY projection and right image sets show YZ projection, scale bar is 2 µm. **F)** Enlargement of yellow arrow from **D** showing Ctbp2 staining within the MG-derived neuronal processes in IPL. Upper right image shows stringent GFP mask used to identify Ctbp2 puncta within MG-derived neurons, scale bar is 5 µm. **G)** Enlargement of yellow arrowhead from **F** showing Ctbp2 within masked GFP process, directly apposed to Psd95 staining, consistent with synaptic specializations. Upper image sets show XY projection and lower image sets show XZ projection, scale bar is 0.5 µm.

Single-cell RNA-seq on reprogrammed Müller glia

To further characterize the effects of STAT inhibition during MG reprogramming, we ran single-cell RNA-seq (scRNA-seq) on FACS-purified MG and MG-derived cells 14 days after ANTSi treatment, similar to that described in an earlier study[106]. In total 648, 823, and 2283 cells were analyzed from WT, ANT, and ANTSi treatments, respectively. All three (WT, ANT, and ANTSi) datasets were combined, normalized, scaled and analyzed in R with Seurat and Monocle[114-116]. Projecting all three treatments onto a single tSNE plot shows ten distinct clusters (Figure 3.4A), differentially associated with the different treatment conditions (Figure 3.4C). We identified the cell types comprising the clusters by their unique expression of specific known marker genes. Some of these genes are shown projected onto the individual clusters (Figure 3.4B) and additional genes are shown associated with the clusters as a heatmap (Figure 3.4F). For example, Clusters 3 and 4 were comprised of cells almost exclusively from the untreated (WT) condition and expressed genes normally present in MG, such as Glul and Aqp4; these were classified as "MG" clusters (Figure 3.4D). Clusters 0 and 2 showed enrichment for progenitor genes (Dll1; Figure 3.4B) but lacked neuronal gene expression (Otx2 and Cabp5) and showed reduced glial gene expression (Glul). We therefore classified clusters 0 and 2 as "Progenitor-like" cells. Clusters 1 and 6 showed enrichment for neuronal genes and greatly reduced expression of glial genes and were classified as "MG-derived Neurons". In addition to these major clusters, there were two contaminating cell populations that we do not think were derived from MG. These include microglial cells, identified by their expression of Aif1 (IBA1), and a small number of cells that express Rho and other photoreceptor genes that we consider contaminating "Rods". These two populations are present in the FACS-purified cells regardless

of treatment group, whereas the progenitor-like cells and MG-derived neurons are only present in the ANT and ANTSi conditions (Figure 3.4C-D). Clusters 8 and 9 contained a small number of cells and were not enriched for any particular retinal cell type (Figure 3.4D; “Other”).

The immunofluorescent analysis of retinas from the ANTSi condition indicated that a greater percentage of progenitor-like cells differentiate into neurons when compared with the ANT treatment. We analyzed the scRNA-seq results to determine whether a similar trend could be detected. Quantifying the number of WT, ANT, and ANTSi cells in the MG, progenitor-like, or MG-derived neuron clusters (Figure 3.4E) revealed nearly double the number of MG-derived neurons in the ANTSi treatment compared to ANT (29% of total ANTSi cells vs. 16% of total ANT cells). The increase in the MG-derived neuron population in the ANTSi treatment was accompanied by a decrease in the number of progenitor-like cells. These data support the immunofluorescent analysis that STAT inhibition results in a population shift of MG from progenitor-like cells to MG-derived neurons and doubles reprogramming efficacy.

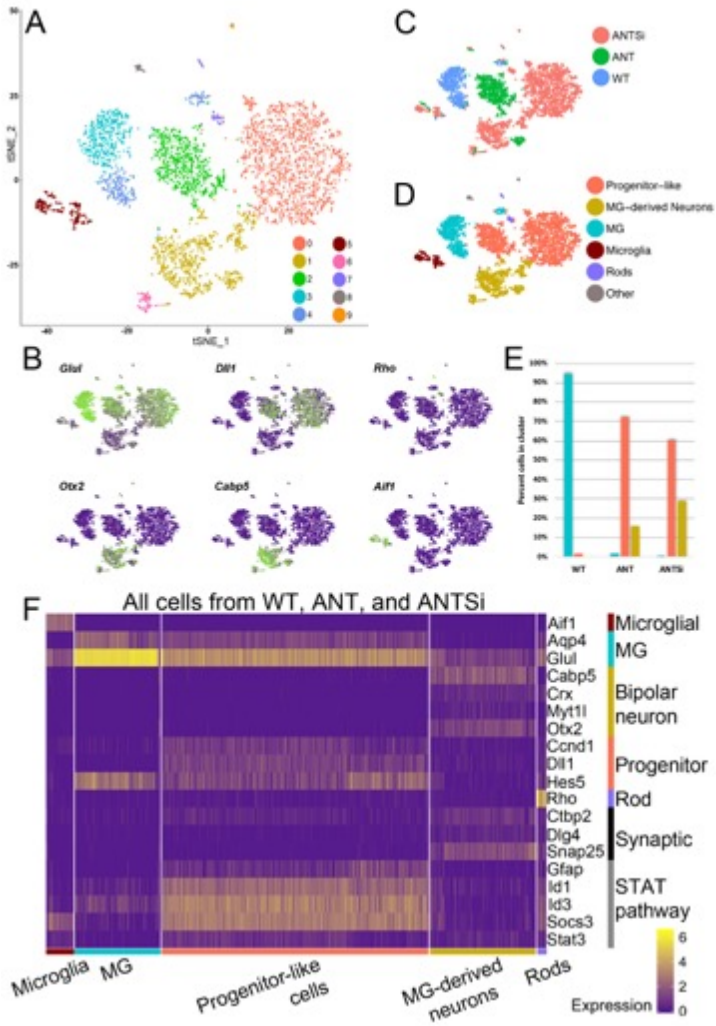

Figure 3.4: ANTSi treatment results in more MG-derived neurons by scRNA-seq. **A)** A tSNE plot of FACS-purified WT MG and ANT-treated cells from out previous study[106], and ANTSi-treated cells. **B)** Feature plots of glial (Glul), progenitor (Dll1), neuronal (Cabp5 and Otx2), rod (Rho), and microglial (Aif1) gene expression to identify clusters by cell type. Green shows high-expressing, purple shows non-expressing cells. **C)** Plot from **A** colored by treatment condition. **D)** Clusters pseudo colored by cell type as determined by **C**. Microglia and rods made up contaminating populations of ~5% and 2% of the total cells in each treatment group, respectively. **E)** Graph showing the fraction of each treatment that was comprised of MG, Progenitor-like cells, and MG-derived neurons. ANTSi treatment increases the population of MG-derived neurons and decreases the number of progenitor-like cells relative to ANT treatment. **F)** Heatmap showing all cells from all three treatments. MG-derived neurons express synaptic genes and do not express Stat pathway targets. Progenitor-like cells highly express Stat pathway targets. Scale shows log2 expression.

To better understand the trajectory of the reprogramming process, we used the Monocle analysis package on a subset of the data that only included MG, progenitor-like cells, and MG-

derived neurons from clusters 0, 1, 2, 3, 4, and 6 (Figure 3.5A). We found the pseudotime scale tracked with our classified cell types, with MG being the root state and transitioning through the progenitor-like cell state and eventually progressing towards MG-derived neurons (Figure 3.5B). We observed cells decreasing expression of glial genes (e.g. Glul) as they progress towards progenitor-like cells and MG-derived neurons (Figures 3.5C-D). Cells in the progenitor-like clusters exclusively express progenitor genes, such as Dll1 and as cells move towards the MG-derived neuronal clusters they upregulate neuronal genes, like Cabp5.

Although the trajectory analysis shows that MG progress to neurons through a progenitor-like state, it also suggests that this state is not identical in the ANT and ANTSi conditions. The progenitor-like cells in these two conditions cluster separately and although both clusters express progenitor genes, like Dll1, the pseudotime plot suggests ANT reprogrammed cells are "closer" to MG than the cells from the ANTSi treated retinas. This led us to hypothesize that progenitor cells may be kept in a stable, but non-neural state, by STAT pathway activation. Indeed, the progenitor-like cells highly express various STAT pathway target genes (e.g. Gfap, Id1, Id3, Socs3, Figure 3.4F), while MG and MG-derived neurons have reduced or no expression of STAT targets.

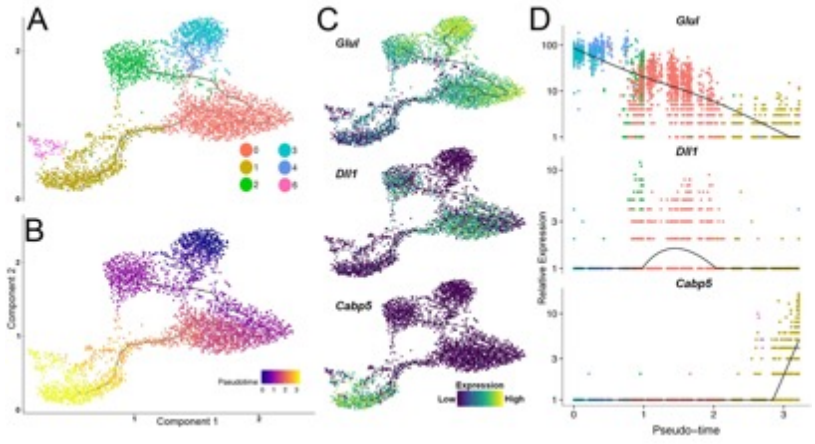

Figure 3.5: Pseudotime analysis of scRNA-seq datasets. **A)** Trajectory analysis in Monocle showing clusters from subset of data that includes MG, Progenitor-like cells, and MG-derived neurons. **B)** Trajectory analysis showing pseudotime progression, with cluster 3 (from **A**) being the root state. **C, D)** Gene expression of Glul, Dll1, and Cabp5 shown as trajectory plot **C**, and pseudotime plot **D**.

ChIP-seq for Ascl1 in P0 mouse retinal progenitors and reprogrammed Müller glia

To explore potential mechanisms by which STAT inhibition promotes Ascl1-mediated retinal regeneration, we carried out ChIP-seq for Ascl1 in MG and compared this with retinal progenitors. In order to determine the endogenous binding pattern of Ascl1 in retinal progenitor cells on a genome-wide scale, we performed ChIP-seq for Ascl1 in P0 retina (Figure 3.6A) and identified 22,251 peaks using HOMER [117] with a False Discovery Rate (FDR) of 0.1%. The top-scoring motif in these peaks (using MEME) was the canonical Ascl1 E-Box[76]. The great majority of the Ascl1 peaks overlapped with an accessible chromatin region (Figure 3.6; P0 DNase Track)[118]. We compared the retinal Ascl1 peaks to previous ChIP-seq for Ascl1 in other neural tissues. For this analysis, we focused on the highest scoring peaks that replicated in two independent P0 retinal Ascl1-ChIP-seq runs (7587 sites, Figure 3.6A). When the three-different neural Ascl1-ChIP-seq datasets were compared, we found that the majority of the Ascl1-bound regions in each type of neural tissue were unique to that tissue (Figure 3.6B); for the peaks present in retina and another neural tissue, there was approximately the same degree of overlap for each of the combinations, while only a relatively small subset of peaks were common to all neural tissues (764; Figure 3.6A-B; Core Ascl1 track). Gene Ontology analysis using the GREAT algorithm[89] showed that those peaks unique to retina were enriched for eye, optic and retinal GO terms (for mouse phenotype), while those regions common to all three neural tissues instead have enrichment for GO terms of non-retinal neural tissues (e.g. telencephalon; Figure

3.6B). In addition, the genes associated with these GO terms for the retinal-specific regions were genes expressed more highly in retina than in other regions of the CNS, like cerebral cortex or spinal cord (e.g. Rax, Six3, Atoh7, Otx2; Figure 3.6B), while those genes associated with the Ascl1-bound regions common to all three neural tissues were potentially representative of a more generic neural program of differentiation (Notch1, Insm1, and Dll1), though it is important to note that there are also region-specific regulatory sites for common targets, like Hes5 and Sox2.

To determine the extent to which Ascl1 binds to similar regions in MG as in retinal progenitors, we performed ChIP-seq for Ascl1 in MG during the reprogramming process. Retinas from P12 mice (germline-rtTA: *tetO*-Ascl1) were dissociated and the MG were grown in culture. After 7 days, Ascl1 expression was induced in the purified MG by addition of doxycycline to the culture medium. Chromatin was then collected after 6 days post-Ascl1 induction and subsequently processed for Ascl1 ChIP-seq. The subsequent sequencing reads were filtered and mapped to the mouse genome (Figure 3.6C) and peaks called using HOMER. In total, 47,507 peaks were called with a False Discovery Rate (FDR) of 0.1%; MEME analysis shows that the top-scoring motif was the canonical Ascl1 E-Box, similar to that described above for the P0 retina.

We performed a binding site overlap analysis between the peaks from the two cell populations. As shown in Figure 3.6E, 31% (14,578/47,507) of Ascl1 binding regions in MG overlap an 'appropriate' Ascl1 binding site (i.e. one present in P0 retinal progenitor cells); however, the majority (~70%) of the Ascl1 bound regions in MG are not present in the P0 retina. This discrepancy is not simply due to the higher number of binding sites in the MG, since 34% (7,673/22,251) of retinal progenitor Ascl1 binding sites are not bound in the MG. Therefore, although the majority of P0 retinal progenitor Ascl1 bound regions are also bound by Ascl1 in

MG, there is substantial binding of Ascl1 to "inappropriate" sites in the genome of MG. In addition, there are also many potential cis-regulatory sites in progenitors that are not bound in the MG.

When we further analyzed the Ascl1 binding sites that are specific to retinal progenitors and compared them with those bound in the MG using the 'GREAT' gene ontology algorithm, the majority of top enriched terms related to neurogenesis (e.g. – 'neural retina development', 'layer formation in cerebral cortex'), suggesting that these Ascl1 binding sites are important for normal neuronal development of the retina and not dispensable binding events. Ascl1 binding sites that occurred in both progenitors and MG were enriched for neurogenic and gliogenic terms (e.g. – 'negative regulation of gliogenesis', 'negative regulation of oligodendrocyte differentiation'). However, the majority of Ascl1 binding sites specific to MG were not associated with retinal development (e.g. – 'filopodium assembly', 'regulation of mitochondrial membrane permeability'). Therefore, while Ascl1 binds 66% of all appropriate sites in retinal progenitors, the majority of binding sites in MG are inappropriate and potentially not productive towards neurogenic reprogramming.

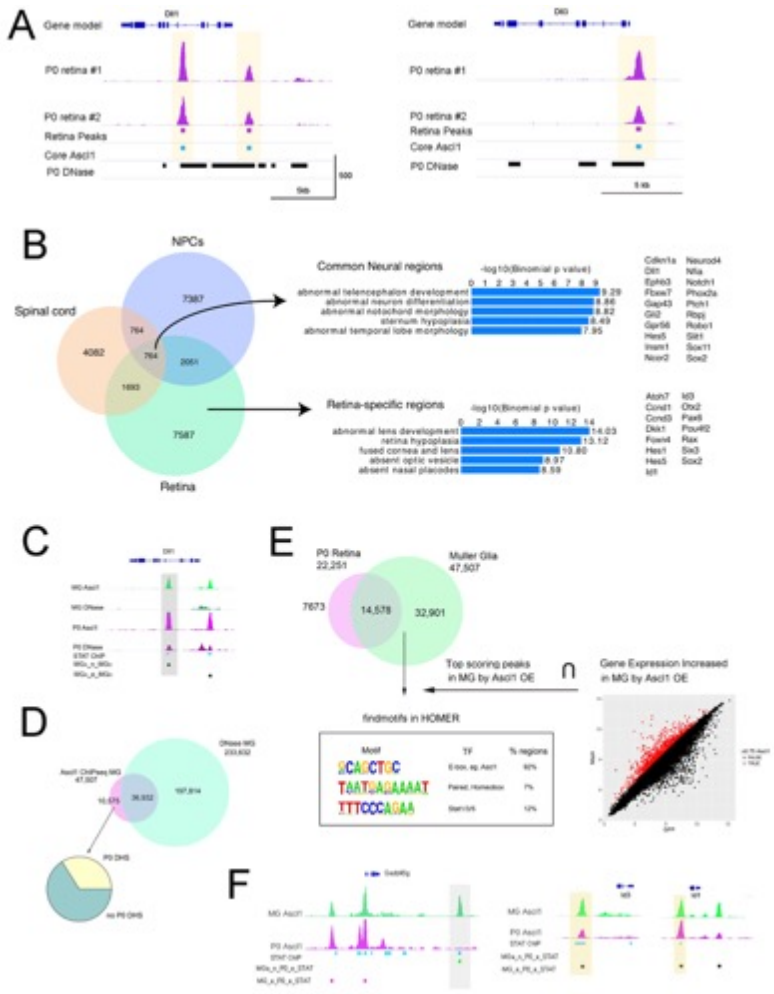

Figure 3.6: Ascl1 ChIP-seq from Ascl1-overexpressing MG and P0 retinal progenitors. **A)** Epigenetic analyses of progenitor genes Dll1 and Dll3. Tracks show biological replicate Ascl1 ChIP-seq peaks from P0 whole retina (P0 retina #1, #2), bars indicate peaks that were called from peak-calling algorithm HOMER with FDR of 0.1% (Retina Peaks track), peaks that were called from retinal, spinal cord, and NPC Ascl1 ChIP-seq datasets (Core Ascl1 track), and DNase-seq peaks from P0 whole retina showing accessible chromatin (P0 DNase track). Yellow highlights indicate core/common binding sites. Scale at the bottom track (X-axis = kilobases of genomic DNA, Y-axis = reads per million, RPM). **B)** Venn diagram showing proportions of overlap for Ascl1 ChIP-seq peaks between P0 retina, NPCs, and spinal cord (Left). Gene Ontology analysis of retinal-specific and core/common Ascl1 ChIP-seq peaks using GREAT algorithm and example genes in these categories (Right). **C)** Epigenetic comparison of Ascl1-overexpressing MG (MG Ascl1 and MG DNase tracks) with P0 developing retina (P0 Ascl1 and P0 DNase tracks). Additional tracks showing previously described Stat3 ChIP-seq peaks from brain oligodendrocytes (STAT ChIP) and comparative peak overlap analyses of Ascl1 peaks without DHSs ($MG_{A\_n}\_MG_D$) or with DHSs ($MG_{A\_e}\_MG_D$). **D)** Above, Venn diagram showing proportions of overlap of Ascl1 ChIP-seq peaks with DNase-seq peaks from Ascl1-overexpressing MG. Below, Pie chart showing the proportion of Ascl1 ChIP-seq peaks that have a P0 DNase peak present. **E)** Venn diagram showing proportions of overlap from Ascl1 ChIP-seq peaks between P0 developing retina and Ascl1-overexpressing MG (Top). Integrative

analysis looking for motifs that were enriched at Ascl1-overexpressing MG-specific Ascl1 peaks (developmentally inappropriate), are located within ±5kb of the T.S.S., and are associated with 0.75 increase in gene expression (from a previous Ascl1-virus vs GFP-virus microarray). Top scoring motifs meeting these criteria are presented in box (E-box 92%, Paired homebox 7%, Stat1/3/5 12%) (Below). **F)** Epigenetic comparison of Gadd45g, Id1, and Id3 gene loci in Ascl1-overexpressing MG (MG Ascl1) and P0 developing retina (P0 Ascl1). Additional tracks showing previously described Stat3 ChIP-seq peaks (STAT ChIP), and comparative peak overlap analyses of sites containing a MG Ascl1 peak, a P0 Ascl1 peak, and a Stat3 peak ($MG_{A\_e}P0_{\_e}STAT$) or sites containing a MG Ascl1 peak, a Stat3 peak, but no P0 Ascl1 peak ($MG_{A\_n}P0_{\_e}STAT$). Yellow highlights indicate strong Ascl1 binding sites during development and forced Ascl1 expression, Grey highlights indicate anomalies.

Studies in induced pluripotent cell reprogramming have shown that induction of pluripotency genes by Yamanaka factors[119] (Oct4, Sox2, cMyc, and Klf4) is initially limited by the accessible chromatin sites in the somatic cell genome already bound by existing transcription factors[120]. We wondered whether the inappropriate sites bound by Ascl1 in MG are due to opportunistic binding to DNase-Hypersensitive sites (DHSs) that are present in the MG and not in the retinal progenitors. Therefore, we quantified the overlap between Ascl1 ChIP-seq peaks and DHSs that are present in MG. As shown in Figure 3.6D, 78% of Ascl1 binding sites occurred within DNase-hotspots in the MG and 22% occurred within non-hypersensitive chromatin. This result suggests that while most of the binding in MG occurs at sites that are already accessible, between one fifth and one quarter of the Ascl1-bound sites in MG were “pioneered” by Ascl1, consistent with prior results in other cells[121]. We hypothesized that these pioneer Ascl1 binding events in MG were actually occurring at regions of DNase-hypersensitivity in the P0 retina. This scenario would be productive towards the goal of reprogramming the cis-regulatory landscape of MG towards that of retinal progenitors. Therefore, we quantified the overlap between pioneer Ascl1 binding sites in MG and P0 DNase-hotspots (Figure 3.6D). We found that 34% (3591/10,575) of the pioneered sites overlap a P0 DNase-Hotspot. However, a much greater

number, 66% (6984/10,575) of the pioneered sites, do not overlap a DNase-Hotspot in either P0 retina or MG, and thus are potentially non-productive pioneered sites.

The preceding analysis suggests that while a third of Ascl1 pioneering events are productive for reprogramming towards a retinal progenitor state, a majority of pioneering events appear to be unproductive towards reprogramming to the retinal progenitor state. We hypothesized that other transcription factors present in the MG might be collaborating with Ascl1 to direct it to these inappropriate[120]. To determine which factors might be associated with the inappropriate Ascl1 ChIP-seq peaks in MG (i.e. not present in progenitors), we used HOMER to identify sequence motifs enriched in these regions (for genes that increase >0.75 fold in reprogrammed MG, over P0 progenitors from our previous microarray[74]). We found that Ascl1 was the top site followed by a generic homeodomain motif, but these regions were also significantly enriched for the STAT consensus site (Figure 3.6E). Thus, the activation of the STAT pathway in the MG after retinal injury may direct Ascl1 to inappropriate sites on the DNA and thereby reduce its ability to reprogram MG more fully to progenitors/neurons.

Among the most highly upregulated genes in the Ascl1-reprogrammed progenitor-like cells include the Inhibitor of Differentiation genes (Id1, Id2, and Id3). These genes code for proteins that are similar to bHLH transcription factors, like Ascl1, except they lack a DNA-binding domain, and thus can form heterodimers with the bHLH family of transcription factors and prevent their ability to activate transcription[122,123]. The scRNA-seq analysis shows that the Ascl1-overexpressing MG that failed to convert to neurons (and retained RPC-like gene expression) highly expressed Id genes Id1, Id2, and Id3 (Figure 3.4F). Ascl1 ChIP-seq and DNase-seq from both P0 and MG show strong binding sites at accessible chromatin at both Id1 and Id3 promoters (Figure 3.6F). Additionally, a previously generated STAT3 ChIP-seq dataset

from oligodendrocytes in the brain (GEO: GSM2650746) indicated STAT3 binding sites in the same region as the Ascl1 binding sites (STAT ChIP track, Figure 3.6F). Taken together, these findings suggest that STAT pathway activation and/or Ascl1 binding may induce Id gene expression, which inhibits Ascl1 from initiating neurogenesis in a subset of MG.

Id genes are dysregulated in the presence of Ascl1

To determine the effects of Ascl1 overexpression and damage on STAT pathway activation and Id1 expression, we performed a NMDA time course (Figure 3.7A). Under normal conditions, in WT animals Id1 is not present at detectable levels in MG (Figure 3.8A). At 1 day and 2 days post-NMDA, Id1 is highly expressed in MG but begins to decline at 4 days and returns to basal levels by 9 days post-NMDA (Figure 3.8B-F). In the Ascl1-overexpressing mice, all MG express Id1 at similarly high levels by 2 days post-NMDA; both the Ascl1-overexpressing GFP+ MG, and the non-Ascl1-overexpressing GFP- Sox2+ MG (Figure 3.7B). By 4 days post-NMDA damage, Id1 was found to be at lower levels in the GFP- MG and highly expressed in the Ascl1 GFP+ MG (Figure 3.7C). Eleven days after TSA treatment, the GFP+ cells that show signs of neuronal morphology and downregulation of Sox2 have basal levels of Id1 expression (Figure 3.7F, orange arrows). By 14 days post-NMDA damage, high Id1 expression became restricted to the MG that express Ascl1 (the GFP+ MG) (Figure 3.7D). Additionally, we performed RT-qPCR for Id1 on whole retinas taken from undamaged WT and Ascl1 overexpressing retinas as well as NMDA treated retinas (Figure 3.7E, n = 4 mice per group). Ascl1 overexpressing retinas treated with NMDA expressed significantly more Id1 at 4 days post-NMDA than all other treatment groups. Interestingly, the Ascl1-overexpressing retinas

have similar levels of Id1 at baseline as the WT mice treated with NMDA. Taken together, these findings suggest that the normally transiently activated target genes of STAT become constitutively active in the presence of Ascl1 overexpression. Constitutive expression of ID proteins in Ascl1 expressing MG likely results in the ID proteins binding Ascl1, antagonizing the pro-neurogenic effects of Ascl1[122,123]. Further evidence supporting this hypothesis is the fact that ANT-treated MG-derived neurons do not have any detectable Id1 expression (Figure 3.7F, orange arrows), while the adjacent non-reprogrammed MG do have Id1 expression (white arrow).

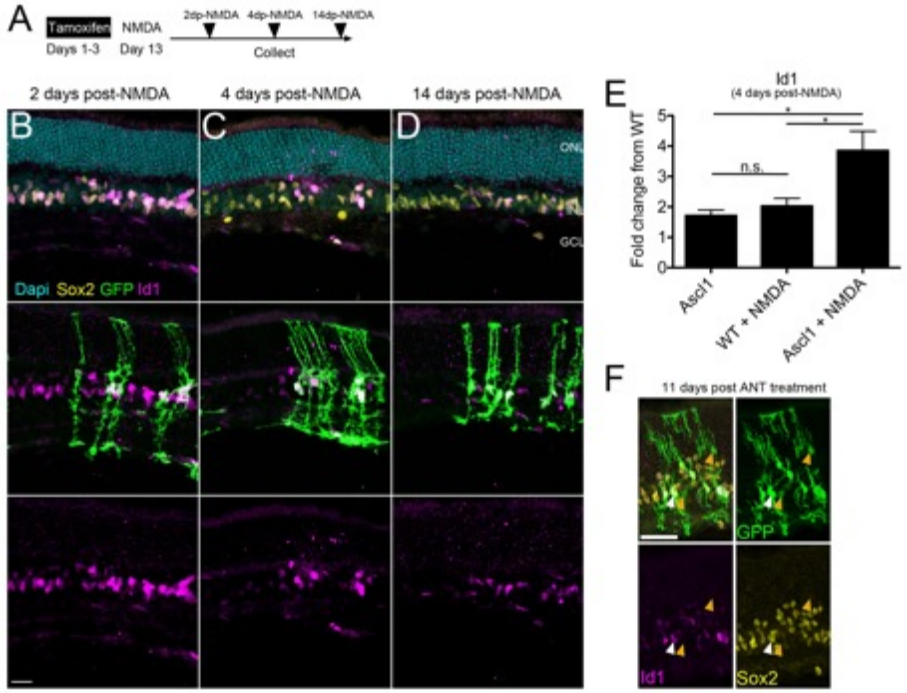

Figure 3.7: Ascl1-overexpression results in dysregulated STAT-target genes. **A)** Experimental paradigm for analyzing STAT-target genes in Ascl1-overexpressing MG. **B)** Both GFP- Sox2+ and Ascl1-expressing GFP+ MG express Id1 2 days after NMDA damage. **C)** Ascl1+ cells have higher expression of Id1 relative to GFP- MG (Sox2+ cells) 4 days after NMDA damage. **D)** Id1 expression is reduced in GFP- MG but remains in the Ascl1-expressing GFP+ MG 14 days after NMDA damage. Note, the flat Id1+ nuclei in all images not labelled with GFP are endothelial cells. Scale bars for **B-D** are 20 μm. **E)** Graph showing RT-qPCR for Id1 gene expression relative to WT on retinas treated 4 days post-NMDA. One-way ANOVA with Tukey's post-test; *P < 0.05, N = 4 biological replicates per condition run in triplicate. **F)** Id1 expression is reduced

in GFP- MG but remains in the Ascl1-expressing GFP+ MG 14 days after ANT treatment (white arrows). MG-derived neurons (orange arrows) do not express Id1. Scale bar is 40 µm.

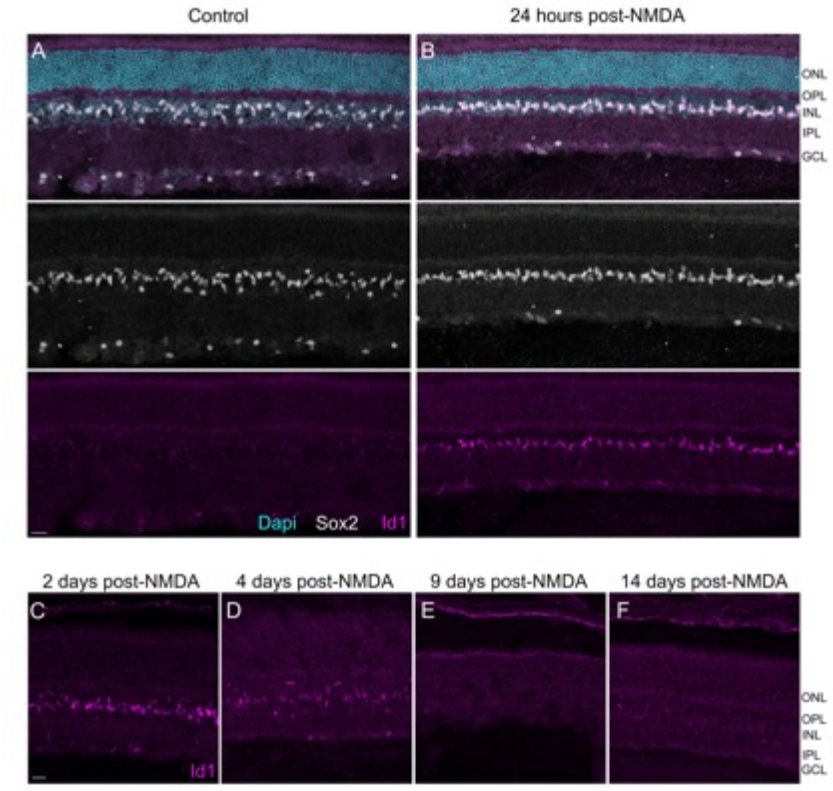

Figure 3.8: Stat pathway is transiently activated during NMDA damage. **A) E**xample image of WT retina stained for MG (Sox2) and Stat pathway activation (Id1). **B)** WT retina 24 hours after NMDA treatment shows Id1 expression in all MG. **C-F)** Id1 expression begins to decrease at 4 days post-NMDA and is undetectable by 9 days. Scale bars are 20 µm.

DISCUSSION

The findings in this report highlight several important features of the reprogramming of glia to neuronal progenitors and neurons. The Ascl1 ChIP-seq and DNase-seq data reveal that the reprogrammed MG show similar Ascl1 binding and chromatin accessibility as the newborn mouse RPCs. However, the reprogrammed MG also have new Ascl1 peaks that are not normally found during development in RPCs, sites we label as "inappropriate." A significant number of

these inappropriate Ascl1 binding sites are found at genes that are not relevant to retinal development and are associated with an increase in expression of these genes in the reprogrammed MG. We further identified a consensus DNA binding motif for STAT3 that was significantly associated with these inappropriate Ascl1 peaks. Potential STAT targets that could underlie the effects we observe, include Id1 and Id3, dominant negative regulators of bHLH gene function. Lastly, this study provides the first evidence combining lineage tracing with EdU-labeling to demonstrate new neurons can arise from proliferating MG in an adult mammal.

One potential target of STAT signaling that could limit the regenerative response in mammalian MG is Id1. Following injury to the retina, the STAT target gene Id1 is transiently expressed in MG, but Id1 returns to basal levels within a week. We found that in Ascl1-overexpressing mice, Id1 expression is maintained in the MG, possibly maintaining the cells in a progenitor-like state and preventing them from generating new neurons. ID proteins are known to form dimers with class I bHLH proteins and inhibit their dimerization with class II bHLH factors to inhibit their transcriptional activation activity[122,123]. Additionally, ID proteins can bind directly with HES proteins to maintain neural progenitors in an undifferentiated state[124-126]. ID proteins have also been shown to play an important role in other organ systems, such as the pancreas, where they can bind Hes1 and participate in the dedifferentiation and fate switching of exocrine cells to endocrine fates[127]. JAK/STAT signaling is known to bias progenitors towards a glial fate in other regions of the nervous system as well[128-130]. For example, inhibition of the JAK/STAT co-receptor gp130 in developing cortical progenitors has been found to increase their neurogenic production at the expense of gliogenesis[131]. Thus, it is possible that STAT activation in astrocytes in other areas of the nervous system may limit their neurogenic potential via ID proteins in a manner similar to that we have described in the retinal MG.

Previous studies have demonstrated the importance of the source cell's epigenetic landscape and presence of endogenous transcription factors of that source cell during reprogramming[120,121]. Fibroblast reprogramming to induced neuronal cells show that the newly generated cell types still retain their source cell signature. We previously found this to be the case in MG reprograming as well[106], where the MG-derived neurons still express low levels of glial genes such as Glul or Aqp4. The present study demonstrates the importance of injury induced STAT pathway activation during reprogramming and shows a successful combinatorial analysis using epigenetic and gene expression datasets to confirm inappropriate transcription factor binding associated with non-productive gene expression.

Chapter 4:

Promoting proliferation and neurogenesis of diverse cell types from Müller glia

INTRODUCTION

In the previous chapters, I was able to show successful reprogramming of MG to retinal neurons in vivo in adult mice. The ANT and ANTSi treatment have thus far resulted in the generation of predominantly bipolar interneurons with a small proportion of amacrine cells being generated. These studies, though foundational to understanding retinal regeneration, have left the field with two critical questions. The first, is how can we promote proliferation of MG in adult mice to increase the absolute number of regenerated neurons? As previously mentioned, the MG comprise 1-3% of all retinal cells, which means even if we convert every MG to a retinal neuron this is only a modest repopulation of newly generated neurons. Ideally, the population of MG could be amplified first by stimulating proliferation followed by reprogramming, resulting in both more MG to maintain the integrity of the retina and more MG-derived neurons to increase the likelihood of vision restoration. The second fundamental question we were left with is how can we promote neurogenesis of diverse cell types besides bipolar interneurons? Few human diseases cause degeneration of retinal interneurons, and instead affect photoreceptor and ganglion cell types, which we have not yet been able to generate. In this chapter, I describe efforts to increase proliferation by adding mitogenic factors to our reprogramming paradigm, as well as efforts to generate more diverse neuronal cell types by studying different damage models or adding additional proneural transcription factors.

RESULTS

Mitogens in combination with Ascl1 increase MG proliferation

To better characterize Ascl1's ability to induce proliferation in the presence or absence of mitogenic factors, I performed various explant experiments. Explants provide a culture system that allows the tissue to be immersed in a treatment of interest for several days, unlike in vivo experiments where the drugs are cleared from the retina within hours. This eliminates the need to establish the narrow windows during which drugs have their effects. The first set of experiments were performed by explanting retinas from P15 mice in Mel's 1% media (see methods) with the addition of 4-OH tamoxifen (1:5000 dilution in media) to induce Ascl1 or GFP expression and EdU (5 ug/mL media) to label proliferating cells. The mitogen mEGF is known to stimulate proliferation of retinal progenitors and MG cells in culture[132-134], and for this reason, I hypothesized that mEGF treatment would stimulate MG proliferation in retinal explants. Thus, retinas were treated with vehicle or mEGF (100 ng/mL media) and cultured for 5 days in vitro (DIV) with media changes every other day, then collected for IHC.

I found that Ascl1 expression alone resulted in an increase in proliferating cells compared to GFP only expressing cells (Figures 4.1A and 4.1C). When mEGF was added to the culture media, I found an increase in proliferating cells in both Ascl1+ and Ascl1- conditions; however, there was a striking increase of proliferation in cells that had both Ascl1 and mEGF treatment over all other treatment conditions (Figures 4.1B and 4.2D). Nearly all GFP+ MG in the Ascl1 + mEGF condition had EdU present, suggesting that Ascl1 may work in concert with the mitogen to induce proliferation. Under normal in vivo conditions the MG do not proliferate, which is why

the findings in Figure 4.1C are interesting and notable. They raised the possibility of stimulating in vivo proliferation by adding mEGF to Ascl1-expressing mice in our reprogramming paradigm.

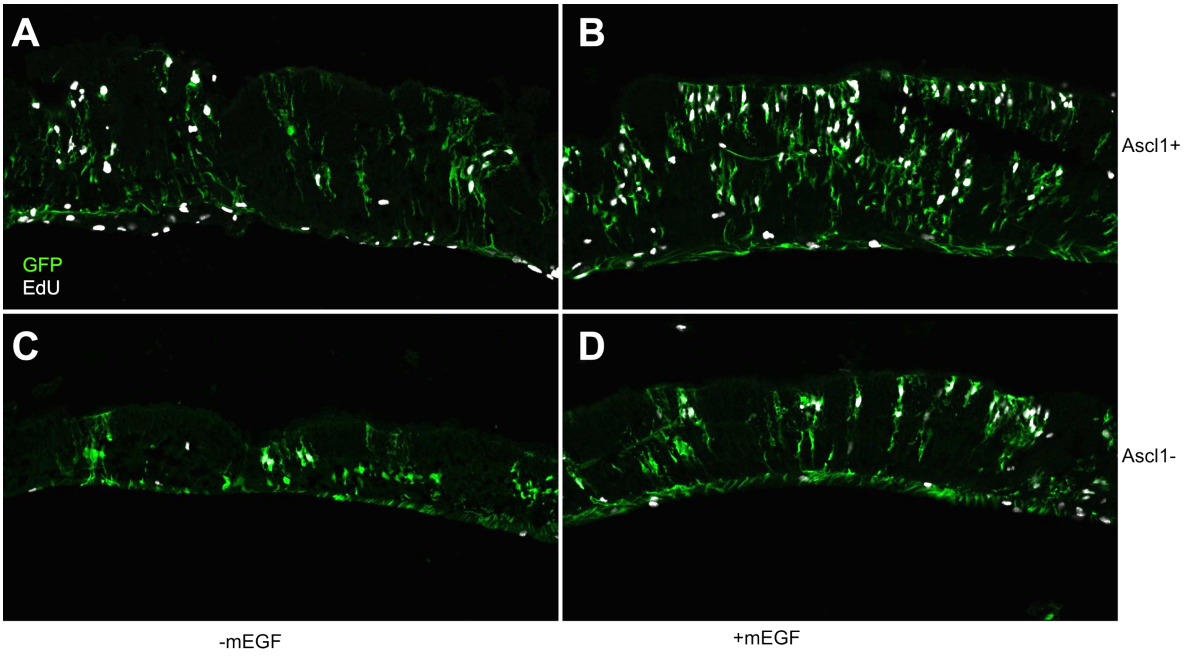

Figure 4.1: Proliferation of P15 MG in explant culture. All images shown were taken from explants after 5 DIV with tamoxifen and EdU. **a**, Image of explanted retina from *Glast*-CreER: Flox-stop-*LNL*-tTA: *tetO*-Ascl1-ires-GFP mouse treated with tamoxifen. **b**, Image of explanted retina from *Glast*-CreER: Flox-stop-*LNL*-tTA: *tetO*-Ascl1-ires-GFP mouse treated with tamoxifen and mEGF. **c**, Image of explanted retina from *Glast*-CreER: Flox-stop-*LNL*-tTA: Flox-stop-*CC*-GFP mouse treated with tamoxifen. **d**, Image of explanted retina from *Glast*-CreER: Flox-stop-*LNL*-tTA: Flox-stop-*CC*-GFP mouse treated with tamoxifen and mEGF. Green shows GFP, white shows EdU.

Previous studies have shown mouse strain-specific differences in the amount of proliferation that can be observed in MG[135]. Our *Glast*-CreER: Flox-stop-*LNL*-tTA: *tetO*-Ascl1-ires-GFP mice that are used for Ascl1 overexpression come from a mixed mouse background that is not directly comparable to any one background strain. In an effort to quantify the basal levels of proliferating MG in our culture system and our Ascl1 mice, I performed another set of explant proliferation studies in adult mice (>P30) from WT C57BL/6 background mice and from our Ascl1 background mice. Retinas were cultured in Mel's 1% media with EdU (5 ug/mL

media) and collected at 2, 4, 6, or 8 DIV with media changes every other day. No tamoxifen was given in this experiment, as the goal was to measure basal levels, not Ascl1-induced levels of proliferation. Retinas were then fixed, sectioned, and stained for EdU and Sox9 to quantify the number of proliferating MG (Sox9 expressing cells).

After explanting at least 4 retinas per condition and timepoint, I found no significant differences between the WT C57BL/6 background and Ascl1 background at the same collection time (Figure 4.2). The significantly different Bonferroni pairwise comparisons are shown by one-way ANOVA. Both strain backgrounds plateau by 8 DIV with around 20% of the Sox9+ MG proliferating. This data suggests that there are no strain specific differences in the Ascl1 overexpressing MG's ability to proliferate at baseline and serves as a benchmark for determining our ability to push the MG with Ascl1 and other mitogenic factors to divide.

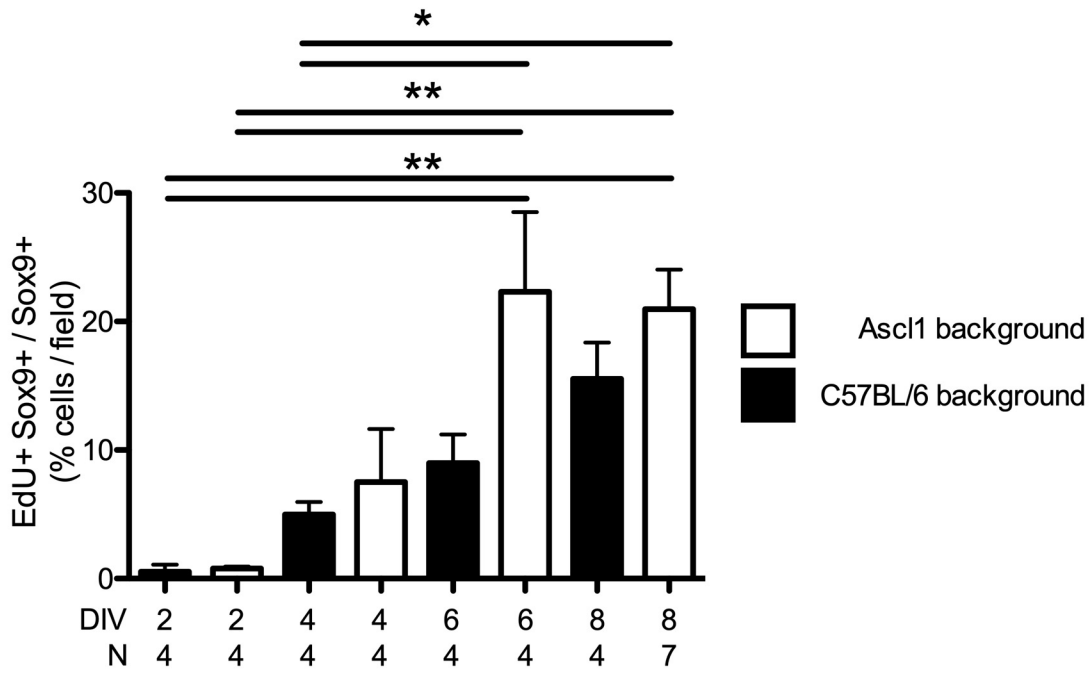

Figure 4.2: Quantification of EdU+ MG in Ascl1 background and C57BL/6 background explants. Retinas were explanted for 2, 4, 6, and 8 DIV with no tamoxifen administration. No significant differences in proliferation were observed between the two background strains at comparable timepoints in vitro. Five images per retina were quantified, with number of retinas shown as N, *P<0.05, **P<0.01, one-way ANOVA with Bonferonni post hoc test.

Next, I decided to test additional mitogens that have been implicated to stimulate MG proliferation, in our explant model[104,136]. Adult retinas (>P60) from our *Glast*-CreER: Flox-stop-*LNL*-tTA: *tetO*-Ascl1-ires-GFP mice were explanted and cultured in Mel's 1% media for 8 DIV with 4-OH tamoxifen (1:5000 dilution) and EdU (5 ug/mL) for the whole duration with media changes occurring every other day. On treatment days 3-4, the explants were treated with TSA, mEGF, the Wnt agonists SC-22416 or CHIR99021, or vehicle. Retinas were then collected, fixed, sectioned, and stained with GFP, EdU, and Sox9 to label proliferating MG.

Similar to my first explant experiments (Figure 4.1), I found Ascl1 alone induced many of the MG to proliferate (Figure 4.3A) and the addition of mEGF resulted in most MG being labeled with EdU (Figure 4.3E). Surprisingly, Ascl1 in combination with the HDAC inhibitor TSA resulted in no EdU labelled MG (Figure 4.3B). In fact, no astrocyte, microglial, or endothelial proliferation was observed either. TSA appeared to completely block proliferation of all cell types in an explant context. Previous studies in cancer models have shown similar anti-proliferative properties of TSA, suggesting that histone deacetylation plays an important role in a cell's ability to divide[137,138]. The addition of Wnt agonists SC-222416 or CHIR99021 resulted in more dividing MG at levels similar to those observed in the mEGF treated condition (Figures 4.3C and 4.3D). Quantification of EdU-labelled MG showed similar levels of proliferation of in Ascl1+ and Ascl1- GFP+ MG at 8 DIV (Figure 4.4, top), in contrasts to our findings from the 5 DIV explants, which showed more proliferation in the Ascl1+ retinas. This suggests that other factors may be stimulating proliferation after a long duration in culture, such as signals from

dying retinal neurons. The addition of a Wnt agonist or mEGF resulted in more EdU-labeled MG compared to the no treatment condition, with mEGF inducing proliferation of more than 90% of the GFP+ MG. Another interesting finding that can be appreciated in both the images and quantification (Figure 4.4, bottom) is that Ascl1 and mEGF led to a greater increase in proliferating GFP+ cells, but Ascl1 and CHIR99021 led to a greater increase in proliferating Sox9+ cells overall. Again, this suggests that mEGF works synergistically with Ascl1, while the Wnt agonist seems to not require Ascl1 (as determined by GFP expression) to induce proliferation of MG. It should be noted that only 2 retinas per condition were used, so statistical tests could not be performed, but the trends I have highlighted were robust across samples.

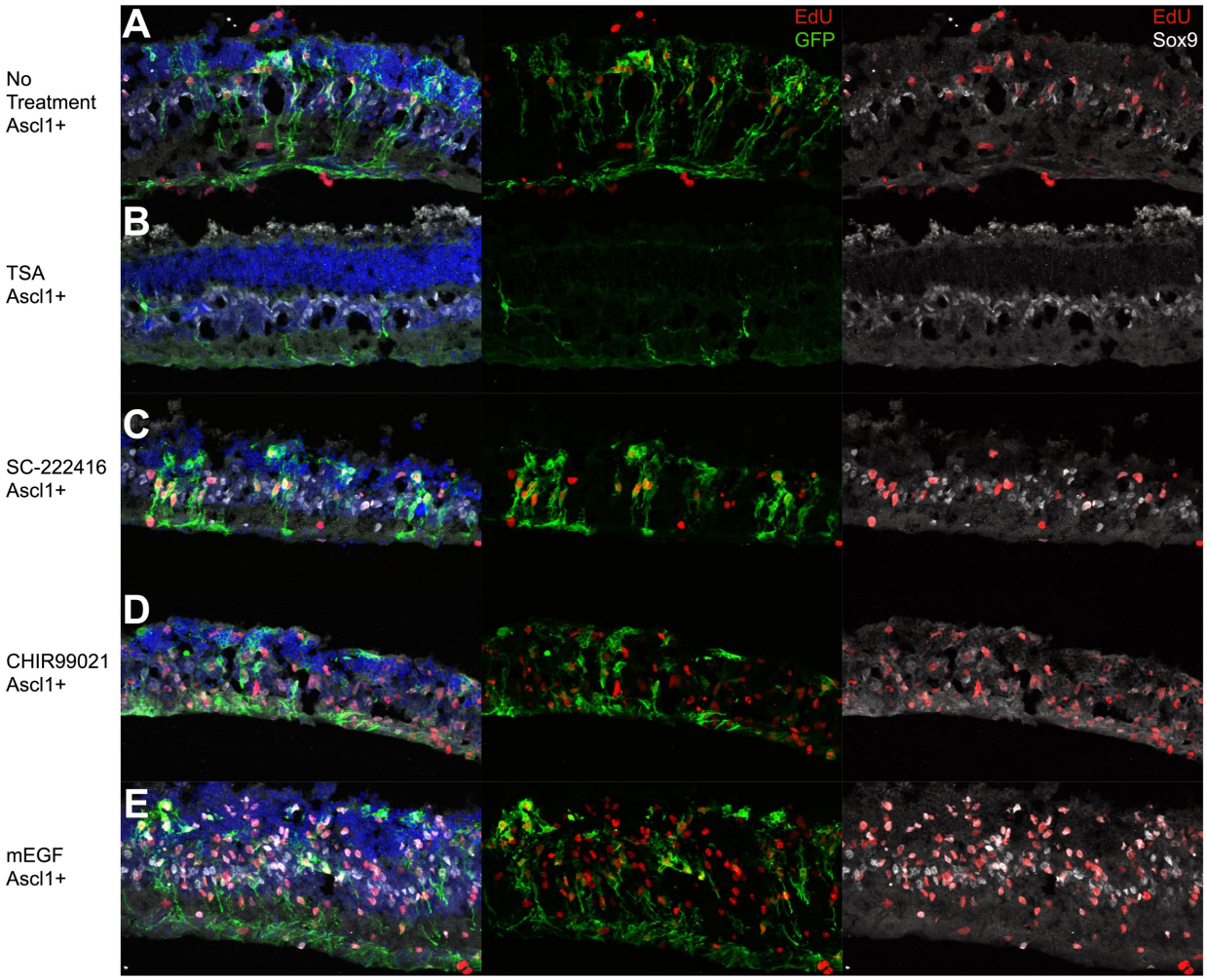

Figure 4.3: Proliferation of adult P60+ MG in explant culture with mitogens. All images shown were taken from explanted *Glast*-CreER: Flox-stop-*LNL*-tTA: *tetO*-Ascl1-ires-GFP mice after 8 DIV with tamoxifen and EdU. Mitogens were administered at 3-4 DIV. **a**, Image of explanted retina treated with tamoxifen. **b**, Image of explanted retina treated with tamoxifen and TSA. **c**, Image of explanted retina treated with tamoxifen and Wnt agonist SC-222416. **c**, Image of explanted retina treated with tamoxifen and Wnt agonist CHIR99021. **d**, Image of explanted retina treated with tamoxifen and mEGF.

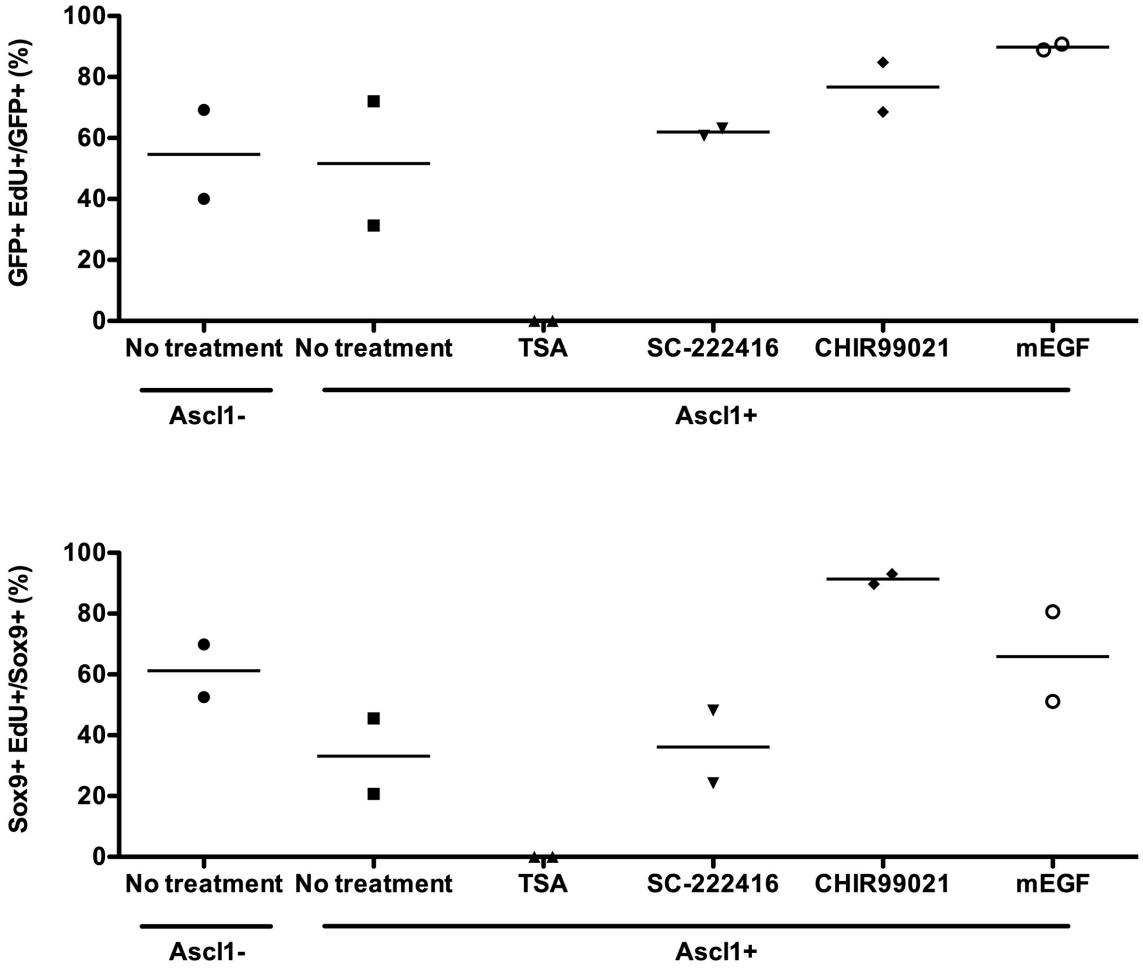

Figure 4.4: Quantification of adult P60+ MG in explant culture with mitogens. **top**, Percent of EdU-labeled GFP+ cells in each treatment condition after 8 DIV. **bottom**, Percent of EdU-labeled Sox9+ cells in each treatment condition after 8 DIV. Five images per retina were quantified, with 2 retinas per condition. Due to small N, statistical tests were not performed.

In vivo, we know that Ascl1 and TSA are sufficient to induce neurogenesis from MG; however, in explants, this combination clearly suppresses the MG's ability to proliferate. To test whether this suppression could be overcome by the addition of a mitogen, I decided to test the Wnt agonists and mEGF in various combinations with Ascl1 and/or TSA. Again, I used the 8 DIV explant paradigm with Wnt agonist or mEGF ± TSA administration on treatment days 3-4. The retinas were collected, fixed, whole-mounted, and stained for EdU to visualize global levels

of proliferation (Figure 4.5). In the absence of Ascl1 and TSA (top row from panel), the Wnt agonists did not appear to increase the level of proliferation over baseline, whereas mEGF had a robust effect (similar to Figures 4.1 and 4.3). Ascl1 expressing retinas in the absence of TSA resulted in more robust proliferation, especially in the CHIR99021 and mEGF treatment conditions. The addition of TSA to both the Ascl1- and Ascl1+ retinas (2nd and 4th row from panel) quenched proliferation in all treatment conditions except the CHIR99021 Wnt agonist treatment. This suggests, that CHIR99021 is able to induce proliferation through Wnt activation in a manner independent from mEGF signaling and is able to circumvent the anti-proliferative effects of TSA accordingly. Interestingly, the other Wnt agonist I tested, SC-222416, was not able to induce proliferation in either the TSA alone condition, or the TSA + Ascl1 treatment. While CHIR99021 activates Wnt signaling by inhibiting GSK-3β, the SC-222416 compound has been shown to activate Wnt signaling through a GSK-3β independent mechanism[139], suggesting that CHIR99021's ability to induce proliferation in the presence of TSA may be acting through the GSK-3β signaling pathway.

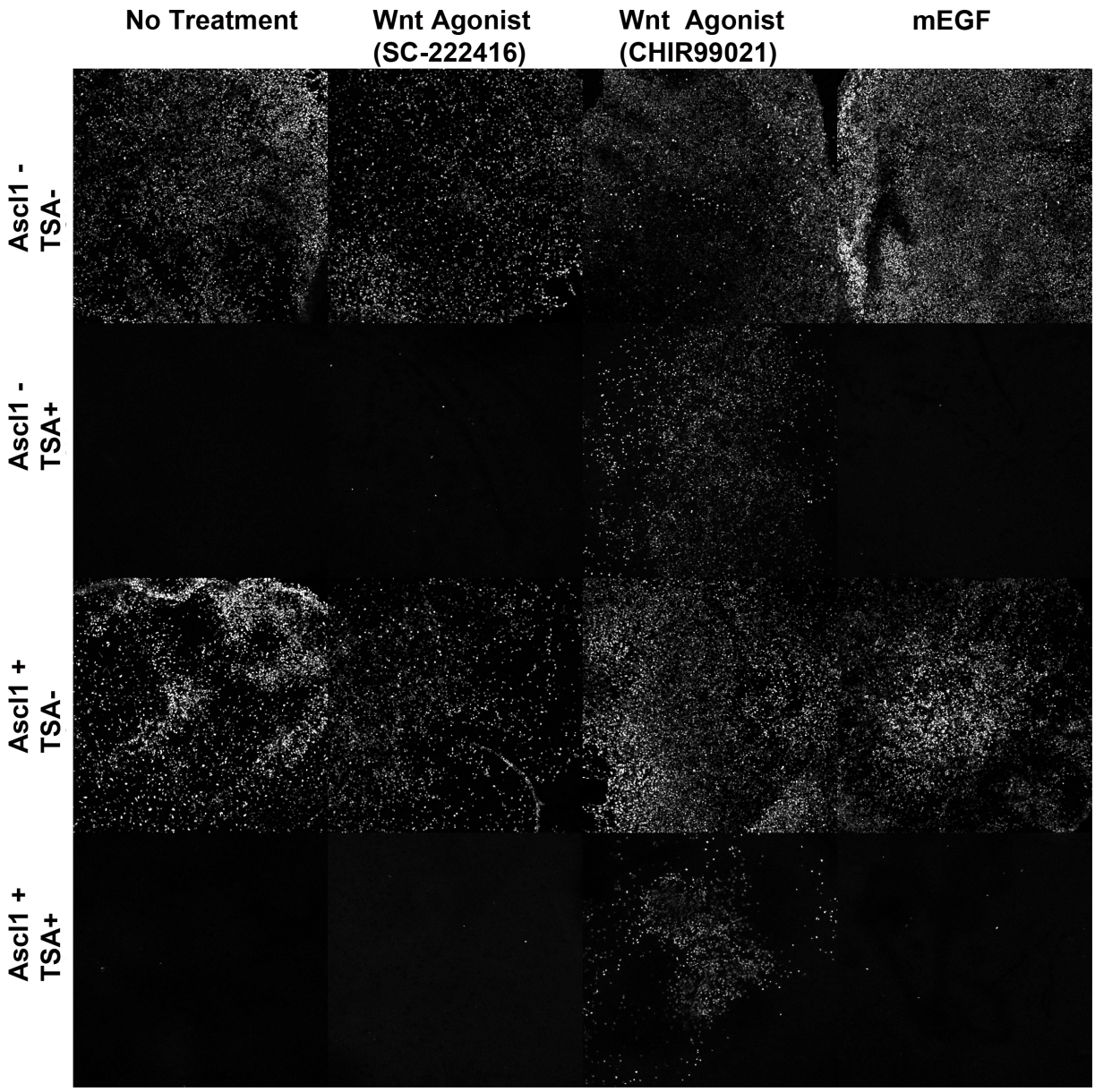

Figure 4.5: Proliferation of adult P60+ MG in explant culture with mitogens ± TSA (whole mount). All images shown were taken from explanted *Glast*-CreER: Flox-stop-*LNL*-tTA: *tetO*-Ascl1-ires-GFP or *Glast*-CreER: Flox-stop-*LNL*-tTA: Flox-stop-*CC*-GFP mice after 8 DIV with tamoxifen and EdU. Mitogens were administered at 3-4 DIV. TSA arrests proliferation in all treatment conditions except CHIR99021.

To assess the effect mitogens have on MG proliferation in vivo in adult mice, I next injected CHIR99021 or mEGF in the ANTSi reprogramming paradigm. I hypothesized that MG would behave in a manner similar to the explant paradigm and would proliferate in the

CHIR99021 condition and fail to proliferate with mEGF, due to the presence of TSA. Mitogens were administered intravitreally at the same time as NMDA on treatment day 8 (Figure 4.6A). EdU was administered during both intravitreal injections in addition to twice daily intraperitoneal injections on treatment days 9-12. Eyes were collected, fixed, sectioned, and stained for GFP and EdU on treatment day 26.

Surprisingly, in an in vivo context, CHIR99021 actually led to less proliferation of MG than did mEGF (Figures 4.6B, 4.6C). Even in the presence of TSA, robust proliferation was observed in the mEGF treatment condition. I have previously shown that TSA robustly increases histone acetylation in vivo up to 24 hours after intravitreal injection, and that acetylation returns to basal levels shortly after. Further experiments are needed to dose response and time course the Wnt agonist, mEGF, and STATi in an in vivo context, but it is likely that the drugs have different half-lives and efficacy in vivo, which is why we see these contradictory responses in vivo. In explant culture experiments (Figure 4.5), the retinas are bathed in the various drugs for two full days and have EdU present the entire 8 DIV, while in vivo, the drugs are cleared from the retina relatively quickly. Additionally, in explants the TSA and mitogens are administered at the same time on treatment days 3-4, whereas in vivo, I administered the mitogens 2 days prior to TSA treatment. Any of these variables may lead to the differences observed between in vivo and explant proliferation responses and subsequent experiments will be needed to fully resolve the effects that timing and dosing of these drugs have on cell division.

Together, these studies indicate that stimulating proliferation of MG in vivo is possible with the addition of mitogenic factors, such as mEGF or Wnt agonists. The most robust effects are seen when mEGF is given to Ascl1 expressing retinas; however, TSA appears to arrest all proliferation in explant models. The Wnt agonist CHIR99021 enables MG proliferation in TSA-

treated explants, possibly through a GSK-3β dependent mechanism, and also leads to robust proliferation of non-Ascl1 expressing, Sox9+ MG. The anti-proliferative effects of TSA were not observed in my ANTSi treatment injection paradigm, with both CHIR99021 and mEGF showed the ability to promote MG proliferation in vivo. Future experiments that test the mitogens' ability to increase the total overall number of MG-derived neurons should be performed to determine if enough new neurons are generated to restore some level of vision in the mice. Quantifying the overall number of GFP+ neurons will likely not be informative due to the fact that Ascl1 and GFP induction is extremely variable from mouse to mouse, and even eye to eye within the same mouse (20-75% of all MG turn on the transgene in a given condition). Instead, a readout of behavioral vision recovery, such as optomotry[140], should be utilized to better characterize the usefulness of mitogens in retinal regeneration.

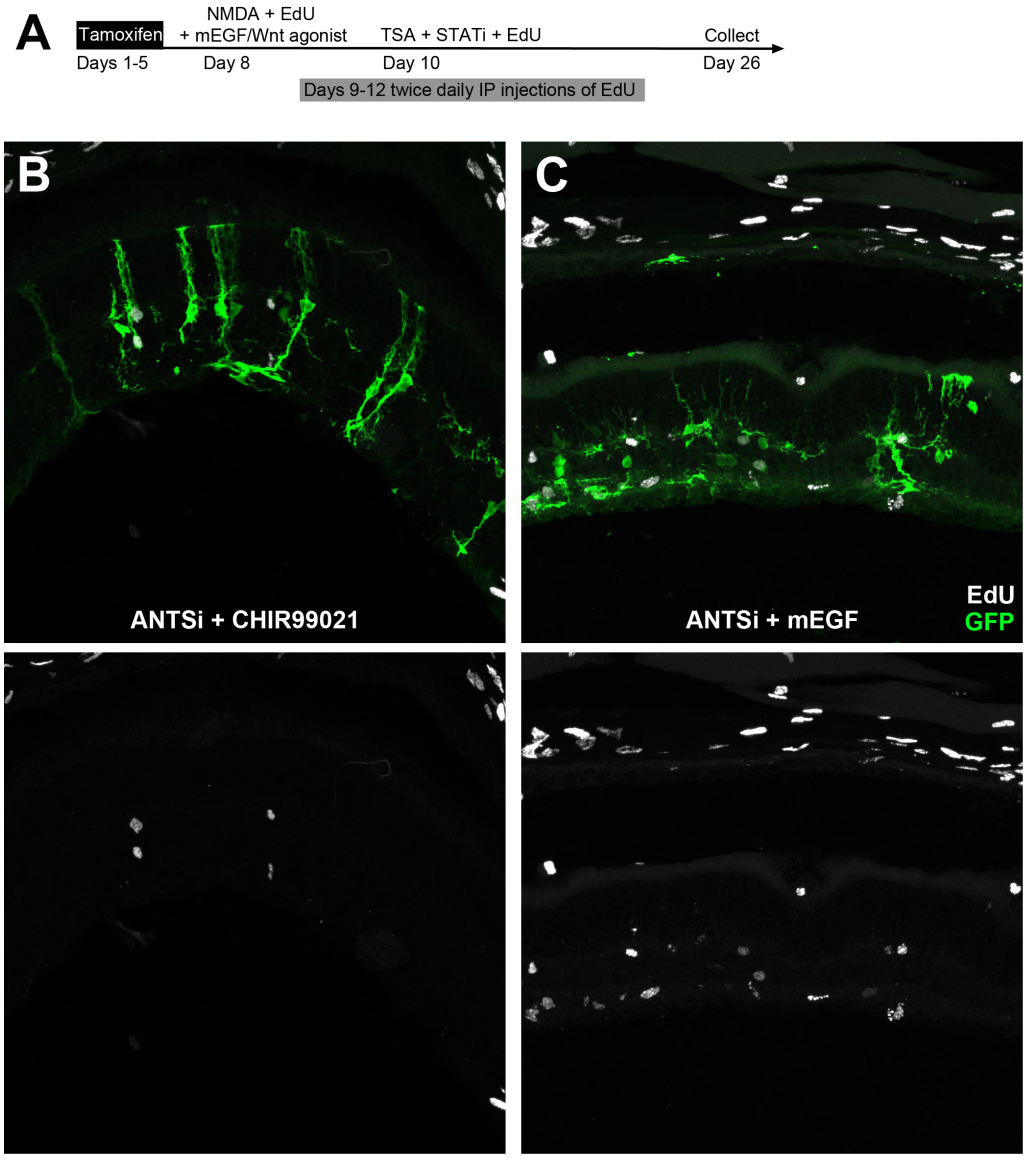

Figure 4.6: Proliferation of adult MG in vivo with mitogens. **a**, *Glast*-CreER: Flox-stop-*LNL*-tTA: *tetO*-Ascl1-ires-GFP mice were treated with 5 consecutive daily intraperitoneal injections of tamoxifen. On treatment day 8, an intravitreal injection of NMDA, EdU, and either mEGF or CHIR99021 was administered. On treatment day 10, an intravitreal injection of TSA, STATi, and EdU was administered. Between treatment days 9-12, twice daily intraperitoneal injections of EdU were administered. Retinas were collected at treatment day 26. **b**, Image from mouse treated with Wnt agonist CHIR99021. **c**, Image from mouse treated with mEGF. Green shows GFP, white shows EdU.

Retinal regeneration from MG in additional neuronal damage models

In zebrafish, MG have the capacity to regenerate all types of lost retinal neurons. Additionally, specific damage models that target particular subtypes of neurons, such as light damage for photoreceptors and NMDA for ganglion cells, show that the MG dedifferentiate into a multipotent progenitor cell that is capable of generating all lost cell types. Although, MG respond to various injuries by forming multipotent progenitor cells, there appear to be biases that give proliferative advantages to progenitor cells in regions where the ablated neurons were located[141]. It is not known for certain if factors released from the dying neurons are responsible for signaling regenerating MG to repopulate the lost cell types or if it is simply a matter of newly available space for the multipotent progenitors that biases MG to repopulate the lost cell types. Interestingly, in our reprogramming paradigm, we specifically target ganglion and amacrine cells for degeneration by NMDA excitotoxic damage and observe predominantly bipolar cell generation from MG. This suggests that in mice, specific dying neuron populations do not pattern the MG to repopulate that cell type. To directly assess this question for a different cell type, I decided to perform two models of photoreceptor-specific degeneration, light damage and a genetic degeneration model of retinitis pigmentosa. I hypothesized that dying rods and cones would release signals instructing the MG to regenerate these dying neurons.

Light damage

To induce a light damage insult in mice, there are numerous complications to consider. In black and agouti mice, the pigment within the iris shields the photoreceptors from experiencing

saturated levels of light exposure due to the constriction of the pupil. Studies have shown that drug-induced dilation of the pupil and prolonged light exposure can cause modest photoreceptor degeneration in pigmented mice[142]. However, in pigment-lacking albino mice, no pupil dilation is necessary, and the photoreceptors have a more robust degenerative response to shorter intervals of light exposure. A second complicating factor to light damage susceptibility, is the genetic contribution of the Rpe65 gene. Rpe65 is a gene that is expressed in the RPE and is essential for the regeneration of the rod photon-detecting protein, rhodopsin. A leucine at residue 450 of the Rpe65 gene renders rods highly susceptible to light damage, while a methionine at this same residue is protective[143,144].

For this reason, I decided to perform a light damage injury model on albino *Glast*-CreER: Flox-stop-*LNL*-tTA: *tetO*-Ascl1-ires-GFP mice that harbored a leucine at residue 450 in the Rpe65 gene. To more closely model my experimental paradigm around how a patient might present to the clinic with a photoreceptor degenerative disorder and receive treatment, I first induced photoreceptor damage in the mice, then provided TSA and tamoxifen to induce Ascl1 expression after damage had already occurred. Adult P86 mice were placed in a cage lined with reflective material (see methods for light damage) and exposed to high intensity light for a duration of 8 hours. The next morning, TSA was administered intravitreally, followed by an intraperitoneal injection of tamoxifen 30 minutes later (Figure 4.7A). Retinas were then collected 10 days later, fixed, sectioned, and stained for various bipolar and photoreceptor markers to determine the neuronal types generated by the MG.

After staining retinas from several different mice with a panel of markers, no MG-derived photoreceptors were observed. Interestingly, I found many instances of MG migrating from the INL to the ONL and expressing Otx2 (Figure 4.7B, orange arrows); however, the pattern of Otx2

expression did not resemble the stereotypical donut-shaped nuclei seen in rods, nor did the cells express rhodopsin or recoverin. Due to the severe reduction in ONL thickness, the morphologies of GFP+ cells were difficult to resolve as having a definite bipolar-like morphology, but they did express bipolar genes, such as Cabp5, similar to the ANT and ANTSi paradigms.

This study provides further evidence that a specific degenerating neuron type does not pattern the MG to regenerate that cell type in mice. The NMDA damage paradigm fails to induce ganglion cell regeneration even though those are the predominant cell type that is lost, and similarly, light damage fails to induce photoreceptor regeneration. Instead, Ascl1 expression and TSA appear to specifically reprogram the MG towards the bipolar fate. It is possible that changing the sequence or timing of TSA administration and Ascl1 induction may yield success in generating photoreceptors, but future experiments involving thorough time courses will be required to address this question.

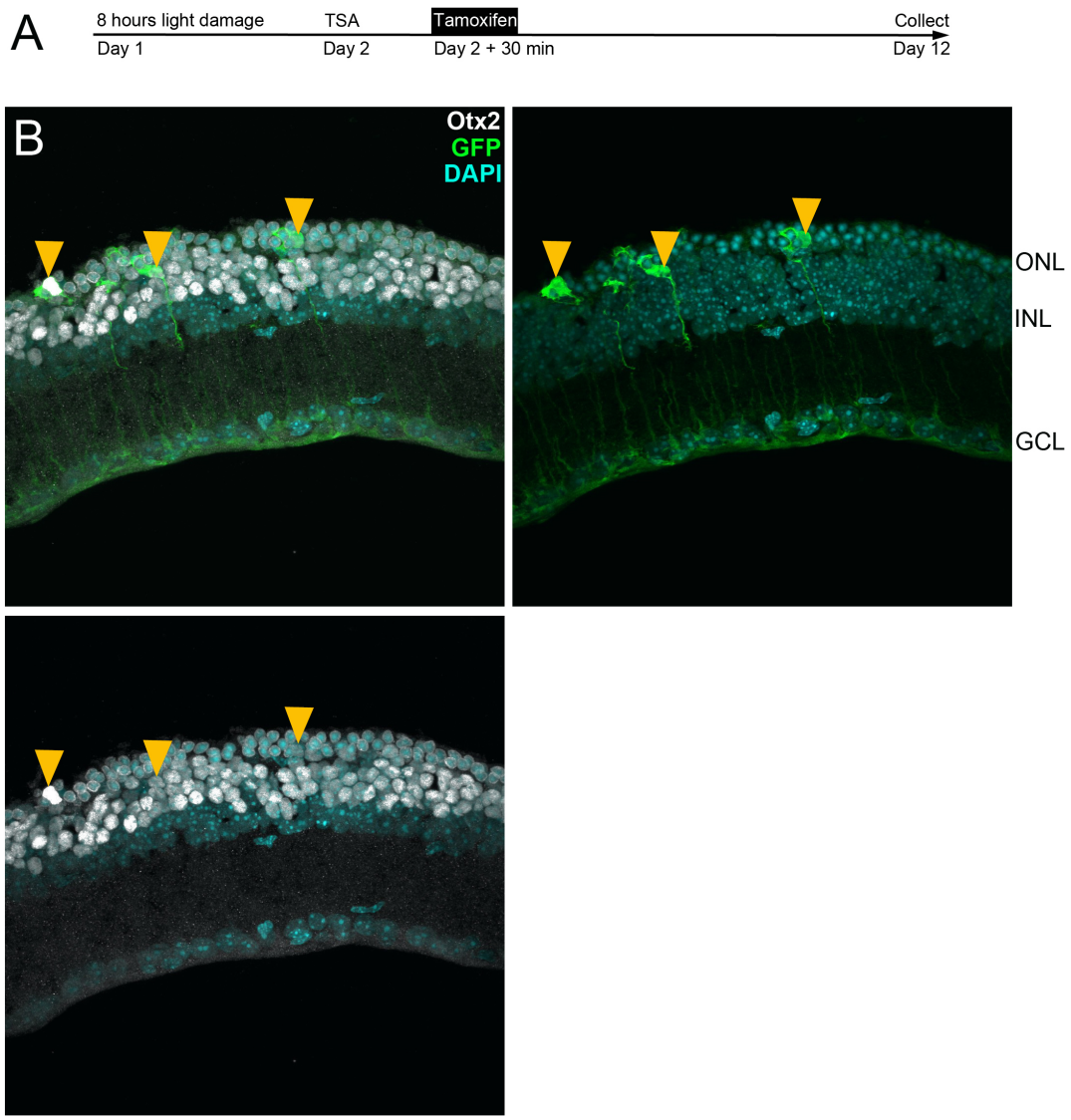

Figure 4.7: Light damage as injury model in MG reprogramming. **a**, Experimental paradigm showing albino *Glast*-CreER: Flox-stop-*LNL*-tTA: *tetO*-Ascl1-ires-GFP mice harboring a leucine at reside 450 of Rpe65 gene being exposed to 8 hours of high intensity light on treatment day 1. An intravitreal injection of TSA was administered on treatment day 2 followed by intraperitoneal injection of tamoxifen 30 minutes later to induce Ascl1 expression. Retinas were collected 10 days later. **b**, Images showing Otx2, GFP, and Dapi staining. ONL thickness is greatly reduced in light damage model. GFP cells express Otx2 in ONL, orange arrows.

P23H damage

Light damage is a robust and very fast model system to induce nearly complete photoreceptor degeneration in the course of hours. To determine the effect of a slower and more clinically relevant model of photoreceptor degeneration on MG's ability to be reprogrammed, I used mice with a proline to histidine substitution at codon 23 (P23H) in rhodopsin. The P23H mutation is the most common cause of autosomal dominant retinitis pigmentosa in humans, resulting in a progressive degeneration of the rod photoreceptors followed subsequently by the loss of cones[145]. Knock-in mice harboring the human disease-causing variant have been generated and show a similar degeneration of rods[146]. In homozygous P23H mice, we find rods are almost completely lost by postnatal day 21, with only a single layer of cells in the ONL remaining. Interestingly, heterozygous P23H mice have a slower degeneration, which occurs over the course of several months, suggesting rods are able to fend off apoptosis for a longer duration due to a single healthy copy of rhodopsin. It should be noted that our LNL-tTA cassette was inserted in the Rosa26 locus, which happens to be just over 1Mb away from the rhodopsin gene on chromosome 6. For this reason, generating homozygous P23H mice that possess all the alleles required for Ascl1 expression is not feasible with our current model.

To test this injury model of retinitis pigmentosa in our *Glast*-CreER: Flox-stop-*LNL*-tTA: *tetO*-Ascl1-ires-GFP mice, I crossed a homozygous P23H mutant mouse with our homozygous Ascl1-expressing strain to generate animals that were heterozygous for all alleles. Similar to the light damage model, I hypothesized that specific signals from dying rods might signal MG to regenerate lost rods; however, instead of the degeneration occurring within hours, this time I would be testing a slower degeneration that occurs over the course of weeks. Because

heterozygous P23H mice begin the degenerative process as soon as the rods are born, I decided to induce Ascl1 expression earlier than usual, at P13, when MG have just reached maturity but before significant rod loss has occurred. This timepoint is also notable because our previous study demonstrated from P12-P14, TSA administration is not required to promote MG-based regeneration in a NMDA injury model[81]. Therefore, I hypothesized that induced MG would sense the photoreceptor degeneration in this crucial window and would not require TSA administration. Mice were thus injected for two consecutive days, starting at P13, with 0.8 mg tamoxifen in 100 uL corn oil (Figure 4.8A). Mice were then allowed to survive for 10 weeks to ensure ample rod loss, then retinas were collected, fixed, sectioned, and stained for a panel of neuronal markers.

Upon analysis of the retinal sections, photoreceptor degeneration was apparent by the thinning of ONL thickness (Figure 4.8B). Unlike the monolayer of rods that is seen in the light damage model, between 3-4 rows of rods could be seen by P83 in the P23H model. Many of the MG maintained their MG morphology; however, a subset of the cells expressed Otx2 (Figure 4.8B, orange arrows) and migrated to the ONL. Like the light damage model, no clear neuronal morphologies (either photoreceptor or bipolar) were observed in this experiment, nor were photoreceptor proteins colocalized with GFP expression, suggesting again, that Ascl1 induction is restricted to regenerating bipolar cells.

The results of this study were promising and showed that a lower level of progressive cell loss was sufficient to induce MG-derived neurogenesis, and that a potent induction of damage from the likes of NMDA and light damage are not necessary. There were numerous caveats to the study, however, the most pressing of which is the developmental timing for Ascl1 induction. I chose the P12-P14 window to induce Ascl1 overexpression as a proof of concept because we

have previously shown that MG are still plastic at this age and do not require TSA administration to generate neurons. In practice, patients who present to the clinic with retinitis pigmentosa will be long past any equivalent developmental window of plastic MG. As a treatment, patients will most likely need Ascl1 induction in combination with TSA to stimulate their terminally differentiated MG to undergo neurogenesis.

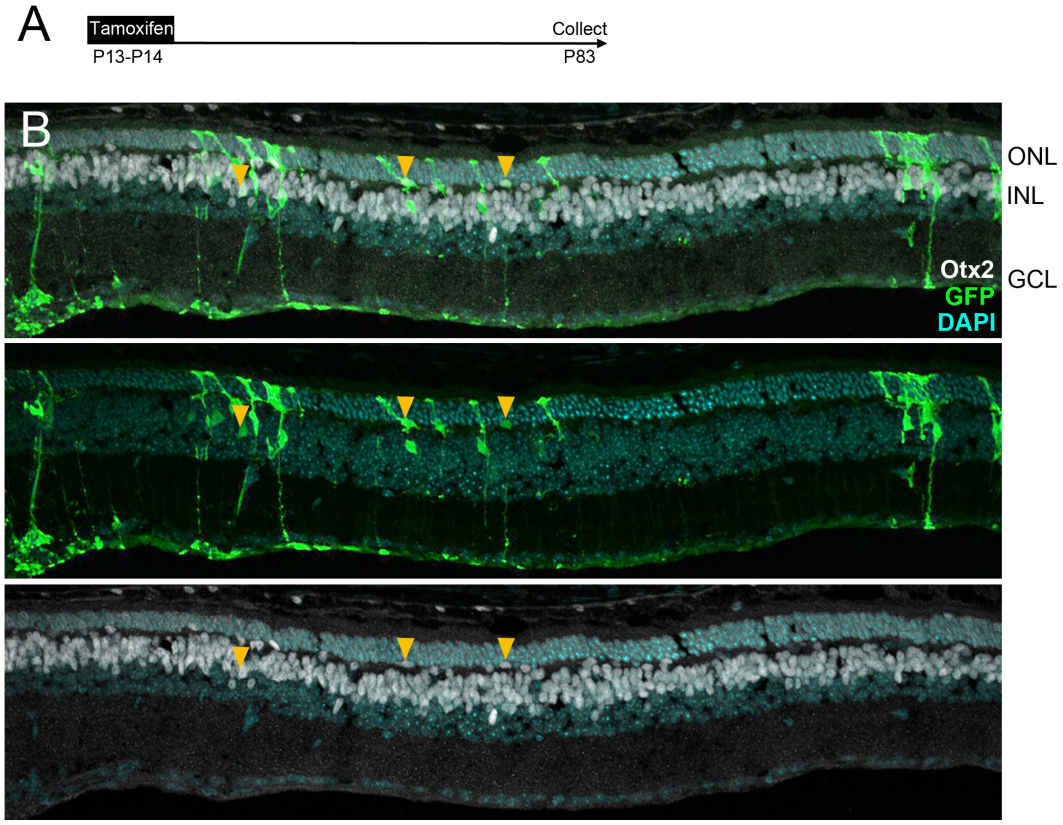

Figure 4.8: P23H as damage model in MG reprogramming. **a**, Experimental paradigm showing *Glast*-CreER: Flox-stop-*LNL*-tTA: *tetO*-Ascl1-ires-GFP: P23H +/- mutant mice being treated with tamoxifen at ages P13-14. Retinas were collected 10 weeks later at P83. **b**, Images showing Otx2, GFP, and Dapi staining. ONL thickness is reduced to 3-4 layers of rods in progressive P23H degeneration model. GFP cells express Otx2, orange arrows.

To determine if Ascl1-induced regeneration could occur in more mature mice in this progressive injury model, I performed an experiment where tamoxifen was administered at P60 for 5 consecutive days, followed by TSA administration. Retinas were collected 2 weeks after TSA and were fixed, sectioned, and stained for a panel of neuronal markers. Again, I found that bipolar markers like Otx2 and Cabp5 were found to be expressed; however, no photoreceptor-specific proteins were colocalized with the GFP.

The results of the light damage, NMDA, and P23H degeneration model demonstrate that Ascl1 expression promotes the specific generation of bipolar neurons regardless of the lost retinal neuron type. Ascl1 is known to induce photoreceptor, bipolar, and MG cell fates in development. Additionally, specific neuron ablation in other species followed by endogenous Ascl1 induction is correlated with a bias towards regenerating the lost neuronal type. For these reasons, I hypothesized that a similar phenomenon may be observed in adult mice. Three different injury models refute this hypothesis and show that in an overexpression context in mature MG, Ascl1 fails to generate any neuronal cell type other than bipolar cells.

Looking at all the genomic datasets we have generated from reprogrammed MG in the previous chapters, some insights can be drawn that probe at the mechanism of action of Ascl1 in adult MG. Firstly, based on gene expression of the MG-derived neurons from single-cell RNA-seq, Ascl1 promotes expression of genes enriched in the bipolar cell fate. No canonical photoreceptor or ganglion cell genes have been observed in these datasets. Next, based on previous ChIP work from a former graduate student in the lab, Dr. Matthew Wilken, and from our Ascl1 ChIP-seq datasets highlighted in previous chapters, Ascl1 is likely the master regulator of Otx2[118]. Interestingly, very few Ascl1 binding sites are found at photoreceptor gene promoters, suggesting that one of Ascl1's downstream target genes is responsible for regulating

photoreceptor cell fate and not Ascl1 itself. It is well known that Otx2 is found in high abundance at both bipolar and photoreceptor gene promoters[90,147]. We know that Otx2 is highly expressed in MG-derived neurons; however, it appears to enrich at bipolar gene promoters rather than photoreceptor genes. Given these observations, there appears to be an unknown mechanism at play that is prompting Otx2 to have a preference for bipolar gene promoters. It is possible that Otx2 fails to bind photoreceptor gene promoters in MG because there is no accessibility at the chromatin level. We have tested this by analyzing MG DNase-seq and ATAC-seq datasets and find evidence of inaccessible chromatin at various sites that are normally open in rods; however, there are also examples of accessible chromatin in a subset of the rod genes that are not expressed. Another hypothesis is that there may be nascent transcription factors expressed in the MG that promote Otx2 binding at bipolar genes; or conversely, there may be repressive transcription factors that actively repress Otx2 binding at photoreceptor genes. In support of this idea, recent work in a model of fibroblast reprogramming has shown that resident transcription factors of the source cell have the ability to effectively recruit the misexpressed transcription factor to other sites along the chromatin[120]. Indeed, Ascl1 ChIP-seq analysis also shows evidence supporting this hypothesis, with STAT motifs being enriched at a large percentage of developmentally inappropriate Ascl1-bound sites. One of these mechanisms is possibly the underlying reason for the lack of MG-derived photoreceptor regeneration, and future experiments are needed to thoroughly probe and address these questions.

An alternative explanation for the lack of photoreceptor and ganglion cell regeneration may simply be due to the lack of an additional but necessary transcription factor. Photoreceptor development has been shown to rely heavily on transcription factor complexes formed by various combinations of Otx2, Crx, Nr2e3, and Nrl. Based on IHC and single-cell RNA-seq, we

have found that MG-derived neurons express Otx2 and Crx; however, the cells lack expression of Nr2e3 and Nrl. Overexpressing these factors in the MG in combination with Ascl1 may result photoreceptor regeneration. Dr. Wilken previously attempted this experiment by infecting MG cultures with a cocktail of lentiviruses for various photoreceptor transcription factors and failed to see any strong evidence of photoreceptor generation. Notably, his readout for these experiments was bulk qPCR for other photoreceptor genes, which may not have been sensitive enough to pick up photoreceptor genesis if only a small proportion of the cells were reprogrammed. Repeating this experiment with newer technologies, such as single-cell RNA-seq as a readout, may yield more promising results. Alternatively, using MG cultures from a photoreceptor gene reporter mouse line, like *Nrl*-GFP or *Rho*-GFP may be a productive way to screen combinations of photoreceptor transcription factors for reprogramming efficacy. Looking to the future of MG-based regeneration, it is likely that additional factors will be necessary to generate photoreceptors and ganglion cells from MG.

Atoh1 in combination with Ascl1 expression promotes generation of diverse cell types and increases reprogramming efficiency

Introducing additional reprogramming transcription factors to the eye in vivo relies predominantly on two methods; transgenic mice or viral-based methods. Viral delivery methods have been met with numerous challenges including tropism, package size, and titer. Groups have partially addressed the issue tropism by creating custom viral capsids that recognize and deliver their payload to specific populations of cell types within the retina, including MG[148-150]. Additionally, libraries of cell type-specific promoters have been generated that can theoretically

be used to drive gene expression in a specific cell type (like MG), even if the virus infects all retinal cell types[151]. AAVs are able to package sequences of ~4.8kbp, which is sufficient for the delivery of most retinal transcription factors and a reporter; however, the package size becomes a limiting factor when the experimenter is attempting to deliver multiple factors in the same payload. To navigate this issue, two viruses, each delivering a factor and possibly a reporter could be introduced in tandem, but this results in issues of multiplicity of infection and the available channels for imaging (usually 4 fluorophores) becomes limiting. High viral titers are crucial to ensure enough cells in the retina are being infected to see a response. Most viruses we have made in the lab have a titer of 10^7-10^8 viral genomes per mL. When these viruses are intravitreally introduced to the retinas of adult mice, very few cells express the reporter and are generally restricted to regions proximal to the injection site. I have attempted injections of a commercially available, high titer virus on the order of 10^{13} viral genomes per mL and found robust labelling of cells throughout the retina of adult mice. Ultimately this approach will require generating a high titer virus that specifically targets MG and harbors our gene of interest. Therefore, I decided to pursue an approach using transgenic mice that contain tetracycline inducible transcription factors of interest, similar to our *tetO*-Ascl1-ires-GFP construct. In this way, a single cross with our *Glast*-CreER: Flox-stop-*LNL*-tTA: *tetO*-Ascl1-ires-GFP mice would yield heterozygous mice that specifically express Ascl1 and another factor in MG after tamoxifen administration.

Atoh1 and Ascl1 overexpression

To determine whether another proneural bHLH transcription factor like Ascl1 would have similar effects, we used mice that had been previously engineered to carry a *tetO*-Atoh1 transgene. Atoh1, like Ascl1, belongs to the bHLH family of transcription factors; however, Atoh1 is in a different subclass of bHLH factors and binds to a related, but not identical, E-box sequence in the DNA to activate transcription. Atoh1 is important for hair cell development in the inner ear, it is not normally expressed in the developing or mature retina[152,153]. However, a highly related gene, Atoh7, is expressed in the developing retina and is important for ganglion cell development in mice[49,154-156]. I therefore hypothesized that Atoh1 would have a similar effect as Atoh7 in development and that inducing Atoh1 expression in MG would result in reprogramming MG towards a ganglion cell fate.

The first cross of the homozygous *tetO*-Atoh1 mice with our heterozygous *tetO*-Ascl1 mice yielded animals that were heterozygous for Atoh1 and/or Ascl1. I first decided to test the effects of Atoh1 alone by administering tamoxifen to adult *Glast*-CreER: Flox-stop-*LNL*-tTA: *tetO*-Atoh1: Flox-stop-*CC*-GFP mice. Like Ascl1 expression alone, I hypothesized I would see GFP+ cells that possessed canonical MG morphology and failed to upregulate neuronal gene expression. I collected, fixed, sectioned, and stained retinas for GFP and various neuronal markers a week after the last tamoxifen injection and surprisingly, I found that nearly all of the MG had undergone apoptosis, with only fragments of MG processes remaining. This result was consistent with previous observations of Atoh1 overexpression toxicity described in the inner ear[157].

I next decided to test if Atoh1 would still be toxic when expressed in combination with Ascl1 in the MG. For these experiments, I injected adult *Glast*-CreER: Flox-stop-*LNL*-tTA: *tetO*-Atoh1: *tetO*-Ascl1-ires-GFP mice with 5 consecutive days of tamoxifen and collected retinas 3-6 weeks later for IHC (Figure 4.9A). I stained for GFP and Atoh1 to determine (1) if there were GFP+ cells present in this paradigm, and (2) if Atoh1 was expressed in MG when co-expressed with Ascl1. I found abundant GFP expressing cells with no obvious signs of injury or apoptosis, suggesting that the combination of Ascl1 and Atoh1 prevent Atoh1's toxicity (Figure 4.9B). Surprisingly, over 80% of the MG had retracted their glial processes and adopted a neuronal morphology. All the MG that maintained their glial morphology failed to express detectable levels of Atoh1 (Figure 4.9B, white arrows), whereas every GFP+ cell with a neuronal morphology expressed high levels of Atoh1 (Figure 4.9B, orange arrows). These data suggest that the combination of Atoh1 and Ascl1expression induces MG reprogramming without the need for retinal damage or a HDAC inhibitor. It is curious that not every GFP+ cell expresses detectable levels of Atoh1 because their *Glast*-CreER is clearly active and enabling the GFP to be expressed. Because the *tetO*-Atoh1 cassette is randomly inserted in the genome, we do not know where it is localized. It is possible that the gene has inserted in a region that is differentially accessible from cell to cell. Nevertheless, the fact that HDAC inhibition and damage are no longer required for reprogramming MG to neurons, make this an attractive system for further understanding the MG reprogramming process..

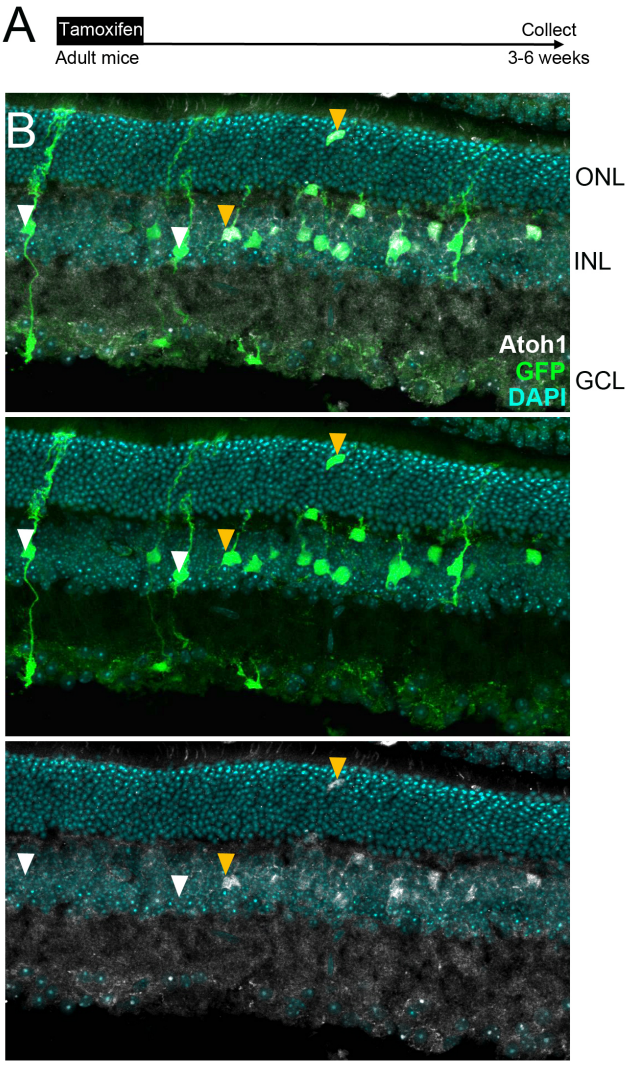

Figure 4.9: Atoh1 and Ascl1 overexpression in adult mice. **a**, Experimental paradigm showing *Glast*-CreER: Flox-stop-*LNL*-tTA: *tetO*-Ascl1-ires-GFP: *tetO*-Atoh1 mice being injected with 5 consecutive daily intraperitoneal injections of tamoxifen. Retinas were collected 3-6 weeks after last tamoxifen injection. **b**, Images showing Atoh1, GFP, and DAPI staining. All GFP+ cells with MG morphology fail to express Atoh1, white arrows. All GFP+ cells with neuronal morphology express Atoh1, orange arrows.

To further characterize the MG-derived neurons in the Ascl1/Atoh1 combination, I used IHC, staining with a panel of neuronal markers. I found every GFP+ cell with a neuronal morphology stained for amacrine marker HuC/D, and none of the cells stained for bipolar markers Otx2 or Cabp5 (Figures 4.10 and 4.11). This is in stark contrast to the ANT and ANTSi

treatment conditions, where Ascl1 generates primarily Otx2+ Cabp5+ neurons and very few HuC/D positive cells. A subset of the neurons in the Atoh1/ Ascl1 expressing cells stained with amacrine marker Pax6, as well. Notably, the neurons had reduced expression of the MG marker Sox9, while the GFP+ MG that failed to undergo neurogenesis still had high levels of Sox9 (Figure 4.10). This is similar to my previous findings from ANT and ANTSi-treated retinas, where MG-derived neurons downregulate glial genes. In addition to Atoh1 and HuC/D being expressed in every GFP+ cell with neuronal morphology, I also observed NeuN expression in every neuronal cell, which was surprising due to the fact that NeuN is normally in every ganglion cell and only a subset of amacrine cells[158,159]. Because these MG-derived neurons appeared to resemble amacrine/ganglion cells, I stained with a panel of amacrine/ganglion cell antibodies against mature markers Ap2, Brn3, Calbindin, Calretinin, and ChAT (Figure 4.11). No colocalization with GFP was observed in any of the sections, suggesting that the MG-derived neurons do not reach the full maturity of a terminally differentiated amacrine or ganglion cell.

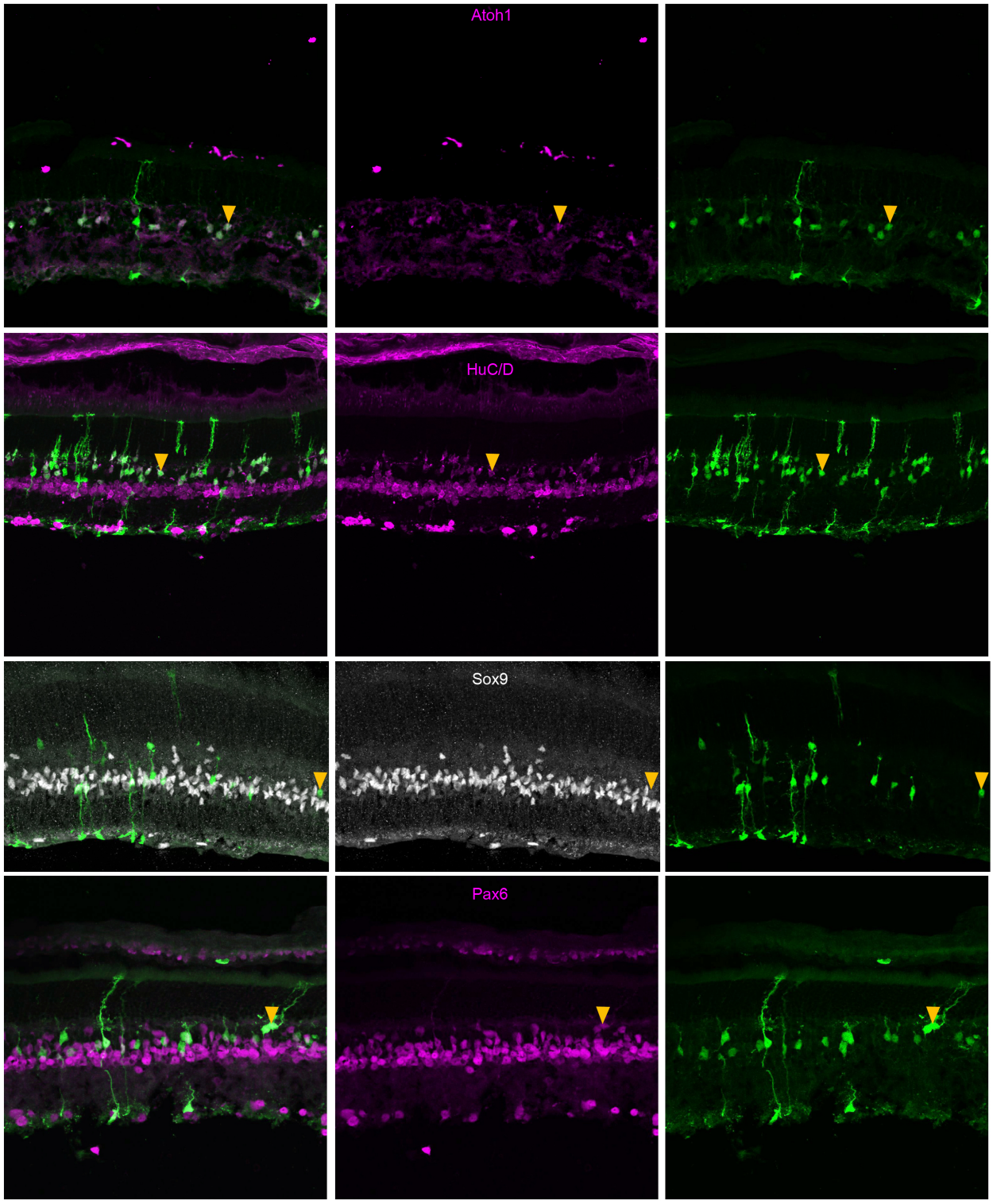

Figure 4.10: Atoh1 and Ascl1-overexpressing cells in adult mice stain for a subset of amacrine markers. Orange arrows indicate examples of cells that express Atoh1, HuC/D, and Pax6. Orange arrow in Sox9 panel highlights MG-derived neuron that lacks Sox9 expression.

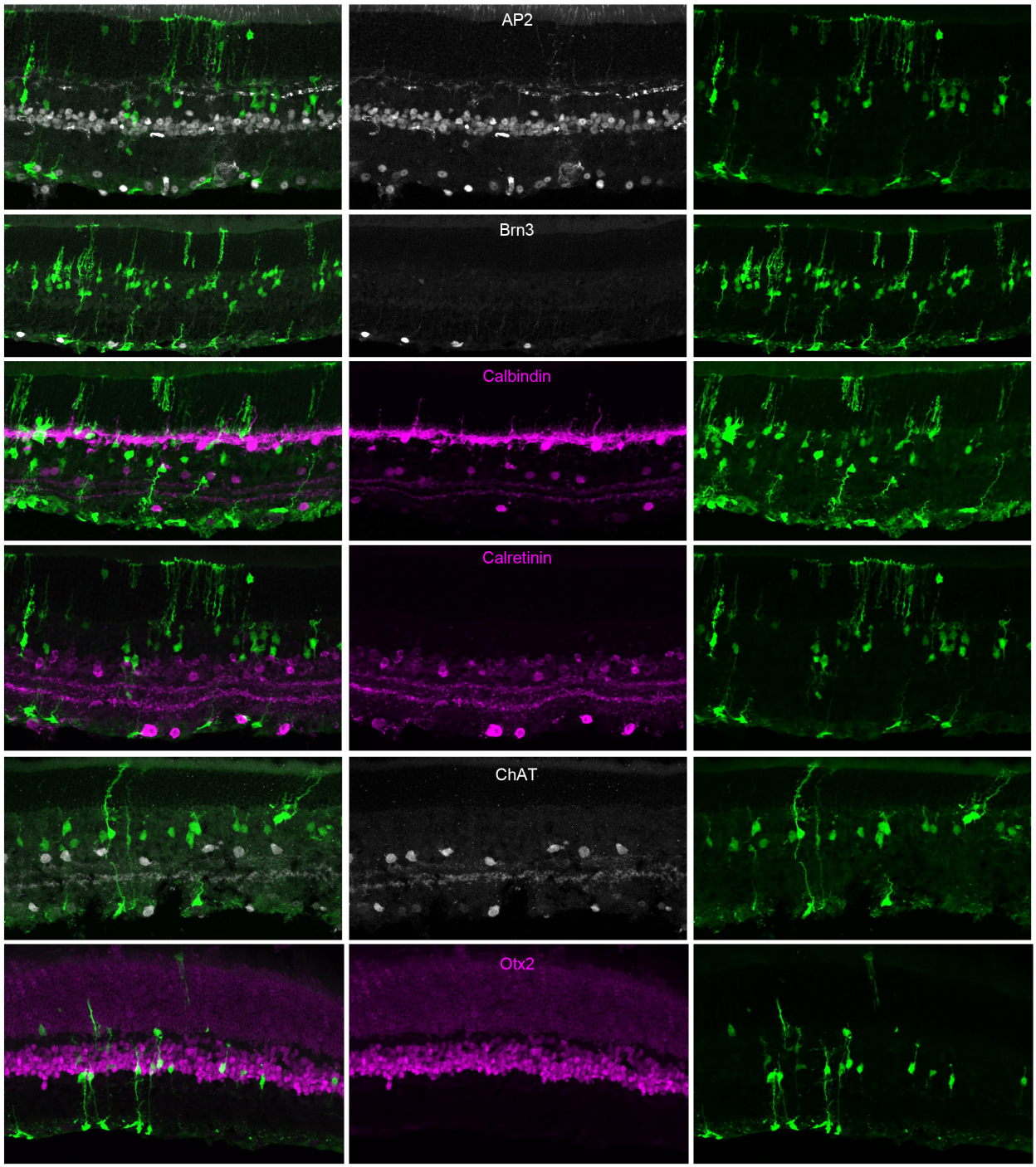

Figure 4.11: Atoh1 and Ascl1-overexpressing cells in adult mice do not express mature amacrine, bipolar, or ganglion cell markers. Example images from staining panel of various neuronal markers, showing no colocalization of neuronal markers with GFP.

In addition to this initial characterization of the retinal phenotype observed from overexpression of proneural bHLH factors in the MG, I also stained brain sections from these mice. Glast is expressed in the retinal MG, but is also highly expressed in astrocytes. For this reason, I hypothesized that brain astrocytes might be reprogrammed to neurons in the Ascl1 and/or Ascl1/Atoh1 expressing mice. I collected brains from several adult mice that received tamoxifen injections and stained for GFP, DCX, and NeuN. In the Ascl1 only mice, I observed robust labelling of GFP+ astrocytes throughout the entire brain (Figure 4.12A). Additionally, the Bergmann glia were labelled throughout the cerebellum (Figure 4.12B). No GFP+ neurons were observed in the cortex; however, the hippocampus and rostral migratory stream (RMS) contained GFP+ DCX+ cells (Figures 4.12C and 4.12D), with a subset being NeuN+. Due to the lack of an Ascl1- GFP+ control, it is not possible to discern whether the radial glia express Glast and their neuronal progeny in the hippocampus and rostral migratory stream, or if Ascl1 expression is driving the neurogenesis. Nevertheless, Ascl1 overexpression did not convert most GFP+ glia to neurons.

When I analyzed the brains of the Ascl1/Atoh1 over-expressing mice, I found distinct changes. In these mice, GFP+ NeuN+ neurons were seen in the deep cortex, suggesting that the combination of Ascl1/Atoh1 does indeed stimulate reprogramming of brain astrocytes to neurons (Figures 4.12E and 4.12F, orange arrows). Future efforts to record from these astrocyte-derived cortical neurons could be an exciting area to pursue to determine if these cells integrate and function within the mature brain circuitry. Additionally, a more thorough characterization involving a panel of antibodies against brain neuron markers, or single-cell RNA-seq would help in identifying the type of cortical neurons that are being generated. Though the brain is not the

focus of my thesis work, this study could potentially benefit researchers attempting to reprogram astrocytes for the treatment of neurodegenerative diseases and psychological disorders.

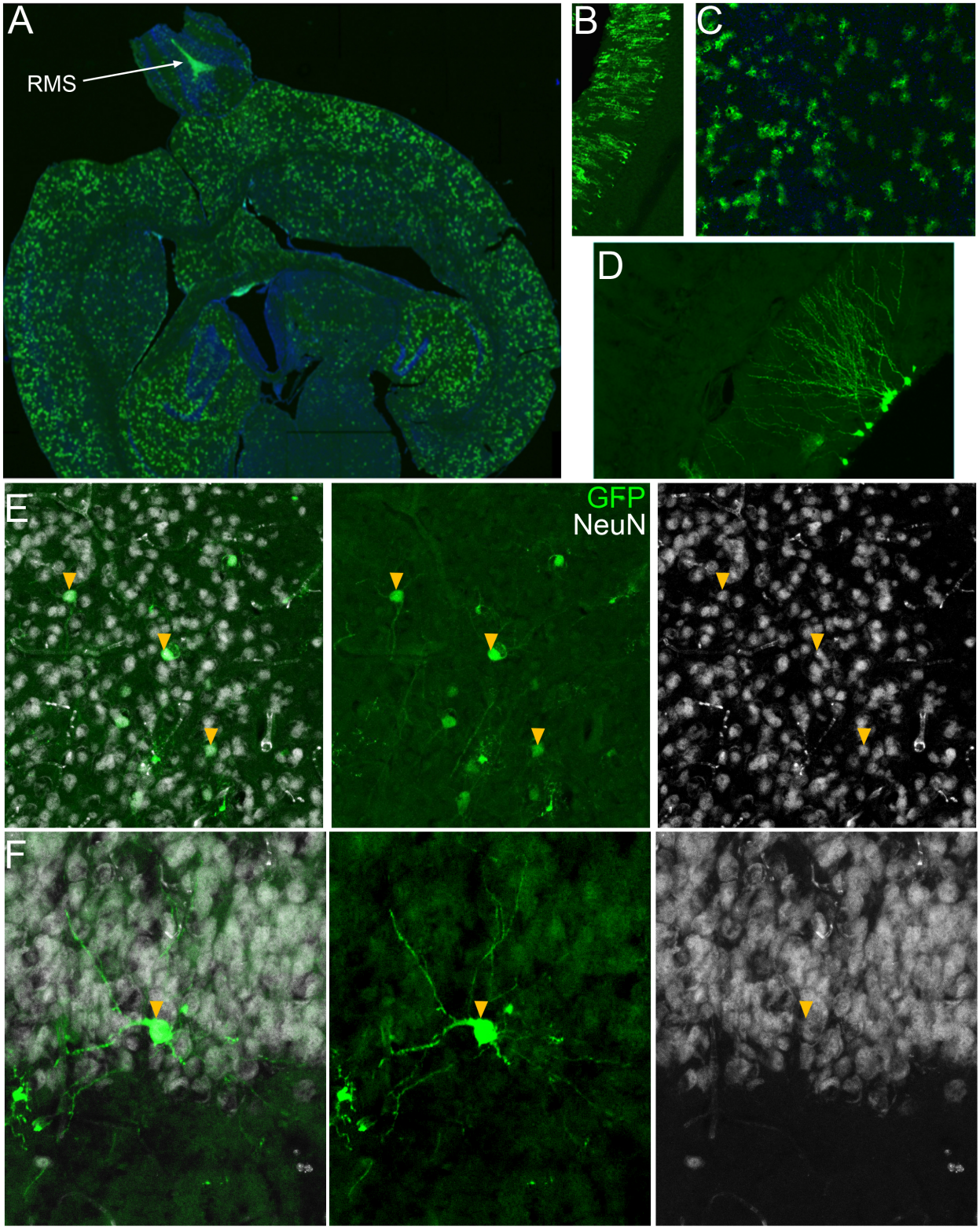

Figure 4.12: Atoh1 and Ascl1-overexpressing cells in adult mouse brain. **a**, Transverse section of whole mouse brain from *Glast*-CreER: Flox-stop-*LNL*-tTA: *tetO*-Ascl1-ires-GFP mouse treated with tamoxifen. Astrocytes are labelled throughout the brain with GFP expression. Arrow

indicates rostral migratory stream (RMS), where neuronal progenitors showed colocalization of GFP with DCX. **b**, Image from cerebellum of *Glast*-CreER: Flox-stop-*LNL*-tTA: *tetO*-Ascl1-ires-GFP mouse showing Bergmann glia labelling with GFP. **c**, Higher magnification image from cortex of *Glast*-CreER: Flox-stop-*LNL*-tTA: *tetO*-Ascl1-ires-GFP mouse showing robust labelling of astrocytes with GFP. **d**, Higher magnification image from hippocampus of *Glast*-CreER: Flox-stop-*LNL*-tTA: *tetO*-Ascl1-ires-GFP mouse showing GFP-labelled neurons. These cells were found to express NeuN and DCX (not shown). **e**, **f**, Higher magnification images from deep cortex of *Glast*-CreER: Flox-stop-*LNL*-tTA: *tetO*-Ascl1-ires-GFP: *tetO*-Atoh1 mouse showing GFP-labelled neurons colocalized with NeuN, orange arrows.

This study in the retina serves as an important step towards generating more diverse populations of neurons from MG but raises numerous questions. For instance, how is the presence of Ascl1 able to reduce the toxicity of Atoh1 in MG? Since both factors are bHLH transcription factors, it is possible that Ascl1 directs Atoh1 to bind at more appropriate sites across the genome. It is also possible that Ascl1 induces expression of downstream target genes that may alleviate Atoh1 toxicity. Future ChIP-seq experiments should provide insights into the binding patterns of each factor and may reveal a mechanism of this rescue of toxicity. Another question that remains is why do these MG-derived neurons fail to mature into terminally differentiated amacrine, or ganglion cells as assessed by canonical protein expression? The presence of HuC/D and NeuN, and the lack of Ap2, Brn3, Calbindin, Calretinin, and ChAT colocalization with GFP suggest that these cells may be immature amacrine or ganglion cells. Future time course experiments are needed to determine whether these MG-derived neurons need more time to turn on these more mature markers or if they are stuck in this immature cell state. Another potential explanation is that keeping Ascl1 and Atoh1 constitutively expressed may prevent further development of the MG-derived neurons. Our transgenes are kept on by the tetracycline transactivator protein after tamofixen is administered; however, this system can be shut off by administering doxycycline. Future experiments in the Ascl1 and Atoh1 expressing mice, and even the ANT/ANTSi treatment paradigm involving the administration of doxycycline

after reprogramming should inform us on the importance of constitutive verses transient transgene expression.

At the time of this writing, numerous molecular biological techniques are underway to further characterize these MG-derived neurons at the functional and mechanistic level. Mice have been treated and are awaiting whole cell electrophysiological recordings to determine if the MG-derived neurons are functioning in a manner similar to amacrine cells. Additionally, GFP+ cells have been FACS-purified from Atoh1/Ascl1-expressing mice and processed for single-cell RNA-sequencing. Combining this data with previous WT, ANT, and ANTSi treatment conditions will aid in the description of the various genes these MG-derived neurons are expressing and how similar or different they are to the bipolar cells generated in the other treatment conditions. Additionally, combining this data with single-cell RNA-seq from whole adult retina will help to determine how similar these MG-derived neurons are to normal amacrine and ganglion cells. Lastly, Ascl1 ChIP-seq experiments are planned to assess how the presence of Atoh1 affects Ascl1 binding across the genome. Hopefully, these techniques will paint a more complete picture of how additional transcription factors can assist Ascl1 to generate more diverse neuronal cell types than the stereotypical bipolar cells that have so far been described.

DISCUSSION

The goals of the studies highlighted in this chapter were to: (1) uncover factors that may promote proliferation of MG in the adult mice; (2) determine whether different models of retinal neuron damage resulted in regeneration of lost cell populations; and (3) to explore the effects of adding additional transcription factors to the reprogramming paradigm in combination with

Ascl1. Though the experiments presented in this chapter have not yet been published in a peer-reviewed journal, they serve as a basis for future regeneration studies.

The explant studies of MG proliferation showed several important findings that may be beneficial when translated to an in vivo context. I found that Ascl1 expression was sufficient to induce MG proliferation at higher levels than WT MG. The addition of mEGF to the culture media increased both WT and Ascl1-expressing MG to undergo even more proliferation, with mEGF and Ascl1 acting synergistically to induce the most proliferation when added together. Comparing C57BL/6 WT MG with our Ascl1 background strain (without tamoxifen induced Ascl1 expression) resulted in comparable basal levels of MG proliferation at all time points out to 8 DIV. This suggests that any novel mitogenic combinations that increase proliferation in the transgenic mice may have a similar effect if administered in combination with an Ascl1 expressing virus in WT animals. This is important because the implications of these studies are meant to serve as the foundation for potential clinical interventions.

Next, I showed that two Wnt agonists (SC-222416 and CHIR99021) are both sufficient to increase MG proliferation in explants when combined with Ascl1 expression, albeit, not to the same extent as mEGF. Surprisingly, I also found that TSA completely arrests proliferation in WT and Ascl1-expressing MG and negates the effects of SC-222416 and mEGF, resulting in no proliferation. CHIR99021 is able to overcome this TSA effect and results in proliferation of MG in both WT and Ascl1 conditions, suggesting that the mechanism by which CHIR99021 stimulates proliferation is different than that for SC-222416 and/or mEGF. Interestingly, CHIR99021 inhibits GSK-3β to activate Wnt, whereas SC-222416 is a GSK-3β independent activator of Wnt signaling. This suggests that GSK-3β inhibition may be important to stimulate proliferation in a treatment paradigm involving TSA.

Lastly, I tested these mitogens in vivo to determine if they were efficacious in increasing MG proliferation in our regeneration paradigm. While I initially hypothesized that mEGF would fail to induce proliferation, based on the explant TSA studies, I found that mEGF actually stimulated more proliferation than CHIR99021 in an in vivo context. There are numerous potential explanations for this contradictory finding; however, future dose responses, time courses, and variations to the sequence of injections for all administered drugs will be required to truly identify why TSA does not arrest mEGF induced proliferation in our current in vivo paradigm.

To explore the idea that loss of specific neurons may result in diverse cell types being regenerated from the MG, I decided to test two models of photoreceptor damage. I hypothesized that dying photoreceptors might release factors that instruct MG to become photoreceptors instead of the bipolar cells that we observe in the NMDA injury model. For the first set of experiments, I chose a light damage model of photoreceptor degeneration and exposed albino Ascl1-expressing mice, harboring a light damage susceptibility mutation at residue 450 in the Rpe65 gene, to 8 hours of high intensity light. To more closely model how a retinitis pigmentosa patient might be treated if they present at the clinic, I chose to administer TSA and tamoxifen after damage had occurred. I found that my initial hypothesis was not supported; light damage resulted in the formation of MG-derived Otx2+ Cabp5+ bipolar neurons, similar to what we observed after NMDA-induced ganglion cell and amacrine cell loss. Although the lack of photoreceptor regeneration was disappointing, this study demonstrated for the first time that an intervention can be given after damage has occurred and this will still stimulate regeneration from Ascl1-expressing MG.

For my second set of experiments, I chose a genetic model of progressive photoreceptor degeneration, by crossing the Ascl1 overexpression mouse strain to the P23H mice that harbor a toxic mutation in the rhodopsin gene. In this study I was testing two questions: (1) is progressive degeneration strong enough to stimulate regeneration, or is a more severe model (like light damage or NMDA) necessary; and (2) will rod specific degeneration result in the regeneration of diverse neuronal types from MG? To the first point, I found that P23H progressive degeneration was indeed strong enough to stimulate MG-derived neurogenesis. Like the light damage model, however, I found that Otx2+ Cabp5+ MG-derived neurons were the only type of retinal neuron generated. Together, the P23H and light damage studies show that intervention can be administered post-damage to stimulate regeneration, that regeneration can be induced in a less severe, progressive model of degeneration, and that loss of specific neuron populations does not affect the diversity of retinal neurons generated from MG.

Because various injury models fail to increase regenerated neuronal diversity, I chose to add an additional reprogramming transcription factor to our paradigm by generating a new mouse with *tetO*-Ascl1 and *tetO*-Atoh1. The expression of Atoh1 alone was seen to be toxic to the MG, as has been observed in similar reprogramming studies in the inner ear; however, when Atoh1 is expressed in MG in combination with Ascl1, I observed the generation of amacrine/ganglion-like cells in the retina. These studies showed that no injury or HDAC inhibitor was necessary, and that merely turning both genes on in MG results in nearly 80% of the cells converting to neurons. Additionally, brain astrocytes were seen to convert to NeuN+ neurons in the cortex, demonstrating the potent reprogramming efficacy of these two factors. Several questions arose from this study, including: (1) how does Ascl1 alleviate the toxicity of Atoh1 expression; and (2) why do these neurons fail to express terminally differentiated markers

of amacrine and ganglion cells? Currently, numerous molecular biological methods are underway to address these questions. This study suggests that viral delivery of a combination of Ascl1 and Atoh1 may be sufficient to induce regeneration, which would be a much simpler clinical intervention than a virus given in combination with a HDAC inhibitor and STAT inhibitor. The Ascl1 and Atoh1 co-expression experiments provide strong evidence that additional reprogramming factors can be used to stimulate different neuronal cell types in retinal regeneration.

Chapter 5:

Discussion

Summary of results

I began this dissertation work with the goal of determining whether or not new neurons could be regenerated in the mature mammalian retina. The prospect of regenerating neurons of the retina captured my imagination because humans are such a highly visual species and so much of our daily interactions with our environment are aided by the sense of sight. The thought that my work might lay the foundation for clinical interventions to treat or cure blinding diseases provided me with a sense of purpose and drive. Key studies in teleost fish demonstrated the natural ability of MG to regenerate all retinal neuron types; since mammals also have MG, retinal regeneration might be feasible in mammals. In the zebrafish, Ascl1 was identified as a critical factor for early reprogramming events during the regenerative process and this led our lab to a model of Ascl1 overexpression in the MG of mice. These early studies by Drs. Pollak and Ueki of the Reh lab demonstrated that Ascl1 could in fact reprogram mammalian MG towards retinal neurons in vitro and in vivo in young mice. Unfortunately, these studies also demonstrated that mammalian MG lose their regenerative capacity before P16 and suggested that epigenetic changes in the aging MG might be responsible for this lost plasticity. When I began my dissertation work, my first objective was to overcome this developmental window by restoring the neurogenic potential of mature MG to the adult animal.

Preliminary results from our lab indicated that epigenetic changes in the chromatin of maturing MG may be restricting Ascl1 from binding at neuronal gene promoters and preventing adult MG from regenerating retinal neurons. In Chapter 2, I explored this hypothesis by administering an HDAC inhibitor, TSA, to the injured retina after Ascl1 had been induced. I hypothesized that HDAC inhibition would reduce the repressive histone mark H3K27me3 and

would instead promote an activated chromatin state by increasing H3K27ac at neuronal gene promoters. Indeed, I found that TSA treatment increased H3K27ac at Ascl1 binding sites in neuronal gene promoters and enabled adult MG to be reprogrammed to a bipolar or amacrine cell fate in vivo. Quantification of stained retinal sections revealed that ~20% of the MG-derived neurons expressed the mature bipolar neuron markers Otx2 and Cabp5. IHC and SBFSEM suggested that these MG-derived bipolar cells were making proper connections with their canonical synaptic partners. Whole-cell patch electrophysiology demonstrated that the MG-derived neurons are functional and receive synaptic input from photoreceptors when exposed to light stimulus. To better assess the neuronal type of these MG-derived neurons, we performed scRNA-seq, ATAC-seq, and Otx2 ChIP-seq on FACS-purified MG and MG-derived neurons. Through scRNA-seq, we found that MG-derived neurons express many mature bipolar genes; however, they also retain a small MG signature by maintaining low levels of glial gene expression, such as Glul and Aqp4. Although the MG-derived neurons are not indicative of truly differentiated bipolar cells, this residual glial gene expression gave us confidence that we really were converting MG towards neuronal fates and that these GFP-labeled neurons were not the result of incorrectly induced transgenes in the wrong cell type. ATAC-seq data from Ascl1 ± NMDA ± TSA treatment conditions showed a similar phenomenon, with many accessible regions of chromatin being found exclusively at neuronal gene promoters in the ANT-treated cells. Interestingly, the MG-specific genes that become downregulated in the ANT condition were accompanied by a reduction in ATAC-seq signal at these same genes, suggesting that MG close down their chromatin at glial gene promoters as they progress towards retinal neurons. Lastly, Otx2 ChIP-seq from Ascl1-expressing cells, ANT-treated cells, and whole retina demonstrated that the ANT treatment results in Otx2 binding patterns that are similar to normal

bipolar interneurons. Together, these results provided the first evidence that mature mammalian MG can be reprogrammed to functional neurons in vivo. This study also demonstrated that our reprogramming paradigm has room for improvement and raised several key issues: (1) only ~20% of the GFP+ MG undergo neurogenesis; (2) the MG that do undergo neurogenesis still retain some of their glial signature; and (3) only interneuron cell fates are observed in the MG-derived population.

In an effort to improve our in vivo reprogramming paradigm and potentially generate more diverse MG-derived neurons, we turned to the zebrafish and avian literature for targetable candidate factors that may improve mammalian reprogramming. Previous work in the teleost fish had shown that STAT3 is required for damage-induced MG-mediated regeneration, and that activation of the JAK/STAT pathway was sufficient to induce retinal regeneration in the absence of injury. Conversely, in mouse, STAT3 was associated with a gliotic response after retinal injury. Additionally, in postnatal chick, STAT signaling had been shown to limit regeneration, and inhibition of STAT3 resulted in increased neurogenesis from MG after injury[110]. We theorized that the conflicting functions of STAT signaling between fish and avian/mammalian species may explain the divergent regenerative potentials of these species after retinal injury. Therefore, we hypothesized that inhibiting the phosphorylation of STAT would reduce the gliotic response of MG after injury and improve the regenerative response in mice. In Chapter 3, I decided to add the potent STAT inhibitor, SH-4-54, in combination with the intravitreal injection of TSA to improve my reprogramming paradigm. After staining and quantifying GFP+ cells from this new ANTSi treatment condition, I found that STAT inhibition doubled the reprogramming efficiency of MG, with nearly 40% of the GFP+ cells staining for mature neuronal markers. The MG-derived neurons continued to express neuronal markers consistent

with bipolar interneurons; there was no evidence of photoreceptors or ganglion cells either morphologically or at the protein level. Single-cell RNA-seq of FACS-purified ANTSi-treated cells confirmed a doubling in the proportion of MG-derived neurons verses the ANT treatment condition. We also observed low levels of residual glial gene expression in this dataset, suggesting that STAT inhibition did not increase the maturation of MG-derived neurons beyond that of the ANT treatment. We also found that MG in the ANT and ANTSi treatment conditions that fail to undergo neurogenesis express high levels of STAT pathway target genes, whereas control WT MG and MG-derived neurons lack enrichment for the same genes. This suggests that in a subset of Ascl1-expressing MG, the JAK/STAT pathway becomes active and keeps the MG in a progenitor-like state.

To better understand how Ascl1 is behaving in our reprogramming paradigm and what implications this has for STAT-signaling, we performed an Ascl1 ChIP-seq on P0 retinal progenitor cells and P12 Ascl1-overexpressing MG. We hypothesized that misexpression of Ascl1 in MG might cause it to bind at different cis-regulatory sites in the DNA than where it does normally during development; this differential binding might be driven in part by STAT signaling. Genome-wide analyses of Ascl1 binding sites in the two samples revealed that there was indeed differential binding of Ascl1 in development versus in an overexpression context in MG. Of the 47,507 high-confidence peaks observed in the Ascl1-overexpressing MG, only about a third of them overlapped with developmentally appropriate Ascl1 binding sites. The other two thirds, or 32,901 peaks, were bound at developmentally inappropriate sites not normally found in P0 RPCs. To determine what factors might be driving this inappropriate binding, we performed a combinatorial analysis of inappropriate Ascl1 binding sites that had a corresponding increase in gene expression. We reasoned that the presence of an inappropriate Ascl1 binding site that

correlated with an increase in expression might be detrimental to reprogramming. Peaks meeting this criterion were fed as input into the motif finding software, HOMER, which returned a list of transcription factor binding motifs. We found that the Ascl1 motif was present in 92% percent of the developmentally inappropriate sites with increased gene expression, which is unsurprising due to this being an Ascl1 ChIP-seq dataset. The next most confident motif returned by HOMER was a paired homeobox motif that was found in 7% of these inappropriate sites. MG have numerous homeobox transcription factors, and this finding suggested that one of these could be playing a role in patterning the chromatin for Ascl1 to bind. Surprisingly, the third most significant motif on the list was the STAT motif, which was present in 12% of the developmentally inappropriate Ascl1 binding sites. This finding supported our hypothesis and suggested that a significant percentage of the inappropriate Ascl1 binding may be attributed to the presence of STAT. This study demonstrated that targeting additional factors in mammalian MG can result in more efficacious reprogramming to a neuronal cell fate. By inhibiting STAT phosphorylation, we were able to double the conversion of MG to neurons. Importantly, while inhibition of STAT signaling increased the efficiency of MG reprogramming with Ascl1, it did not change the types of neurons generated after NMDA damage, with bipolar cells making up the great majority and some evidence for amacrine cells, but none of the cells expressed genes or had features of photoreceptors or ganglion cells.

In Chapter 4 of my dissertation, I performed various experiments to stimulate the proliferation of mature MG and tested various injury models and additional factors to generate diverse retinal neuron types. Stimulating proliferation of mature MG in vivo is an important goal to achieve for the translation of retinal regeneration to the clinic for two main reasons. The first, is that the MG make up only a fraction of the total retinal cells (about 3%). This means that even

if every MG was converted to a retinal neuron, it would only be a modest repopulation of new neurons and likely would not lead to vision recovery, except in diseases of other rare cell types, like cone loss in macular degeneration. The second reason is that MG are critical for the maintenance of retinal integrity. If too many MG are converted to neurons, the structural and trophic support for the neurons will likely be reduced as a consequence. By expanding the pool of MG in the retina prior to reprogramming through stimulating proliferation, we would likely be able to address both these issues at once.

I began by adding various mitogens to retinal explant cultures to determine which factors induce MG proliferation in vitro in the adult retina. I performed these experiments in both WT and Ascl1-expressing retinas and found that Ascl1 alone was sufficient to increase MG cell division. Additionally, I found that combining Ascl1 expression with a Wnt agonist (SC-222416 or CHIR99021) or mEGF increased the total number of proliferating MG in vitro. Surprisingly, when TSA was added to the culture medium, I found that all proliferation was completely arrested, even when administered in combination with mEGF or SC-222416. The other Wnt agonist, CHIR99021, was sufficient to overcome this TSA effect and showed high levels of MG proliferation in both Ascl1-expressing and WT MG. The two Wnt agonists I used in this study increase Wnt signaling through two separate mechanisms, with CHIR99021 acting through inhibition of GSK-3β and SC-222416 acting through a GSK-3β independent mechanism. This suggested that increasing proliferation in the TSA-dependent reprogramming paradigm in vivo might require manipulation of GSK-3β, using a drug like CHIR99021. To test this hypothesis, I administered either CHIR99021 or mEGF via intravitreal injection in the ANT reprogramming paradigm in combination with the NMDA injection. I found mEGF to be a more potent stimulator of proliferation than CHIR99021 in this paradigm, which was contradictory to my in

vitro explant TSA results. CHIR99021, mEGF, and TSA are likely all metabolized in vivo at different rates, which may partially explain the conflicting in vivo versus in vitro proliferation responses. Regardless, I was able to successfully demonstrate that both mEGF and CHIR99021 can increase levels of mature MG proliferation in vivo, which may be useful in future retinal regeneration studies as a way of expanding the pool of MG to reprogram.

The next studies I presented in Chapter 4 were designed to test whether the loss of specific neuron populations would promote the MG to regenerate retinal neurons other than bipolar and amacrine cells. In the ANT and ANTSi treatment conditions, NMDA is given to kill ganglion and amacrine cells, and consequently, we are able to regenerate bipolar and amacrine cells as a result. I decided to test two models of photoreceptor-specific damage by performing either a light damage injury model or a genetic rod degeneration model in the Ascl1-based reprogramming paradigm. For the light damage model, adult albino *Glast*-CreER: Flox-stop-*LNL*-tTA: *tetO*-Ascl1-ires-GFP mice harboring a light damage susceptibility mutation in the Rpe65 gene were exposed to 8 hours of high intensity light. TSA and tamoxifen were administered the following day to induce MG reprogramming, and eyes were collected 10 days later. I found many GFP+ cells labelled with Otx2 in the INL and ONL; however, none of these cells stained with markers or had morphologies indicative of photoreceptors or ganglion cells. For the genetic rod degeneration model, adult *Glast*-CreER: Flox-stop-*LNL*-tTA: *tetO*-Ascl1-ires-GFP mice harboring an unstable mutation in the rhodopsin gene (P23H mutation) were used. Normally, the heterozygous P23H mice undergo a progressive degeneration of their rod photoreceptors over the course of several months. For this reason, I injected tamoxifen to induce Ascl1 expression, then allowed the mice to survive for 10 weeks prior to collecting eyes. Similar to the light damage model, I found many GFP+ Otx2+ MG in both the INL and ONL; however,

no evidence for photoreceptor or ganglion cell genesis was observed. Together, these two studies and the result from the ANT and ANTSi treatment paradigms suggest that Ascl1-based reprogramming of MG is restricted to bipolar and amacrine cell fates, regardless of which neuronal cell type is lost in injury.

In the last section of Chapter 4, I decided to introduce another bHLH transcription factor in combination with Ascl1. I crossed the *Glast*-CreER: Flox-stop-*LNL*-tTA: *tetO*-Ascl1-ires-GFP mice with a *tetO*-Atoh1 mouse, to express Gfp, Ascl1, and Atoh1 in MG when tamoxifen is administered. Atoh1 is not normally found in the retina during retinal development, but its paralog, Atoh7, is a critical transcription factor that is necessary for ganglion cell development. I hypothesized that Atoh1 overexpression in MG would promote the regeneration of ganglion cells rather than the bipolar and amacrine cells we have observed in Ascl1 conditions. Notably, in the absence of Ascl1, Atoh1 expression alone appeared to induce an apoptotic response in the MG, with no viable GFP+ MG being observed one week after induction. When Atoh1 expression was induced in the presence of Ascl1, I observed robust reprogramming of MG to retinal neurons. Over 80% of the GFP+ cells expressed amacrine and ganglion cell markers HuC/D and NeuN; and surprisingly, no Otx2 or Cabp5 was seen to colocalize with GFP. Additionally, no retinal injury, HDACi, or STATi was necessary to stimulate this robust reprogramming. The results of this study suggested that two bHLH transcription factors (Ascl1 and Atoh1) were sufficient to induce the most efficient reprogramming observed to date, and that this reprogramming does not require damage or additional drugs. This study also demonstrates the ability to generate diverse retinal neuron subtypes by inducing expression of different transcription factors in MG. Several important questions surfaced after this study, such as: (1) why is Atoh1 alone toxic to MG and how does Ascl1 rescue this effect; (2) how does the addition of Atoh1 change the MG-derived

neuron fate from predominantly Otx2+ Cabp5+ bipolar cells to amacrine/ganglion cell fates; and (3) why do Atoh1-Ascl1-expressing MG-derived neurons fail to express mature ganglion cell markers like Brn3 or Isl1? Future studies in the lab are planned to address these questions, but the finding that additional transcription factors may aid Ascl1-based reprogramming is exciting and sets a precedent for adding additional tetracycline inducible transcription factors to generate diverse neuronal types.

Reprogramming MG to diverse neuronal types

My dissertation work in Chapter 2 demonstrated for the first time that retinal neurons could be regenerated from MG in an adult mouse. Through several follow up studies in Chapters 3 and 4, I have shown that Ascl1 expression appears to restrict MG towards regenerating bipolar cells, and to a lesser extent amacrine cells. I have found no evidence of photoreceptor or ganglion cell gene expression, proteins, or morphologies in any treatment involving Ascl1 alone. In Chapter 4, I was able to observe markers of immature ganglion/amacrine cells when Ascl1 was expressed in combination with Atoh1, providing strong evidence that MG might be able to generate diverse cell types other than interneurons if the correct cocktail of transcription factors is found. Our lab is currently awaiting the arrival of a mouse from Dr. Xiuqian Mu at the University of Buffalo that contains a *tetO*-Pou4f2/Isl1 gene cassette. By crossing this mouse onto our *Glast*-CreER: Flox-stop-*LNL*-tTA: *tetO*-Ascl1-ires-GFP: *tetO*-Atoh1 mouse, we will be able to test if adding additional ganglion cell transcription factors will enable MG to generate more terminally differentiated ganglion cell types. If more *tetO* mice become available, generating a

similar transgenic animal that expresses important photoreceptor transcription factors would be interesting to determine if MG can generate rods or cones with the right combination of factors.

In November 2018, *Yao et al* published the first evidence of regenerated rod photoreceptors in an adult mouse[160]. They chose to pursue a different approach for retinal regeneration by virally introducing genes of interest to the MG via intravitreal injections of a modified AAV, ShH10, which has been mutated to specifically recognize and infect MG in the retina[161]. In their paradigm, *Yao et al* first administered a shH10 AAV containing β-catenin under the MG-specific promoter Gfap. A previous study by the same group had shown that β-catenin is capable of activating the Wnt pathway and stimulated proliferation of adult MG in vivo without injury[104]. To reprogram the proliferating MG into rods, they next administered a ShH10 AAV containing a *Gfap*-Otx2-Crx-Nrl construct. As previously mentioned, Otx2, Crx, and Nrl are three key transcription factors necessary for the development of rods and act together to activate expression of critical rod-specific genes. After 2-4 weeks post-infection, rods were shown to be labelled with their viral reporters, suggesting that the MG had been successfully reprogrammed. *Yao et al* next decided to test if these MG-derived rods could restore visual function to a mouse harboring a mutation that results in lack of photoreceptor-mediated light responses. These Gnat1/2 mutant mice were first treated with a ShH10 AAV containing a fluorescent reporter, β-catenin, and a healthy copy of Gnat1 to enable MG-derived rods to conduct light responses. Next, the *Gfap*-Otx2-Crx-Nrl construct was delivered to reprogram the dividing MG into rods. After 4 weeks post-infection, they demonstrated that the new reporter-labelled cells indeed had light responses indicative of functional rods by electrophysiological recordings, thus demonstrating the first evidence of MG-derived rod-genesis in a mature mammal.

This work, though exciting, has been met with caution and skepticism by retinal regeneration experts. In an editorial published in *Science Magazine* shortly after this study, a respected retinal regeneration expert expressed his concerns with the results by offering an alternative explanation that, "the existing rod and cones in the blind mice were repaired in the procedure either because they took up the virus carrying the corrective [Gnat1] gene, or because Müller glia shared that gene's products with them. In either case, the visual signals to their brains didn't come from newly created rods, but from existing photoreceptors with restored function." *Yao et al* performed numerous EdU-pulse experiments to demonstrate β-catenin's ability to induce proliferation, but failed to show any EdU-labelled rods, resulting in a failure to convince some that these labelled rods are MG-derived. Results from our reprogrammed MG-derived neurons present with atypical neuronal morphologies and maintain a low level of residual glial gene expression, giving us confidence that our cells were in fact once MG and are not the result of a false positively-labeled GFP+ neurons. The perfect recapitulation of rod morphologies and function in *Yao et al*'s study are incredible, but if the results prove reproducible with EdU-labelling, their reprogramming paradigm holds great potential for clinical interventions.

Validating reprogramming factors in non-transgenic animals

The approach of viral-mediated in vivo reprogramming of MG to neurons taken by *Yao et al* provides a model paradigm for how such a clinical intervention would be implemented. Transgenic overexpression of transcription factors in humans is not possible, so demonstrating the ability to regenerate neurons with a viral-based method in WT mice after injury is the perfect clinically relevant model to study retinal regeneration. For my line of research, delivering a

ShH10 AAV harboring an Ascl1 and/or Atoh1 overexpression construct to reprogram MG in a WT mouse would directly demonstrate the translational potential of my dissertation work. I attempted this experiment by sourcing the production of a ShH10-Ascl1-ires-GFP virus to a commercial manufacturer. When I administered this virus to adult WT mice as an intravitreal injection, I found very few GFP-labelled cells. Additionally, introducing this virus to adult retinal explant cultures resulted in little GFP expression. Although the sequence of the viral construct appeared correct, none of my experiments demonstrated robust labelling of MG with GFP or Ascl1. This suggests that either viral packaging of the payload or the payload itself was not correctly processed into a viable therapeutic agent. Future work could be performed in-house to troubleshoot the viral production process and ensure the generation of a viable product to reproduce this experiment.

Numerous mouse strains with transgenic tetracycline-inducible factors are in the process of being screened in our lab for their ability to generate diverse retinal neuron types from reprogrammed MG. Additionally, other post-docs and graduate students in the lab are currently screening various transcription factors important for photoreceptor and ganglion cell development via lentiviruses to test their neurogenic potential in cultured MG. If any of these factors show promise in reprogramming MG, they will need to be tested in vivo in WT adult mice to demonstrate their efficacy in a relevant model system. Using AAVs with modified capsids, such as ShH10, is one approach to deliver genes of interest to the MG; however, recent studies have also demonstrated the potential for synthetic cell type-specific promoters. The lab of Botond Roska has developed a library of 230 AAVs, each with its own cell type-specific promoter to target various cell types within the retina[151]. These promoters were validated in mice, non-human primates, and human tissue and show robust specificity across species. MG-

specific promoters from this library could be used to deliver Ascl1 or other candidate factors to MG across various species to validate their reprogramming efficacy in WT animals, and potentially in humans. Recent clinical trials have demonstrated the efficacy of AAV-based gene therapies for the treatment of congenital diseases, like Leber's amaurosis, and have also shown that such strategies have promising safety profiles[162,163]. If additional factors being screened in our lab are able to reprogram MG into rods or ganglion cells, it is reasonable to assume that an AAV-based therapy delivering these factors to human MG could be used for the treatment of neurodegenerative diseases like retinitis pigmentosa, macular degeneration, or glaucoma.

Glial-based reprogramming in the CNS

In addition to our efforts in the retina, much work has been done in the brain to reprogram the resident astroglia towards neuronal cell fates. Converting the glia of the CNS into new neurons is a potential therapeutic strategy for generating new neurons in patients afflicted with neurodegenerative diseases like Alzheimer's, Parkinson's, and amyotrophic lateral sclerosis. Strategies targeting astrocytes, NG2 glia, or striatal progenitors with reprogramming factors, such as Ascl1, Brn2, Myt1l, Sox2, and Neurod1 have demonstrated the feasibility of this approach[92,94,164-168]. Although these strategies only have modest efficacy, with the majority of the reprogrammed cells residing directly adjacent to the injection site, the cells that are converted stain with various markers indicative of mature neurons, such as NeuN, Tbr1, and Gad65. Additionally, these reprogrammed neurons show evidence of mature excitability and reception of synaptic input[98].

A more mechanistic characterization of the reprogramming process has been elucidated in the conversion of mouse embryonic fibroblasts (MEFs) to neurons. In an Ascl1 overexpression context, *Wapinski et al* have demonstrated the importance of the chromatin state of MEFs at Ascl1 target genes for their ability to be reprogrammed[121]. Cells that lacked an active trivalent chromatin state (H3K4me1, H3K27ac, and H3K9me3) at predicted Ascl1 target loci fail to be reprogrammed into neurons. This demonstrates the importance of the epigenetic landscape at Ascl1 binding sites within the source cell during reprogramming events. The results presented in Chapter 2 of my dissertation provide a potential new avenue of research that could be applied to increase reprogramming efficiency of MEFs to neurons and potentially astroglia to neurons. HDAC inhibition promotes the acetylation of the H3K27 residue and consequently results in a more accessible chromatin state for Ascl1 binding. If TSA or another HDAC inhibitor were added to MEF or astrocyte reprogramming paradigms, their overexpressed transcription factor binding sites might become more accessible and enable more robust conversion to neurons.

A recent study by *Chronis et al* highlights another detrimental phenomenon during reprogramming that might be improved by findings in my dissertation work. ChIP-seq of various transcription factors, epigenetic regulators, and histone modifications was performed at numerous timepoints during the conversion of MEFs to induced pluripotent stem cells[120]. Reprogramming of MEFs was induced by overexpression of the four Yamanaka factors (Oct4, Sox2, Klf4, and cMyc)[119]. When the epigenetic landscapes of these various transitional states were compared to the control embryonic stem cell state, *Chronis et al* found evidence that somatic transcription factors within the source cell directed the binding of the overexpressed Yamanka factors to inappropriate sites at early reprogramming timepoints. Similar to the MEF studies, in Chapter 3 of my dissertation we observed inappropriate Ascl1 binding in MG at sites

predicted for STAT binding motifs. The endogenous STAT signaling after retinal injury in the MG likely patterned the chromatin to enable this inappropriate Ascl1 binding and consequently resulted in a failure to convert the majority of MG to retinal neurons. By adding a STAT inhibitor, I was able to reduce this STAT effect and double the reprogramming efficiency of MG to neurons. Astroglial reprogramming in different regions of the CNS is likely affected by similar mechanisms of endogenous transcription factor patterning and could be improved by targeted suppression of these pathways. For instance, the addition of a STAT inhibitor to an astrocyte reprogramming paradigm may prevent STAT from directing overexpressed transcription factors to non-productive gene loci during reprogramming and result in more efficient conversion to neurons.

Taken together, the findings from my dissertation work demonstrate the importance of chromatin accessibility and endogenously expressed transcription factors in the source cell's ability to be reprogrammed. I have successfully shown that promoting an accessible chromatin state with a HDAC inhibitor enables exogenously expressed transcription factor binding and reprogramming of MG to neuronal fates. Additionally, I have shown that targeted suppression of endogenous transcription factors, such as STAT signaling, results in a higher rate of conversion of MG to neurons. In Chapter 4, I demonstrated that overexpressing Ascl1 and Atoh1 resulted in a high rate of MG reprogramming (~80%) and that this reprogramming occurred in the absence of injury. Astrocytes in the brain were also converted to NeuN-expressing neurons in the cortex, suggesting that adding multiple bHLH transcription factors may be more efficacious than a single factor approach. These studies have implications for other reprogramming models in the CNS and potentially in other organ systems, such as the reprogramming of α-cells in the pancreas to insulin producing β-cells[169-172]. Identifying common hurdles in cellular

reprogramming has enabled my work to inform other model systems of potential strategies to improve reprogramming efficacy. Additionally, findings in other model systems may provide insights that will aid in the reprogramming of MG to retinal neurons. For instance, overexpression of neurogenic transcription factors Brn2, Myt1l, Sox2, and Neurod1 have shown efficacy in astroglial reprogramming but have yet to be tested in vivo in the retinal MG. Factors that are successful in reprogramming astroglia in the CNS or MEFs to neurons serve as potential candidate factors to test in mammalian MG. Monitoring reprogramming phenomena in other model systems will likely elucidate important molecular pathways that could be targeted to improve MG-derived neurogenesis, as well.

Considerations in MG reprogramming

The field of mammalian retinal regeneration via reprogrammed MG has seen significant advances in recent years; however, there are numerous issues to consider before translating this work to the clinic. One of the most critical considerations is the preservation of a healthy MG population. As previously stated, MG are critical for maintaining the structural integrity of the retina and providing trophic support to the retinal neurons. If too many MG are converted to neurons or a neurogenic state, the retina will be compromised and begin to degenerate due to lack of ionic and neurotransmitter regulation. Limiting the reprogramming treatment to convert a subset of MG to retinal neurons, or adding mitogens to stimulate proliferation of MG prior to reprogramming, will be key to ensuring sufficient MG remain in the retina for proper tissue function. Fortunately, the *Glast*-CreER: Flox-stop-*LNL*-tTA: *tetO*-Ascl1-ires-GFP mice only induce Ascl1 expression in a subset of the MG (<50%) and have shown evidence of

proliferation. Viral-based reprogramming of MG in WT animals, however, might result in more robust conversion that may need to be dialed back to ensure the maintenance of endogenous MG. Interestingly, all of the Ascl1-expressing MG exhibit electrophysiological changes; MG-derived neurons have properties similar to endogenous retinal neurons, while GFP+ Ascl1-expressing cells with MG morphology display electrical properties that are starkly different from normal MG. This suggests the MG that fail to generate neurons may have altered glial function based on their electrophysiology. Additionally, single-cell RNA-seq analysis shows MG that fail to generate neurons in the ANT and ANTSi treatment conditions (ie. progenitor-like cells) down-regulate expression of key glutamate transporter genes, like Slc1a3, and change expression of their potassium channel genes, providing further evidence that their glial function may be impaired. Monitoring the overall percentage of converted MG and the consequences of a given treatment on the endogenous MG function will be important for future studies of retinal regeneration.

Another important consideration, not only for retinal regeneration but reprogramming in general, is the possibility that a given treatment might affect non-target cell types. For instance, the reprogramming paradigms I have used include intravitreal injections of a HDAC inhibitor and STAT inhibitor, which are not cell-type specific drugs. This means they are acting on the MG as well as all other cell types within the retina. We have recorded from endogenous retinal neurons from animals treated with these drugs and their function appears unaltered; however, if this combination were to move forward into pre-clinical trials, thorough characterization of all cell types in the retina after treatment will be important to ensure no adverse drug effects are present. For viral-based reprogramming, it is also crucial to prove that regenerated neurons are actually derived from MG and are not the result of a leaky or treatment-induced reporter. The

Glast-CreER: Flox-stop-*LNL*-tTA: *tetO*-Ascl1-ires-GFP mice used in my study only label MG under normal conditions, and retinal neurons are only observed when all three factors, Ascl1, NMDA, and TSA are present. Additionally, the MG-derived neurons have atypical and heterogenous morphologies that do not fully recapitulate canonical bipolar/amacrine morphologies. The MG-derived neurons also have residual traces of glial gene expression and chromatin accessibility. Lastly, the MG-derived neurons label with EdU, as well as the MG-specific reporter, all of which give us high confidence that the newly generated neurons did indeed originate from a MG. Viruses, even when modified to recognize specific cell types, such as MG, can infect normal retinal neurons and give the appearance of retinal regeneration. For this reason, it is important that viral-based reprogramming paradigms show EdU colocalization within the MG-derived neurons to give confidence that the new neurons actually arose from a proliferating MG. Based on my findings of residual MG traits in MG-derived neurons, researchers should be skeptical if their MG-derived neurons fully recapitulate gene expression, epigenetic, and electrophysiological properties of normal retinal neurons.

Many blinding diseases are caused by detrimental somatic mutations in the phototransduction pathway. In retinitis pigmentosa for instance, the P23H mutation in the rhodopsin gene causes a progressive degeneration of rod photoreceptors. If a retinitis pigmentosa patient were treated with a therapeutic agent to reprogram their MG into new rods, the P23H mutation would still be present in the MG-derived neurons and would eventually result in their degeneration as well. In cases of genetic disorders, such as retinitis pigmentosa, it is important to consider the genotype of the patient and what implications this may have for MG-derived neurons. Gene therapy or CRISPR-mediated gene correction may be necessary to ensure the MG-derived neurons are viable and functional, and that they survive. Although our lab is not yet

able to regenerate rods from MG, the pathological consequences of genotype should not be dismissed and will likely play an important role in translating this work to the clinic.

Currently, the MG-derived neurons that are generated in the ANT and ANTSi paradigms resemble bipolar and amacrine cells, but maintain a residual level of glial gene expression. MG-derived neurons also have electrical properties that resemble immature interneurons. Both of these observations should be considered in future studies and the eventual pre-clinical trials. Although the MG-derived neurons receive synaptic input from photoreceptors, it is possible that they do not properly integrate into the retinal circuitry to facilitate vision recovery due to their immaturity. Future studies aimed at promoting MG-derived neuron maturity and suppressing the residual glial fate may be necessary to make behaviorally functional neurons from MG.

Clinical implications of this work

My dissertation work has shown that MG have the ability to generate new bipolar and amacrine cells in the mature mammalian retina. Unfortunately, few blinding diseases exist that result in the loss of interneurons. The most common forms of retinal degeneration are retinitis pigmentosa and macular degeneration, which cause the death of photoreceptors; and glaucoma, which causes the death of ganglion cells. Generating additional interneurons in patients with these degenerative diseases could potentially amplify the sensitivity of the remaining neurons and improve vision; however, this approach is speculative and would still fail to address the underlying pathology. Ideally, future work will build on my results and develop strategies for generating photoreceptors and ganglion cells for treating these diseases.

Interestingly, a rare condition called central retinal artery occlusion (CRAO), causes the death of retinal interneurons by cutting off the blood supply to the INL, resulting in an ischemic loss of bipolar and amacrine cells. Patients with CRAO experience a sudden loss of vision, usually in a single eye, and have no viable treatment options to preserve or restore vision. Administering an intravitreal injection of a MG-specific AAV delivering an Ascl1-overexpression construct may show promise in these patients and allow their photoreceptors to reconnect with the ganglion cells by restoring the interneurons and restore vision. Our lab is currently exploring a CRAO damage model in mice by increasing the intraocular pressure high enough to occlude the INL vasculature and induce ischemic injury. The behavioral vision assay, optomotry, will be performed before injury, after injury, and after regeneration is induced to determine if our reprogramming paradigm can restore sight to mice in a model of CRAO. If this study shows beneficial results, a similar experiment using viral-based delivery methods will be performed in larger model organisms.

Four years ago, I set out to determine if new retinal neurons could be regenerated in mature mice. My dissertation work demonstrated for the first time that bipolar and amacrine cells can be generated from MG and successfully integrate into the retinal circuitry. There is room to improve upon the reprogramming paradigm to stimulate the generation of photoreceptors and ganglion cells; however, my work has laid a robust and reproducible foundation for others to build on. We have contributed knowledge to the field of regenerative medicine by demonstrating the importance of the epigenetic landscape in an overexpressed transcription factor's ability to bind its target genes. We have also highlighted the importance of endogenous transcription factors in the source cell, and how these factors may restrict the cell's ability to be reprogrammed. I look forward to seeing how researchers incorporate findings from my results

into their reprogramming studies and anticipate an eventual viral-based treatment for blinding diseases, such as CRAO.

Chapter 6:

Materials and Methods

Injections

Intraperitoneal injections of 100 µL of tamoxifen (Sigma) in corn oil were given to induce expression of Ascl1 and GFP. CreER induction for *Glast* and *Rlbp* animals is variable, but this did not correlate with a specific treatment. Tamoxifen was administered for 5 consecutive days at a concentration of 1.5 mg per 100 µL of corn oil. For proliferation studies, 100 µL of 1 µg/µL EdU (Invitrogen) in PBS was given intraperitoneally at the time of NMDA daily until eyes were collecting for histology.

Intravitreal injections were performed on mice anesthetized with isoflurane using a Hamilton syringe with 32-gauge needle (Hamilton). All intravitreal injections were given in 2 µL volumes. N-Methyl-D-aspartic acid (NMDA) was injected at a 100 mM concentration in PBS. Trichostatin-A (TSA)(Sigma) was injected at a concentration of 1 µg/µL in DMSO. Control animals were injected with an equal volume of vehicle.

For proliferation experiments, either 2 µL of mEGF [0.05 µg/µL] and EdU [2.5 µg/µL] in PBS or 2 µL of EdU [2.5 µg/µL] in PBS was intravitreally injected for 3 consecutive days, 2 days after NMDA injections.

In Chapter 3, Intravitreal injections of SH-4-54 STAT-inhibitor (Selleck Chem) were administered at a concentration of 10 mM in TSA containing DMSO at a volume of 1.5 µL. All intravitreal injections were performed on isoflurane-anesthetized mice using a 32-gauge Hamilton syringe. For EdU-labelling experiments, NMDA and EdU were intravitreally co-injected in a mixture containing 1 µL of 34mM NMDA, 0.5 µL EdU (5 mg/mL), and 0.5 µL PBS at a volume of 2 µL. Two days later the TSA, STATi, and EdU were intravitreally co-injected in a mixture containing 1 µL TSA (2 mg/mL), 0.5 µL EdU (5 mg/mL), and 0.5 µL SH-

4-54 (25 mg/mL) at a volume of 2 μL. From treatment days 9 through 12, EdU was intraperitoneally injected twice daily for a total of 8 injections at a concentration of 1 mg/mL EdU at a volume of 100uL in PBS.

Immunohistochemistry (IHC)

For in vivo studies, animals were euthanized and the eyes removed for dissection and removal of the cornea and lens. Eye cups containing the retina were then fixed in 4% PFA in PBS for 1 hour before being transferred to a 30% sucrose in PBS solution overnight at 4 ºC. Eyes were then frozen and stored at -80 ºC in O.C.T. (Sakura Finetek) until being sectioned at 14-16 μm on a cryostat (Leica). Slides were incubated at room temperature in blocking solution (10% normal horse serum, 0.5% Triton X-100, in PBS) for 2 hours. Slides were then washed 3 times in PBS for half an hour each prior to overnight incubation at 4 ºC in primary antibody diluted in blocking solution. Slides were then washed 3 times in PBS for half an hour each prior to a 3 hour incubation in secondary antibodies (Life Technologies) diluted in blocking solution with 1:100,000 DAPI (Sigma) covered from light. At this point, slides were then washed 3 times in PBS for half an hour each and either coverslipped with Fluoromount-G (SouthernBiotech) or were stained for EdU with the Click-iT EdU Kit (Invitrogen), washed, then coverslipped. Primary antibodies: rabbit anti-Cabp5 (gift from Dr. F. Haeseleer, 1:500), rabbit anti-Pax6 (Convance, 1:300), rabbit anti-PSD95 (Abcam, 1:100), rabbit anti-Sox9 (Millipore, 1:300), rabbit anti-Opn1sw (Millipore, 1:30, AB5407), rabbit anti-Id1 (Biocheck, 1:1000, BCH-1/#37-2), mouse anti-CtBP2 (BD Biosciences, 1:500), mouse anti-HuC/D (Invitrogen, 1:100), chicken

anti-GFP (Abcam, 1:500), goat anti-Otx2 (R&D Systems, 1:100), goat anti-Sox2 (Santa Cruz, 1:100, SC-17320). TUNEL staining was performed using the Promega TUNEL kit.

Microscopy and Cell Counts

Slides were imaged via confocal microscopy on either an Olympus FluoView FV1000 for cell counts, or a Zeiss LSM880 with Airyscan (voxel size = 0.0426 x 0.0426 x 0.185 um^3) for high-resolution imaging and synaptic colocalization. For cell counts, 5 fields were imaged with a 20x objective at 2 μm thick *z*-stacks and counts were averaged for each eye analyzed.

For synaptic colocalization figures, the GFP channel was used to generate a mask of the neuronal processes (shown in Figure 3.7e-e'') using Amira image software (FEI). From within this mask, a more stringent GFP mask was generated, only highlighting the brightest intensity pixels (not shown). This stringent mask was then applied to the CtBP2 staining to show clear GFP-containing presynaptic ribbons.

For morphology panels shown in Figure 3.1k, Z-stacks were processed in Amira to mask around the cell's soma and processes to generate clear examples of various MG-derived cell morphologies.

Western Blotting (WB)

Whole retina was dissected and homogenized in a dounce homogenizer and histones isolated with the Histone Extraction Kit (ab113476, Abcam). Extracts were run on a 4-20% gel (Bio-Rad) prior to blotting. PVDF membranes (Bio-Rad) were then blocked overnight at 4 ºC in

a milk blocking solution (5% powdered milk, 0.5% Triton X-100, 0.1% NaN_3 in PBS). Following 3 half hour washes in a wash buffer (0.5% Tween in PBS), membranes were then incubated with primary antibodies in milk blocking solution overnight at 4 ºC. Membranes were then washed 3 times with wash buffer and incubated with at room temperature with 1:10,000 rabbit anti-HRP in TBS-T for 2 hours. Following a final wash step, membranes were developed with SuperSignal West Dura Extended Duration Substrate (Thermo Scientific) and exposed on Autoradiography Film (Blue Devil West). All blots were scanned at 600 DPI and quantified in ImageJ (NIH, Bethesda, MD) by transforming the image to 8-bit format and quantifying the gray value via Uncalibrated OD in a region of interest drawn around histone bands.
Primary antibodies: rabbit anti-Histone H3 (Cell Signaling, 1:10,000), rabbit anti-H3K27ac (Abcam, 1:10,000).

In Chapter 3, retinas from P11 *rtTA germline***:** *tetO-mAscl1-ires-GFP* mice were dissociated and MG were grown in culture as previously described[74,173]. Confluent monolayers of MG were passaged and doxycycline (1:500) was added to the media to overexpress Ascl1 for 6 days, and a subset of cultures received SH-4-54 STAT-inhibitor (Selleck Chem) on the fifth day of treatment for 24 hours. MG cultures were lysed with buffer containing 25 mM Tris-HCl pH 7.5, 150 mM NaCl, 1 mM EDTA, 1 % Triton X-100, 5 % glycerol, 1X protease inhibitor cocktail, and 1X phosphatase inhibitor cocktail and equal amounts of protein samples were loaded and run in a 4 % to 20 % SDS gel (Bio-Rad Laboratories). Protein was transferred to a polyvinylidene fluoride membrane (Thermo Fisher Scientific, Waltham, MA, USA), blocked (5 % BSA and 0.1 % Tween 20 in 1X TBS) for at least 1 hour at room temperature and stained with primary antibodies (Phospho-STAT3 Y705 and STAT3, R&D Systems 9131S and 9132S) diluted in blocking solution overnight at 4 ºC. Membranes were washed with 0.1 % Tween 20 in

1X TBS and then incubated with HRP-conjugated secondaries (Bio-Rad Laboratories) diluted in blocking solution for 1 hour at room temperature. Signals were visualized on X-ray film with a commercial substrate (SuperSignal West Dura Extended Duration Substrate; Thermo Fisher Scientific) and quantified using ImageJ software.

Fluorescence activated cell sorting (FACS)

Retinas were dissected, isolated from vitreous humor and retinal pigment epithelium (RPE), and then washed in PBS. Retinas were confirmed to have expression of GFP or RFP via live imaging under an inverted fluorescent microscope (Zeiss) prior to dissociation. Retinas were then incubated on a nutator in Papain and DNase I for 20 minutes at 37 ºC. Retinas were then triturated to generate a single-cell suspension and transferred to a tube containing Ovomucoid. The suspension was then spun down at 300 g for 10 minutes at 4 ºC. For Otx2 ChIP-seq, pellets were then resuspended and fixed in 0.5% formaldehyde in PBS for 7 minutes at room temperature. After fixation, 1.25 M glycine was added to the suspension to quench fixation. Cells were passed through a 35 μm filter then sorted using a BD FACSAria III Cell Sorter (BD Biosciences). Gating was performed to isolate intact cells from debris and to isolate positive fluorescent MG-derived cells. Positive fractions containing fluorescently labeled MG were then spun down at 300 g and either resuspended at appropriate concentrations for various assays or frozen at -80 ºC for Otx2 ChIP-seq.

Single-cell mRNA-sequencing (10x Genomics)

Three ANT-treated *Glast*-CreER animals had their retinas pooled and were dissociated for FACS purification. Live purified cells were then pelleted at 300 g for 10 minutes at 4 ºC and resuspended in 0.04% BSA in PBS at a concentration of 2,000 cells per µL. Cells were then loaded onto the Single Cell 3' Chip with a targeted cell recovery of 4000 cells. For control animals, two *Rlbp*-CreER: tdTomato animals had their retinas pooled and were run in parallel at equal cell concentrations. GEM generation and barcoding, RT, cleanup, cDNA amplification, and library construction were performed according to the Chromium Single Cell 3' Reagent Kits User Guide. Library QC was determined by TapeStation (Agilent Technologies, Inc., Santa Clara, CA). Single Cell libraries were sequenced on the Illumina NextSeq 500/550 v2 kit. Reads were processed in Cell Ranger (10x Genomics) and aligned to mm10 and aggregate filtered outputs (from the combined WT and ANT-treated libraries) were analyzed in Loupe (10x Genomics) to generate PCA plots of tSNE scores. Single-cell data shown in Figure 3.11b is from this dataset.

Single-cell mRNA-sequencing (Fluidigm)

Three ANT-treated *Glast*-CreER animals had their retinas pooled and were dissociated for FACS purification. Live purified cells were then pelleted at 300 g for 10 minutes at 4 ºC and resuspended in neurobasal medium. A fraction of the resuspended cells were analyzed on a Countess II FL Automated Cell Counter (Invitrogen) for quality control and to determine final cell density. Cells were loaded onto a 5-10 µm 96-well Fluidigm© C1 IFC at a concentration of

400 cells per µL. A separate group of two control *Rlbp*-CreER: tdTomato animals were run in parallel in a similar manner and were loaded onto a second IFC at a concentration of 1400 cells per µL. IFCs were imaged under a fluorescent microscope to visualize which capture sites contained GFP or RFP cells for the ANT-treated and control cells, respectively. Wells that contained intact GFP or RFP cells and were free of cellular debris were then chosen for sequencing. After selecting for wells that contained viable cells (as stated above) and for wells that had similarly high DNA concentrations, a total of 9 ANT-treated and 48 control cells were used for all analyses. Reads that passed Illumina's base call quality filter were aligned to mm9 using TopHat v2.1.0. Counts for each gene were generated using htseq-count v0.6.1p1 in the "intersection-strict" overlap mode. Raw reads were then processed using the Monocle suite in Bioconductor[174]. Data was analyzed and presented using R.

Assay for Transposase-Accessible Chromatin (ATAC)-sequencing

Purified cells from live cell FACS were input into a 15 µL transposase reaction[175] with an input of 65,000 cells for wild type (*Rlbp*-creER: tdTomato), 85,000 cells for tamoxifen (*Glast*-CreER Ascl1-overexpressing animals) only, 100,000 cells for tamoxifen + NMDA, 85,000 cells for tamoxifen + TSA, and 130,000 cells for ANT treatment. For *Grm6*-tdTomato mice, 100,000 cells were collected. Transposition was carried out with reagents from the Nextera DNA Sample prep kit: 7.5 µL 2X TD Buffer, 0.75 µL Tn5 Transposases, and nuclease-free water to 15 µL. The reaction was mixed and incubated at 37 °C for one hour before being purified with the Qiagen Reaction Cleanup Minelute kit and eluted into 10 µL. Samples were then amplified by PCR with Nextera primers (Nextera barcodes N701-N706) in a 50 µL reaction with 2x PCR master mix

(NEB Cat no.: M0541) and 0.5 µL 100x SYBR Green I. PCR cycled as: 1) 72 °C, 5 min, 2) 98 °C, 30 sec, 3) 98 °C, 10 sec, 4) 63 °C, 30 sec, 5) 72 °C, 1 min, 6) Repeat 3-5 for 4 cycles. Libraries were then monitored with qPCR: 5 µL PCR sample in a 15 µL reaction with the same Nextera primers, NEB 2x PCR master mix and SYBR green. qPCR cycled as: 1) 98 °C, 30 sec, 2) 98 °C, 10 sec, 3) 63 °C, 30 sec, 4) 72 °C, 1 min, 5) Repeat 2-4 for 29 cycles. qPCR output was monitored for the delta RN; ¼ ΔRN cycle number was used to estimate the number of additional cycles of the PCR reaction needed for the remaining PCR samples. WT received 9 cycles, tamoxifen-only 6 cycles, tamoxifen + NMDA 12 cycles, tamoxifen + TSA 9 cycles, and ANT treatment 6 cycles. Amplified libraries were purified with the Qiagen PCR cleanup minelute kit and eluted into 20 µL. Library QC was performed using gel electrophoresis. 6 µL of each library sample was run on a 5 % Bio-Rad mini-Protean TBE Precast Gel in TBE. Gel was stained using 1x SYBR Gold in TBE for 30 minutes before imaging. Libraries were quantitated on a Qubit 3.0 Fluorometer with the dsDNA HS Assay kit and A260/280 and A260/230 checked by nanodrop before sending for Illumina NextGen sequencing on a HiSeq 2500 in rapid mode employing a paired-end 50 base read length sequencing strategy. Image analysis and base calling were performed using Illumina's Real Time Analysis v1.18 software, followed by 'demultiplexing' of indexed reads and generation of FASTQ files, using Illumina's bcl2fastq Conversion Software v1.8.4.

Reads were mapped using Bowtie. Files were downsampled to normalize for equivalent peaks across samples, using Samtools,. Mapped reads for downsampled files were: WT 6662388, A+N 20292142, A+T 4154220, A+N+T 16146406. Peaks were called using HOMER (Hypergeometric Optimization of Motif EnRichment) findPeaks histone style with a minimum distance of 415 and size of 150. Final peak call numbers were: WT 42535, Ascl1 41345, A+N

43429, A+T 42599, A+N+T 43267. Bedops was used to compare peak files. Gene ontology was first analyzed by the Genomic Regions Enrichment of Annotations Tool (GREAT) to get annotations of peak associations with genes. Gene lists were further filtered in R to enrich for those genes with the greatest changes in accessibility by selecting those genes with 5 or more associated peaks. Gene lists were analyzed for ontology using G:profiler. Bam files were converted to bigwig files for track visualization,and loaded onto the Integrative Genomics View browser. Motif enrichment was performed with HOMER software using the findMotifs program with default parameters.

Chromatin Immunoprecipitation (ChIP)

For Otx2 ChIP-seq, all cells from FACS purification were input into the respective ChIP reactions: 490,430 cells in ANT-treated condition and 692,271 cells in untreated condition. Post-FACS-purified cells were pelleted at 400 g for 20 minutes and washed in PBS at 4 °C. Chromatin shearing by sonication was performed with a probe sonicator (Fisher Scientific ultrasonic dismembrator model 150e) with parameters: 12 pulses of 100 Joules, amplitude 35, offset of 45 seconds at 4 °C. 1200 µL of sheared chromatin was divided into 2 x 500 µL samples for anti-OTX2/IgG control IPs and 150 µL for input DNA controls. Immunoprecipitation was performed with 11 µL Protein-G coated beads (DiaMag Protein-G coated magnetic beads, Diagenode Cat. No.: C03010021-150) and 2 µg goat anti-hOTX2 antibody (R&D Systems BAF1979) or 2 µg goat IgG (R&D Systems AB-108-C) per IP reaction according to LowCell# ChIP Kit (Diagenode, Liège, Belgium). DNA was purified with phenol/chloroform/isoamyl-alcohol and resuspended in 30 µL of TE buffer.

Libraries were prepared from ChIP DNAs with the KAPA Hyper Library prep kit (KAPA Biosystems, Wilmington, MA) using SeqCap Adapters (Roche-Nimblegen, Pleasanton, CA). Library size distributions were validated using the Agilent High Sensitivity D1000 ScreenTape run on an Agilent 2200 TapeStation (Agilent Technologies, Inc., Santa Clara, CA). Additional library QC, blending of pooled indexed libraries, and cluster optimization was performed using Life Technologies- Invitrogen Qubit® 2.0 Fluorometer (Life Technologies-Invitrogen, Carlsbad, CA, USA). ChIP-seq libraries were pooled (4-plex) and clustered onto a flow cell lane. Sequencing was performed using an Illumina HiSeq 2500 in rapid mode employing a paired-end, 50 base read length (PE50) sequencing strategy. Image analysis and base calling were be performed using Illumina's Real Time Analysis v1.18 software, followed by 'demultiplexing' of indexed reads and generation of FASTQ files, using Illumina's bcl2fastq Conversion Software v1.8.4.

Paired end reads were aligned to mm9 using bowtie2 v2.2.8 using default parameters. The number of aligned, mapped fragments were: Input-Ascl1, 18,967,599; Input-ANT, 27,060,224; OTX2-IP-Ascl1, 3,627,010; OTX2-IP-ANT, 5,917,349. Peak calling and motif enrichment was performed with HOMER software. Peaks were called using DNA input samples as controls with findPeaks parameters: Tag Threshold = 4, fold threshold (L) = 3, and Poisson p-value (LP) = 0.001. Motif enrichment used the findMotifs program with default parameters. Overlap analysis of Otx2 peaks and motifs was performed with Bedops[176] using a 1bp overlap requirement. Heat maps were generated with Bioconductor Genomation.

For H3K27ac ChIP-qPCR, FACS ANT (80,000 cells) and WT (*Rlbp*-CreER: tdTomato, 100,000 cells) cells were digested with 0.5 U MNase in Digestion buffer (50 mM TrisHCl pH 7.5, 1 mM CaCl2, 0.2% Triton X-100, 1X EDTA-free proteinase inhibitors) at 37 °C for 10

minutes before stopping with 5 mM EDTA. Digested chromatin was immunoprecipitated with rabbit anti-H3K27ac (Abcam, 3 μg per IP) according to Valensisi et al[177]. Eluted DNA was run by qPCR for promoter regions of Hes5, Dll3, Nefl, and HoxB2 (primers available upon request) and were run in triplicate. All samples were compared to an equivalent volume input chromatin by equation $2^{(input-IP)}$. Percent input was normalized for each gene to WT=100%.

For Ascl1-ChIP-seq, P0 retinas or cultured, post-natal day 12, Müller glia (+/- Ascl1 overexpression, *rtTA germline:tetO-Ascl1-ires-GFP* mice ± doxycycline) were digested with papain/DNase to single cells and fixed with 0.75 % formaldehyde for 10 minutes at room temperature. Sonication was performed with a probe sonicator (Fisher Scientific): 12 pulses, 100 J/pulse, Amplitude: 45, 45 seconds cooling at 4 ºC between pulses. Immunoprecipitation performed with 40 μL anti-mouse IgG magnetic beads (Invitrogen Cat: 110.31) and 4 μg mouse anti-MASH1 antibody (BD Pharmingen Cat: 556604) or 4 μg mouse IgG against chromatin from 5 million cells per condition according to Diagenode LowCell Number Kit using IP and Wash buffers as described in[76]. Libraries were prepared with standard Illumina adaptors and sequenced to an approximate depth of 36 million reads each. Sequence reads (36 bp) were mapped to the mouse mm9 genome using bwa (v 0.7.12-r1039). Merging and sorting of sequencing reads from different lanes was performed with SAMtools (v1.2). The HOMER software suite was used to determine and score peak calls ('findPeaks' function, v4.7) as well as motif enrichment ('findMotifs' function, v4.7, using repeat mask). Peak overlap analyses were performed using Bedops.

DNase I Hypersensititivy-Sequencing (DNase-Seq)

Detailed protocols can be found at encodeproject.org. In brief: nuclei from retina were isolated using 25 strokes of a dounce homogenizer, tight pestle, in 3 mL homogenization buffer (20 mM tricine, 25 mM D-sucrose, 15 mM NaCl, 60 mM KCl, 2 mM $MgCl_2$, 0.5 mM spermidine, pH 7.8) and filtered through a 100 μm filter and washed with Buffer A (15 mM Tris-HCl, 15 mM NaCl, 60 mM KCl, 1 mM EDTA, 0.5 mM EGTA, 0.5 mM spermidine). Nuclei from Müller glia were isolated using TrypLE (Thermofisher) to obtain single cells, followed by incubation with 0.04 % IGEPAL in Buffer A for 10 minutes at 4 ºC. Nuclei were incubated at 37 ºC for 3 minutes in limiting concentrations of DNaseI enzyme in Buffer A with calcium supplement. The reaction was stopped using equal volume of Stop Buffer (50 mM Tris-HCl, 100 mM NaCl, 0.1 % SDS, 100 mM EDTA, 1 mM spermidine, 0.5 spermine pH 8.0) and subsequently treated with proteinase K and RNase A at 55 ºC. Small (<750 bp) DNA fragments were isolated by sucrose ultracentrifugation and end repaired and ligated with Illumina compatible adaptors. Sequence reads were mapped to mm9 using bowtie (v 0.12.7) and DNaseI peak calling performed with Hotspot (http://www.uwencode.org/proj/hotspot/).

Primary Cell Culture

Postnatal day 0, 11/12 retinas of both sexes from *rtTA germline:tetO-Ascl1-ires-GFP* mice were digested with papain/DNase to single cells and MG were grown in culture as previously described[74,173]. In brief, retinas were placed in a papain solution with 180 units/mL DNase (Worthington) and incubated at 37 ºC for 10 min. Cells were triturated and added to an

equal ovomucoid (Worthington) volume then spun down at 300 g at 4 ºC to pellet. Cells were then resuspended in Neurobasal with 10 % FBS (Clontech), mEGF (100 ng/mL; R&D Systems), 1 mM L-glutamine (Invitrogen), N2 (Invitrogen), and 1 % Penicillin-Streptomycin (Invitrogen) with two retinas plated per 10 cm^2 at 37 ºC. Media was changed every 2 days until confluent monolayers of MG were passaged after 7 DIV and doxycycline was added to induce expression of Ascl1.

Electrophysiology

Electrophysiology experiments were conducted in retinal slice (200 μm thick) preparations taken from dark-adapted mice. Retinas were isolated under infrared visualization and stored in oxygenated (95% O_2/5% CO_2) Ames medium (Sigma) at ~32-34 °C. Once under the microscope, tissue preparations were perfused by the same Ames solution at a rate of ~8 mL/min. Isolated retinas were embedded in agarose and sliced as previously described[178,179]. Retinal neurons were visualized and targeted for whole-cell recordings using video DIC with an infrared light source (>950 nm) and GFP-positive cells were targeted using two-photon (□=980 nm) or confocal (□=488 nm) microscopy. For all cells targeted under infrared illumination, a full field illumination (diameter: 560 μm) was delivered to the preparation through a customized condenser from blue (peak power at 470 nm) or green (peak power at 510 nm) LEDs. Cells targeted using the visible 488 nm laser were primarily used for measurements of input resistance and resting membrane potential. Images shown are 2D projections of 3D image stacks acquired with a two-photon or confocal microscope.

Whole-cell recordings were obtained using pipettes (5-6 MΩ) filled with an intracellular solution containing (in mM): 123 K-aspartate, 10 KCl, 10 HEPES, 1 $MgCl_2$, 1 $CaCl_2$, 2 EGTA, 4 Mg-ATP, 0.5 Tris-GTP and 0.1 Alexa (594) hydrazide (~280 mOsm; pH ~7.2 with KOH). To isolate excitatory or inhibitory synaptic input, cells were held at the estimated reversal potential for inhibitory or excitatory input of ~-60 mV and ~+10 mV. Absolute voltage values were not corrected for liquid junction potentials (K+-based = -10.8 mV; Cs+-based = -8.5 mV). MG-derived GFP+ cells exhibited much higher input resistance than normal MG, characteristic of excitable cells near their resting potential; this would be expected to lead to the sizeable voltage changes in response to synaptic input that we observed.

Due to technical limitations, we were not able to assess outputs of the GFP+ cells with the same methods. Many of the ganglion cells were destroyed by the NMDA, and to record from the approximately 20% that remain to confirm that they receive direct input from the MG-derived neurons would be technically challenging. Demonstrating direct MG-derived neuronal output onto a ganglion cell would require random patching onto ganglion cells downstream of the GFP+ processes with paired recording techniques on rare cell populations. Additionally, ensuring both cells are at a feasible recording depth within the retinal slice would compound the complexity of such an experiment.

Serial Block-Face Scanning Electron Microscopy (SBFSEM)

Freshly dissected retinas were fixed in 4% glutaraldehyde in 0.1 M sodium cacodylate buffer (pH 7.4) for 30 minutes, then trimmed into 2 x 2 mm trapezoidal sections to maintain orientation. Sections were then coverslipped on a slide within an insert and imaged on a two-

photon microscope with Ti:sapphire laser (Spectra-Physics) at 60x magnification. Once the cell of interest was located, a ~50 x 50 μm box was branded using the two-photon laser[180] (near-infrared branding or NIRB) around the soma by increasing the laser power of the 880 nm beam and exposing the tissue to it for 5 seconds. Two notches were NIRBed in the X and Y planes of the box that point to and demarcate the soma of the cell of interest. To localize the region containing the cell of interest prior to serial sectioning, a larger 100 x 100 μm box was NIRBed above the cell in the ganglion cell layer. The issue was then stained, dehydrated, and embedded in Durcupan resin following a previously established protocol[181]. SBFSEM was performed on the Zeiss 3 View of a region of interest comprising 2 x 2 tiles, each 7000 x 7000 pixels (~40 x 40 μm) at a section thickness of 70 nm. Images were then aligned and the cell of interest was traced using TrackEM2 (NIH, Bethesda).

Quantitative reverse transcription PCR (RT-qPCR)

Glast-CreER:LNL-tTA:tetO-mAscl1-ires-GFP mice received 3 days of tamoxifen injections to induce Ascl1 expression on treatment days 1 through 3. On treatment day 13, WT and Ascl1 expressing mice received an intravitreal injection of 100 mM NMDA in 1.5 μL volume. Four days after NMDA administration WT and Ascl1 expressing mice were euthanized and retinas collected and digested in TRIzol reagent (Thermo Fischer). RNA was extracted and collected in miRNeasy Mini Kit columns in accordance with manufacturer instructions (Qiagen). Reverse transcription was performed on 1 μg of purified RNA using the iScript Reverse Transcription Supermix kit (Bio-Rad). The cDNA was then added to SsoFast (Bio-Rad) for qPCR. A total of 4 biological replicates were run for each condition (WT, WT + NMDA, Ascl1,

Ascl1 + NMDA) and each biological replicate was run in triplicate. Id1 cycles were subtracted from housekeeping gene Gapdh (ΔCt) and then subtracted from WT (ΔΔCt) to determine fold change $2^{(-\Delta\Delta Ct)}$. Primers for Gapdh were (5′-GGCATTGCTCTCAATGACAA-3′ and 5′-CTTGCTCAGTGTCCTTGCTG-3′) and primers used for Id1 were (5′-TACGACATGAACGGCTGCTACTCA-3′ and 5′-TTACATGCTGCAGGATCTCCACCT-3′).

Statistics

All statistics for WB and IHC were performed on Prism GraphPad 5, or with R, version 3.2.3 "Wooden Christmas Tree". The Shapiro-Wilks test (R) or Kolmogorov-Smirnov test (Prism) were used to determine normality. *t*-tests were two-tailed. Both *t*-tests and ANOVA were significant if $P<0.05$. Primary findings shown in Figure 3.1 were repeated five times in separate cohorts of animals.

Animals

All mice were housed at the University of Washington and treated with protocols approved by the University of Washington's Institutional Animal Care and Use Committee. Mice expressed cre-recombinase under one of two different promoters (*Rlbp*-CreER from Dr. E. Levine (Vanderbilt University) and *Glast*-CreER from Jackson Labs) and mice with Rosa-Flox-stop-tTA (Jackson labs) have been previously described. tetO-mAscl1-ires-GFP mice were a gift from Dr. M. Nakafuku (University of Cincinnati). *Grm6*-tdTomato mice have been previous described[182]. The *rtTA germline*: *tetO-mAscl1-ires-GFP* mice for in vitro experiments were

generated by crossing Nakafuku's *tetO-mAscl1-ires-GFP* mice onto the germline rtTA mice from Jackson Labs. Adult mice of both sexes were used for this study and analyzed together in their respective treatment groups.

References

1 Cajal, S. R. Die Retina der Wirbelthiere. *Рипол Классик* (1894).

2 Rheaume, B. A. *et al.* Single cell transcriptome profiling of retinal ganglion cells identifies cellular subtypes. *Nat Commun* **9**, 2759, doi:10.1038/s41467-018-05134-3 (2018).

3 Franke, K. *et al.* Inhibition decorrelates visual feature representations in the inner retina. *Nature* **542**, 439-444, doi:10.1038/nature21394 (2017).

4 Greene, M. J., Kim, J. S., Seung, H. S. & EyeWirers. Analogous Convergence of Sustained and Transient Inputs in Parallel On and Off Pathways for Retinal Motion Computation. *Cell Rep* **14**, 1892-1900, doi:10.1016/j.celrep.2016.02.001 (2016).

5 Shekhar, K. *et al.* Comprehensive Classification of Retinal Bipolar Neurons by Single-Cell Transcriptomics. *Cell* **166**, 1308-1323 e1330, doi:10.1016/j.cell.2016.07.054 (2016).

6 Balasubramanian, R. & Gan, L. Development of Retinal Amacrine Cells and Their Dendritic Stratification. *Curr Ophthalmol Rep* **2**, 100-106, doi:10.1007/s40135-014-0048-2 (2014).

7 Demb, J. B. & Singer, J. H. Functional Circuitry of the Retina. *Annu Rev Vis Sci* **1**, 263-289, doi:10.1146/annurev-vision-082114-035334 (2015).

8 Vlasits, A. L., Euler, T. & Franke, K. Function first: classifying cell types and circuits of the retina. *Curr Opin Neurobiol* **56**, 8-15, doi:10.1016/j.conb.2018.10.011 (2018).

9 Bassett, E. A. & Wallace, V. A. Cell fate determination in the vertebrate retina. *Trends Neurosci* **35**, 565-573, doi:10.1016/j.tins.2012.05.004 (2012).

10 Masland, R. H. The neuronal organization of the retina. *Neuron* **76**, 266-280, doi:10.1016/j.neuron.2012.10.002 (2012).

11 Famiglietti, E. V., Jr. & Kolb, H. A bistratified amacrine cell and synaptic cirucitry in the inner plexiform layer of the retina. *Brain Res* **84**, 293-300 (1975).

12 Nelson, R. AII amacrine cells quicken time course of rod signals in the cat retina. *J Neurophysiol* **47**, 928-947, doi:10.1152/jn.1982.47.5.928 (1982).

13 Nelson, R. & Kolb, H. A17: a broad-field amacrine cell in the rod system of the cat retina. *J Neurophysiol* **54**, 592-614, doi:10.1152/jn.1985.54.3.592 (1985).

14 Strettoi, E., Dacheux, R. F. & Raviola, E. Synaptic connections of rod bipolar cells in the inner plexiform layer of the rabbit retina. *J Comp Neurol* **295**, 449-466, doi:10.1002/cne.902950309 (1990).

15 Strettoi, E., Raviola, E. & Dacheux, R. F. Synaptic connections of the narrow-field, bistratified rod amacrine cell (AII) in the rabbit retina. *J Comp Neurol* **325**, 152-168, doi:10.1002/cne.903250203 (1992).

16 Macadam, D. L. Color Science - Concepts and Methods, Quantitative Data and Formulas, 2nd Edition - Wyszecki,G, Stiles,Ws. *Opt Eng* **22**, S116-S117 (1983).

17 Saine, P. J. Ophthalmic photography books: an historical bibliography. *J Ophthalmic Photogr* **16**, 78-82 (1994).

18 Breuninger, T., Puller, C., Haverkamp, S. & Euler, T. Chromatic bipolar cell pathways in the mouse retina. *J Neurosci* **31**, 6504-6517, doi:10.1523/JNEUROSCI.0616-11.2011 (2011).

19 Li, W. & DeVries, S. H. Bipolar cell pathways for color and luminance vision in a dichromatic mammalian retina. *Nat Neurosci* **9**, 669-675, doi:10.1038/nn1686 (2006).

20 Swaroop, A., Kim, D. & Forrest, D. Transcriptional regulation of photoreceptor development and homeostasis in the mammalian retina. *Nat Rev Neurosci* **11**, 563-576, doi:10.1038/nrn2880 (2010).

21 Nishida, A. *et al.* Otx2 homeobox gene controls retinal photoreceptor cell fate and pineal gland development. *Nat Neurosci* **6**, 1255-1263, doi:10.1038/nn1155 (2003).
22 Koike, C. *et al.* Functional roles of Otx2 transcription factor in postnatal mouse retinal development. *Mol Cell Biol* **27**, 8318-8329, doi:10.1128/MCB.01209-07 (2007).
23 Furukawa, T., Morrow, E. M., Li, T., Davis, F. C. & Cepko, C. L. Retinopathy and attenuated circadian entrainment in Crx-deficient mice. *Nat Genet* **23**, 466-470, doi:10.1038/70591 (1999).
24 Mitton, K. P. *et al.* The leucine zipper of NRL interacts with the CRX homeodomain. A possible mechanism of transcriptional synergy in rhodopsin regulation. *J Biol Chem* **275**, 29794-29799, doi:10.1074/jbc.M003658200 (2000).
25 Pittler, S. J. *et al.* Functional analysis of the rod photoreceptor cGMP phosphodiesterase alpha-subunit gene promoter: Nrl and Crx are required for full transcriptional activity. *J Biol Chem* **279**, 19800-19807, doi:10.1074/jbc.M401864200 (2004).
26 Mears, A. J. *et al.* Nrl is required for rod photoreceptor development. *Nat Genet* **29**, 447-452, doi:10.1038/ng774 (2001).
27 Oh, E. C. *et al.* Transformation of cone precursors to functional rod photoreceptors by bZIP transcription factor NRL. *Proc Natl Acad Sci U S A* **104**, 1679-1684, doi:10.1073/pnas.0605934104 (2007).
28 Oh, E. C. *et al.* Rod differentiation factor NRL activates the expression of nuclear receptor NR2E3 to suppress the development of cone photoreceptors. *Brain Res* **1236**, 16-29, doi:10.1016/j.brainres.2008.01.028 (2008).
29 Peng, G. H., Ahmad, O., Ahmad, F., Liu, J. & Chen, S. The photoreceptor-specific nuclear receptor Nr2e3 interacts with Crx and exerts opposing effects on the transcription of rod versus cone genes. *Hum Mol Genet* **14**, 747-764, doi:10.1093/hmg/ddi070 (2005).
30 Cheng, H. *et al.* In vivo function of the orphan nuclear receptor NR2E3 in establishing photoreceptor identity during mammalian retinal development. *Hum Mol Genet* **15**, 2588-2602, doi:10.1093/hmg/ddl185 (2006).
31 Chen, J., Rattner, A. & Nathans, J. The rod photoreceptor-specific nuclear receptor Nr2e3 represses transcription of multiple cone-specific genes. *J Neurosci* **25**, 118-129, doi:10.1523/JNEUROSCI.3571-04.2005 (2005).
32 Cheng, H. *et al.* Photoreceptor-specific nuclear receptor NR2E3 functions as a transcriptional activator in rod photoreceptors. *Hum Mol Genet* **13**, 1563-1575, doi:10.1093/hmg/ddh173 (2004).
33 Jia, L. *et al.* Retinoid-related orphan nuclear receptor RORbeta is an early-acting factor in rod photoreceptor development. *Proc Natl Acad Sci U S A* **106**, 17534-17539, doi:10.1073/pnas.0902425106 (2009).
34 Srinivas, M., Ng, L., Liu, H., Jia, L. & Forrest, D. Activation of the blue opsin gene in cone photoreceptor development by retinoid-related orphan receptor beta. *Mol Endocrinol* **20**, 1728-1741, doi:10.1210/me.2005-0505 (2006).
35 Ng, L. *et al.* A thyroid hormone receptor that is required for the development of green cone photoreceptors. *Nat Genet* **27**, 94-98, doi:10.1038/83829 (2001).
36 Eldred, K. C. *et al.* Thyroid hormone signaling specifies cone subtypes in human retinal organoids. *Science* **362**, doi:10.1126/science.aau6348 (2018).
37 MacNeil, M. A., Heussy, J. K., Dacheux, R. F., Raviola, E. & Masland, R. H. The population of bipolar cells in the rabbit retina. *J Comp Neurol* **472**, 73-86, doi:10.1002/cne.20063 (2004).

38 Wassle, H., Puller, C., Muller, F. & Haverkamp, S. Cone contacts, mosaics, and territories of bipolar cells in the mouse retina. *J Neurosci* **29**, 106-117, doi:10.1523/JNEUROSCI.4442-08.2009 (2009).
39 Kuffler, S. W. Discharge patterns and functional organization of mammalian retina. *J Neurophysiol* **16**, 37-68, doi:10.1152/jn.1953.16.1.37 (1953).
40 Jackman, S. L., Babai, N., Chambers, J. J., Thoreson, W. B. & Kramer, R. H. A positive feedback synapse from retinal horizontal cells to cone photoreceptors. *PLoS Biol* **9**, e1001057, doi:10.1371/journal.pbio.1001057 (2011).
41 Hirano, A. A., Brandstatter, J. H. & Brecha, N. C. Cellular distribution and subcellular localization of molecular components of vesicular transmitter release in horizontal cells of rabbit retina. *J Comp Neurol* **488**, 70-81, doi:10.1002/cne.20577 (2005).
42 Erskine, L. & Herrera, E. Connecting the retina to the brain. *ASN Neuro* **6**, doi:10.1177/1759091414562107 (2014).
43 Decembrini, S., Andreazzoli, M., Vignali, R., Barsacchi, G. & Cremisi, F. Timing the generation of distinct retinal cells by homeobox proteins. *PLoS Biol* **4**, e272, doi:10.1371/journal.pbio.0040272 (2006).
44 Vitorino, M. *et al.* Vsx2 in the zebrafish retina: restricted lineages through derepression. *Neural Dev* **4**, 14, doi:10.1186/1749-8104-4-14 (2009).
45 Elshatory, Y. *et al.* Islet-1 controls the differentiation of retinal bipolar and cholinergic amacrine cells. *J Neurosci* **27**, 12707-12720, doi:10.1523/JNEUROSCI.3951-07.2007 (2007).
46 Feng, L. *et al.* Requirement for Bhlhb5 in the specification of amacrine and cone bipolar subtypes in mouse retina. *Development* **133**, 4815-4825, doi:10.1242/dev.02664 (2006).
47 Brzezinski, J. A. t., Lamba, D. A. & Reh, T. A. Blimp1 controls photoreceptor versus bipolar cell fate choice during retinal development. *Development* **137**, 619-629, doi:10.1242/dev.043968 (2010).
48 Masai, I., Stemple, D. L., Okamoto, H. & Wilson, S. W. Midline signals regulate retinal neurogenesis in zebrafish. *Neuron* **27**, 251-263 (2000).
49 Kay, J. N., Finger-Baier, K. C., Roeser, T., Staub, W. & Baier, H. Retinal ganglion cell genesis requires lakritz, a Zebrafish atonal Homolog. *Neuron* **30**, 725-736 (2001).
50 Liu, W., Mo, Z. & Xiang, M. The Ath5 proneural genes function upstream of Brn3 POU domain transcription factor genes to promote retinal ganglion cell development. *Proc Natl Acad Sci U S A* **98**, 1649-1654, doi:10.1073/pnas.98.4.1649 (2001).
51 Turner, D. L. & Cepko, C. L. A common progenitor for neurons and glia persists in rat retina late in development. *Nature* **328**, 131-136, doi:10.1038/328131a0 (1987).
52 Jadhav, A. P., Roesch, K. & Cepko, C. L. Development and neurogenic potential of Muller glial cells in the vertebrate retina. *Prog Retin Eye Res* **28**, 249-262, doi:10.1016/j.preteyeres.2009.05.002 (2009).
53 Tomita, K. *et al.* Mammalian hairy and Enhancer of split homolog 1 regulates differentiation of retinal neurons and is essential for eye morphogenesis. *Neuron* **16**, 723-734 (1996).
54 Hojo, M. *et al.* Glial cell fate specification modulated by the bHLH gene Hes5 in mouse retina. *Development* **127**, 2515-2522 (2000).
55 Hippert, C. *et al.* Muller glia activation in response to inherited retinal degeneration is highly varied and disease-specific. *PLoS One* **10**, e0120415, doi:10.1371/journal.pone.0120415 (2015).

56 Powell, C., Grant, A. R., Cornblath, E. & Goldman, D. Analysis of DNA methylation reveals a partial reprogramming of the Muller glia genome during retina regeneration. *Proc Natl Acad Sci U S A* **110**, 19814-19819, doi:10.1073/pnas.1312009110 (2013).

57 Lenkowski, J. R. & Raymond, P. A. Muller glia: Stem cells for generation and regeneration of retinal neurons in teleost fish. *Prog Retin Eye Res* **40**, 94-123, doi:10.1016/j.preteyeres.2013.12.007 (2014).

58 Raymond, P. A. Movement of retinal terminals in goldfish optic tectum predicted by analysis of neuronal proliferation. *J Neurosci* **6**, 2479-2488 (1986).

59 Moshiri, A., Close, J. & Reh, T. A. Retinal stem cells and regeneration. *Int J Dev Biol* **48**, 1003-1014, doi:10.1387/ijdb.041870am (2004).

60 Kubota, R., Hokoc, J. N., Moshiri, A., McGuire, C. & Reh, T. A. A comparative study of neurogenesis in the retinal ciliary marginal zone of homeothermic vertebrates. *Brain Res Dev Brain Res* **134**, 31-41 (2002).

61 Sperry, R. W. Patterning of central synapses in regeneration of the optic nerve in teleosts. *Physiol Zool* **21**, 351-361 (1948).

62 Maier, W. & Wolburg, H. Regeneration of the goldfish retina after exposure to different doses of ouabain. *Cell Tissue Res* **202**, 99-118 (1979).

63 Raymond, P. A., Reifler, M. J. & Rivlin, P. K. Regeneration of goldfish retina: rod precursors are a likely source of regenerated cells. *J Neurobiol* **19**, 431-463, doi:10.1002/neu.480190504 (1988).

64 Otteson, D. C. & Hitchcock, P. F. Stem cells in the teleost retina: persistent neurogenesis and injury-induced regeneration. *Vision Res* **43**, 927-936 (2003).

65 Fischer, A. J. & Reh, T. A. Muller glia are a potential source of neural regeneration in the postnatal chicken retina. *Nat Neurosci* **4**, 247-252, doi:10.1038/85090 (2001).

66 Fausett, B. V. & Goldman, D. A role for alpha1 tubulin-expressing Muller glia in regeneration of the injured zebrafish retina. *J Neurosci* **26**, 6303-6313, doi:10.1523/JNEUROSCI.0332-06.2006 (2006).

67 Bernardos, R. L., Barthel, L. K., Meyers, J. R. & Raymond, P. A. Late-stage neuronal progenitors in the retina are radial Muller glia that function as retinal stem cells. *J Neurosci* **27**, 7028-7040, doi:10.1523/JNEUROSCI.1624-07.2007 (2007).

68 Kassen, S. C. *et al.* Time course analysis of gene expression during light-induced photoreceptor cell death and regeneration in albino zebrafish. *Dev Neurobiol* **67**, 1009-1031, doi:10.1002/dneu.20362 (2007).

69 Morris, A. C., Forbes-Osborne, M. A., Pillai, L. S. & Fadool, J. M. Microarray analysis of XOPS-mCFP zebrafish retina identifies genes associated with rod photoreceptor degeneration and regeneration. *Invest Ophthalmol Vis Sci* **52**, 2255-2266, doi:10.1167/iovs.10-6022 (2011).

70 Qin, Z., Barthel, L. K. & Raymond, P. A. Genetic evidence for shared mechanisms of epimorphic regeneration in zebrafish. *Proc Natl Acad Sci U S A* **106**, 9310-9315, doi:10.1073/pnas.0811186106 (2009).

71 Ramachandran, R., Zhao, X. F. & Goldman, D. Insm1a-mediated gene repression is essential for the formation and differentiation of Muller glia-derived progenitors in the injured retina. *Nat Cell Biol* **14**, 1013-1023, doi:10.1038/ncb2586 (2012).

72 Fausett, B. V., Gumerson, J. D. & Goldman, D. The proneural basic helix-loop-helix gene ascl1a is required for retina regeneration. *J Neurosci* **28**, 1109-1117, doi:10.1523/JNEUROSCI.4853-07.2008 (2008).

73 Gorsuch, R. A. & Hyde, D. R. Regulation of Muller glial dependent neuronal regeneration in the damaged adult zebrafish retina. *Exp Eye Res* **123**, 131-140, doi:10.1016/j.exer.2013.07.012 (2014).

74 Pollak, J. *et al.* ASCL1 reprograms mouse Muller glia into neurogenic retinal progenitors. *Development* **140**, 2619-2631, doi:10.1242/dev.091355 (2013).

75 Nelson, B. R. *et al.* Acheate-scute like 1 (Ascl1) is required for normal delta-like (Dll) gene expression and notch signaling during retinal development. *Dev Dyn* **238**, 2163-2178, doi:10.1002/dvdy.21848 (2009).

76 Castro, D. S. *et al.* A novel function of the proneural factor Ascl1 in progenitor proliferation identified by genome-wide characterization of its targets. *Genes Dev* **25**, 930-945, doi:10.1101/gad.627811 (2011).

77 Cao, R. *et al.* Role of histone H3 lysine 27 methylation in Polycomb-group silencing. *Science* **298**, 1039-1043, doi:10.1126/science.1076997 (2002).

78 Boyer, L. A. *et al.* Polycomb complexes repress developmental regulators in murine embryonic stem cells. *Nature* **441**, 349-353, doi:10.1038/nature04733 (2006).

79 Karlic, R., Chung, H. R., Lasserre, J., Vlahovicek, K. & Vingron, M. Histone modification levels are predictive for gene expression. *Proc Natl Acad Sci U S A* **107**, 2926-2931, doi:10.1073/pnas.0909344107 (2010).

80 Mori, T. *et al.* Inducible gene deletion in astroglia and radial glia--a valuable tool for functional and lineage analysis. *Glia* **54**, 21-34, doi:10.1002/glia.20350 (2006).

81 Ueki, Y. *et al.* Transgenic expression of the proneural transcription factor Ascl1 in Muller glia stimulates retinal regeneration in young mice. *Proc Natl Acad Sci U S A* **112**, 13717-13722, doi:10.1073/pnas.1510595112 (2015).

82 Raymond, P. A., Barthel, L. K., Bernardos, R. L. & Perkowski, J. J. Molecular characterization of retinal stem cells and their niches in adult zebrafish. *BMC Dev Biol* **6**, 36, doi:10.1186/1471-213X-6-36 (2006).

83 Wan, J. & Goldman, D. Retina regeneration in zebrafish. *Curr Opin Genet Dev* **40**, 41-47, doi:10.1016/j.gde.2016.05.009 (2016).

84 Thummel, R., Kassen, S. C., Montgomery, J. E., Enright, J. M. & Hyde, D. R. Inhibition of Muller glial cell division blocks regeneration of the light-damaged zebrafish retina. *Dev Neurobiol* **68**, 392-408, doi:10.1002/dneu.20596 (2008).

85 Ramachandran, R., Fausett, B. V. & Goldman, D. Ascl1a regulates Muller glia dedifferentiation and retinal regeneration through a Lin-28-dependent, let-7 microRNA signalling pathway. *Nat Cell Biol* **12**, 1101-1107, doi:10.1038/ncb2115 (2010).

86 Karl, M. O. & Reh, T. A. Regenerative medicine for retinal diseases: activating endogenous repair mechanisms. *Trends Mol Med* **16**, 193-202, doi:10.1016/j.molmed.2010.02.003 (2010).

87 Biedermann, B., Bringmann, A. & Reichenbach, A. High-affinity GABA uptake in retinal glial (Muller) cells of the guinea pig: electrophysiological characterization, immunohistochemical localization, and modeling of efficiency. *Glia* **39**, 217-228, doi:10.1002/glia.10097 (2002).

88 Newman, E. A. Physiological properties and possible functions of Muller cells. *Neurosci Res Suppl* **4**, S209-220 (1986).

89 McLean, C. Y. *et al.* GREAT improves functional interpretation of cis-regulatory regions. *Nat Biotechnol* **28**, 495-501, doi:10.1038/nbt.1630 (2010).

90 Samuel, A., Housset, M., Fant, B. & Lamonerie, T. Otx2 ChIP-seq reveals unique and redundant functions in the mature mouse retina. *PLoS One* **9**, e89110, doi:10.1371/journal.pone.0089110 (2014).

91 Brzezinski, J. A. t., Kim, E. J., Johnson, J. E. & Reh, T. A. Ascl1 expression defines a subpopulation of lineage-restricted progenitors in the mammalian retina. *Development* **138**, 3519-3531, doi:10.1242/dev.064006 (2011).

92 Guo, Z. *et al.* In vivo direct reprogramming of reactive glial cells into functional neurons after brain injury and in an Alzheimer's disease model. *Cell Stem Cell* **14**, 188-202, doi:10.1016/j.stem.2013.12.001 (2014).

93 Liu, Y. *et al.* Ascl1 Converts Dorsal Midbrain Astrocytes into Functional Neurons In Vivo. *J Neurosci* **35**, 9336-9355, doi:10.1523/JNEUROSCI.3975-14.2015 (2015).

94 Niu, W. *et al.* SOX2 reprograms resident astrocytes into neural progenitors in the adult brain. *Stem Cell Reports* **4**, 780-794, doi:10.1016/j.stemcr.2015.03.006 (2015).

95 Torper, O. *et al.* In Vivo Reprogramming of Striatal NG2 Glia into Functional Neurons that Integrate into Local Host Circuitry. *Cell Rep* **12**, 474-481, doi:10.1016/j.celrep.2015.06.040 (2015).

96 Srivastava, D. & DeWitt, N. In Vivo Cellular Reprogramming: The Next Generation. *Cell* **166**, 1386-1396, doi:10.1016/j.cell.2016.08.055 (2016).

97 Gotz, M., Sirko, S., Beckers, J. & Irmler, M. Reactive astrocytes as neural stem or progenitor cells: In vivo lineage, In vitro potential, and Genome-wide expression analysis. *Glia* **63**, 1452-1468, doi:10.1002/glia.22850 (2015).

98 Heinrich, C., Spagnoli, F. M. & Berninger, B. In vivo reprogramming for tissue repair. *Nat Cell Biol* **17**, 204-211, doi:10.1038/ncb3108 (2015).

99 Sherpa, T. *et al.* Ganglion cell regeneration following whole-retina destruction in zebrafish. *Dev Neurobiol* **68**, 166-181, doi:10.1002/dneu.20568 (2008).

100 Reh, T. A., Nagy, T. & Gretton, H. Retinal pigmented epithelial cells induced to transdifferentiate to neurons by laminin. *Nature* **330**, 68-71, doi:10.1038/330068a0 (1987).

101 Coulombre, J. L. & Coulombre, A. J. Regeneration of neural retina from the pigmented epithelium in the chick embryo. *Dev Biol* **12**, 79-92 (1965).

102 Wilken, M. S. & Reh, T. A. Retinal regeneration in birds and mice. *Curr Opin Genet Dev* **40**, 57-64, doi:10.1016/j.gde.2016.05.028 (2016).

103 Karl, M. O. *et al.* Stimulation of neural regeneration in the mouse retina. *Proc Natl Acad Sci U S A* **105**, 19508-19513, doi:10.1073/pnas.0807453105 (2008).

104 Yao, K. *et al.* Wnt Regulates Proliferation and Neurogenic Potential of Muller Glial Cells via a Lin28/let-7 miRNA-Dependent Pathway in Adult Mammalian Retinas. *Cell Rep* **17**, 165-178, doi:10.1016/j.celrep.2016.08.078 (2016).

105 Elsaeidi, F. *et al.* Notch Suppression Collaborates with Ascl1 and Lin28 to Unleash a Regenerative Response in Fish Retina, But Not in Mice. *J Neurosci* **38**, 2246-2261, doi:10.1523/JNEUROSCI.2126-17.2018 (2018).

106 Jorstad, N. L. *et al.* Stimulation of functional neuronal regeneration from Muller glia in adult mice. *Nature* **548**, 103-107, doi:10.1038/nature23283 (2017).

107 Nelson, C. M. *et al.* Stat3 defines three populations of Muller glia and is required for initiating maximal muller glia proliferation in the regenerating zebrafish retina. *J Comp Neurol* **520**, 4294-4311, doi:10.1002/cne.23213 (2012).

108 Peterson, W. M., Wang, Q., Tzekova, R. & Wiegand, S. J. Ciliary neurotrophic factor and stress stimuli activate the Jak-STAT pathway in retinal neurons and glia. *J Neurosci* **20**, 4081-4090 (2000).

109 Ueki, Y., Wang, J., Chollangi, S. & Ash, J. D. STAT3 activation in photoreceptors by leukemia inhibitory factor is associated with protection from light damage. *J Neurochem* **105**, 784-796, doi:10.1111/j.1471-4159.2007.05180.x (2008).

110 Todd, L., Squires, N., Suarez, L. & Fischer, A. J. Jak/Stat signaling regulates the proliferation and neurogenic potential of Muller glia-derived progenitor cells in the avian retina. *Sci Rep* **6**, 35703, doi:10.1038/srep35703 (2016).

111 Kassen, S. C. *et al.* CNTF induces photoreceptor neuroprotection and Muller glial cell proliferation through two different signaling pathways in the adult zebrafish retina. *Exp Eye Res* **88**, 1051-1064, doi:10.1016/j.exer.2009.01.007 (2009).

112 Zhao, X. F. *et al.* Leptin and IL-6 family cytokines synergize to stimulate Muller glia reprogramming and retina regeneration. *Cell Rep* **9**, 272-284, doi:10.1016/j.celrep.2014.08.047 (2014).

113 Erickson, P. A., Fisher, S. K., Anderson, D. H., Stern, W. H. & Borgula, G. A. Retinal detachment in the cat: the outer nuclear and outer plexiform layers. *Invest Ophthalmol Vis Sci* **24**, 927-942 (1983).

114 Butler, A., Hoffman, P., Smibert, P., Papalexi, E. & Satija, R. Integrating single-cell transcriptomic data across different conditions, technologies, and species. *Nat Biotechnol* **36**, 411-420, doi:10.1038/nbt.4096 (2018).

115 Trapnell, C. *et al.* The dynamics and regulators of cell fate decisions are revealed by pseudotemporal ordering of single cells. *Nat Biotechnol* **32**, 381-386, doi:10.1038/nbt.2859 (2014).

116 Qiu, X. *et al.* Single-cell mRNA quantification and differential analysis with Census. *Nat Methods* **14**, 309-315, doi:10.1038/nmeth.4150 (2017).

117 Heinz, S. *et al.* Simple combinations of lineage-determining transcription factors prime cis-regulatory elements required for macrophage and B cell identities. *Mol Cell* **38**, 576-589, doi:10.1016/j.molcel.2010.05.004 (2010).

118 Wilken, M. S. *et al.* DNase I hypersensitivity analysis of the mouse brain and retina identifies region-specific regulatory elements. *Epigenetics Chromatin* **8**, 8, doi:10.1186/1756-8935-8-8 (2015).

119 Takahashi, K. & Yamanaka, S. Induction of pluripotent stem cells from mouse embryonic and adult fibroblast cultures by defined factors. *Cell* **126**, 663-676, doi:10.1016/j.cell.2006.07.024 (2006).

120 Chronis, C. *et al.* Cooperative Binding of Transcription Factors Orchestrates Reprogramming. *Cell* **168**, 442-459 e420, doi:10.1016/j.cell.2016.12.016 (2017).

121 Wapinski, O. L. *et al.* Hierarchical mechanisms for direct reprogramming of fibroblasts to neurons. *Cell* **155**, 621-635, doi:10.1016/j.cell.2013.09.028 (2013).

122 Benezra, R., Davis, R. L., Lockshon, D., Turner, D. L. & Weintraub, H. The protein Id: a negative regulator of helix-loop-helix DNA binding proteins. *Cell* **61**, 49-59 (1990).

123 Ruzinova, M. B. & Benezra, R. Id proteins in development, cell cycle and cancer. *Trends Cell Biol* **13**, 410-418 (2003).

124 Bai, G. *et al.* Id sustains Hes1 expression to inhibit precocious neurogenesis by releasing negative autoregulation of Hes1. *Dev Cell* **13**, 283-297, doi:10.1016/j.devcel.2007.05.014 (2007).

125 Boareto, M., Iber, D. & Taylor, V. Differential interactions between Notch and ID factors control neurogenesis by modulating Hes factor autoregulation. *Development* **144**, 3465-3474, doi:10.1242/dev.152520 (2017).
126 Nam, H. S. & Benezra, R. High levels of Id1 expression define B1 type adult neural stem cells. *Cell Stem Cell* **5**, 515-526, doi:10.1016/j.stem.2009.08.017 (2009).
127 Gomez, D. L. *et al.* Neurogenin 3 Expressing Cells in the Human Exocrine Pancreas Have the Capacity for Endocrine Cell Fate. *PLoS One* **10**, e0133862, doi:10.1371/journal.pone.0133862 (2015).
128 Guillemot, F. Cell fate specification in the mammalian telencephalon. *Prog Neurobiol* **83**, 37-52, doi:10.1016/j.pneurobio.2007.02.009 (2007).
129 Bonni, A. *et al.* Regulation of gliogenesis in the central nervous system by the JAK-STAT signaling pathway. *Science* **278**, 477-483 (1997).
130 He, F. *et al.* A positive autoregulatory loop of Jak-STAT signaling controls the onset of astrogliogenesis. *Nat Neurosci* **8**, 616-625, doi:10.1038/nn1440 (2005).
131 Barnabe-Heider, F. *et al.* Evidence that embryonic neurons regulate the onset of cortical gliogenesis via cardiotrophin-1. *Neuron* **48**, 253-265, doi:10.1016/j.neuron.2005.08.037 (2005).
132 Levine, E. M., Close, J., Fero, M., Ostrovsky, A. & Reh, T. A. p27(Kip1) regulates cell cycle withdrawal of late multipotent progenitor cells in the mammalian retina. *Dev Biol* **219**, 299-314, doi:10.1006/dbio.2000.9622 (2000).
133 Close, J. L., Gumuscu, B. & Reh, T. A. Retinal neurons regulate proliferation of postnatal progenitors and Muller glia in the rat retina via TGF beta signaling. *Development* **132**, 3015-3026, doi:10.1242/dev.01882 (2005).
134 Lillien, L. & Cepko, C. Control of proliferation in the retina: temporal changes in responsiveness to FGF and TGF alpha. *Development* **115**, 253-266 (1992).
135 Suga, A., Sadamoto, K., Fujii, M., Mandai, M. & Takahashi, M. Proliferation potential of Muller glia after retinal damage varies between mouse strains. *PLoS One* **9**, e94556, doi:10.1371/journal.pone.0094556 (2014).
136 Gallina, D., Palazzo, I., Steffenson, L., Todd, L. & Fischer, A. J. Wnt/beta-catenin-signaling and the formation of Muller glia-derived progenitors in the chick retina. *Dev Neurobiol* **76**, 983-1002, doi:10.1002/dneu.22370 (2016).
137 Vigushin, D. M. *et al.* Trichostatin A is a histone deacetylase inhibitor with potent antitumor activity against breast cancer in vivo. *Clin Cancer Res* **7**, 971-976 (2001).
138 Ailenberg, M. & Silverman, M. Trichostatin A-histone deacetylase inhibitor with clinical therapeutic potential-is also a selective and potent inhibitor of gelatinase A expression. *Biochem Biophys Res Commun* **298**, 110-115 (2002).
139 Liu, J. *et al.* A small-molecule agonist of the Wnt signaling pathway. *Angew Chem Int Ed Engl* **44**, 1987-1990, doi:10.1002/anie.200462552 (2005).
140 and, K. P. M. a. S. S. a. J. M. a. A. B. a. D. H. a. K. E. a. J.-P. V. a. T. G. H. Validation of an OptoMotry system for measurement of visual acuity in Han Wistar rats. *Journal of Pharmacological and Toxicological Methods* **58**, 152 (2008).
141 Powell, C., Cornblath, E., Elsaeidi, F., Wan, J. & Goldman, D. Zebrafish Muller glia-derived progenitors are multipotent, exhibit proliferative biases and regenerate excess neurons. *Sci Rep* **6**, 24851, doi:10.1038/srep24851 (2016).

142 Micah Chrenek, J. S., Stephanie Foster, Dustin Zuelke, Tiffany Liao, John Nickerson, Jeffrey Boatright. Light induced retinal damage in 129sv pigmented mice. *Invest Ophthalmol Vis Sci* **54** (2013).
143 Kim, S. R. *et al.* Rpe65 Leu450Met variant is associated with reduced levels of the retinal pigment epithelium lipofuscin fluorophores A2E and iso-A2E. *Proc Natl Acad Sci U S A* **101**, 11668-11672, doi:10.1073/pnas.0403499101 (2004).
144 Wenzel, A., Reme, C. E., Williams, T. P., Hafezi, F. & Grimm, C. The Rpe65 Leu450Met variation increases retinal resistance against light-induced degeneration by slowing rhodopsin regeneration. *J Neurosci* **21**, 53-58 (2001).
145 Chen, Y. *et al.* Inherent instability of the retinitis pigmentosa P23H mutant opsin. *J Biol Chem* **289**, 9288-9303, doi:10.1074/jbc.M114.551713 (2014).
146 Olsson, J. E. *et al.* Transgenic mice with a rhodopsin mutation (Pro23His): a mouse model of autosomal dominant retinitis pigmentosa. *Neuron* **9**, 815-830 (1992).
147 Aldiri, I. *et al.* The Dynamic Epigenetic Landscape of the Retina During Development, Reprogramming, and Tumorigenesis. *Neuron* **94**, 550-568 e510, doi:10.1016/j.neuron.2017.04.022 (2017).
148 Hickey, D. G. *et al.* Tropism of engineered and evolved recombinant AAV serotypes in the rd1 mouse and ex vivo primate retina. *Gene Ther* **24**, 787-800, doi:10.1038/gt.2017.85 (2017).
149 Day, T. P., Byrne, L. C., Schaffer, D. V. & Flannery, J. G. Advances in AAV vector development for gene therapy in the retina. *Adv Exp Med Biol* **801**, 687-693, doi:10.1007/978-1-4614-3209-8_86 (2014).
150 Watanabe, S. *et al.* Tropisms of AAV for subretinal delivery to the neonatal mouse retina and its application for in vivo rescue of developmental photoreceptor disorders. *PLoS One* **8**, e54146, doi:10.1371/journal.pone.0054146 (2013).
151 Juettner, J. *et al.* Targeting neuronal and glial cell types with synthetic promoter AAVs in mice, non-human primates, and humans. *bioRxiv* (2018).
152 Cafaro, J., Lee, G. S. & Stone, J. S. Atoh1 expression defines activated progenitors and differentiating hair cells during avian hair cell regeneration. *Dev Dyn* **236**, 156-170, doi:10.1002/dvdy.21023 (2007).
153 Chen, P., Johnson, J. E., Zoghbi, H. Y. & Segil, N. The role of Math1 in inner ear development: Uncoupling the establishment of the sensory primordium from hair cell fate determination. *Development* **129**, 2495-2505 (2002).
154 Brown, N. L., Dagenais, S. L., Chen, C. M. & Glaser, T. Molecular characterization and mapping of ATOH7, a human atonal homolog with a predicted role in retinal ganglion cell development. *Mamm Genome* **13**, 95-101, doi:10.1007/s00335-001-2101-3 (2002).
155 Brown, N. L., Patel, S., Brzezinski, J. & Glaser, T. Math5 is required for retinal ganglion cell and optic nerve formation. *Development* **128**, 2497-2508 (2001).
156 Wang, S. W. *et al.* Requirement for math5 in the development of retinal ganglion cells. *Genes Dev* **15**, 24-29 (2001).
157 Walters, B. J. *et al.* In Vivo Interplay between p27(Kip1), GATA3, ATOH1, and POU4F3 Converts Non-sensory Cells to Hair Cells in Adult Mice. *Cell Rep* **19**, 307-320, doi:10.1016/j.celrep.2017.03.044 (2017).
158 Schlamp, C. L. *et al.* Evaluation of the percentage of ganglion cells in the ganglion cell layer of the rodent retina. *Mol Vis* **19**, 1387-1396 (2013).

159 Raymond, I. D., Vila, A., Huynh, U. C. & Brecha, N. C. Cyan fluorescent protein expression in ganglion and amacrine cells in a thy1-CFP transgenic mouse retina. *Mol Vis* **14**, 1559-1574 (2008).
160 Yao, K. *et al.* Restoration of vision after de novo genesis of rod photoreceptors in mammalian retinas. *Nature* **560**, 484-488, doi:10.1038/s41586-018-0425-3 (2018).
161 Klimczak, R. R., Koerber, J. T., Dalkara, D., Flannery, J. G. & Schaffer, D. V. A novel adeno-associated viral variant for efficient and selective intravitreal transduction of rat Muller cells. *PLoS One* **4**, e7467, doi:10.1371/journal.pone.0007467 (2009).
162 Bainbridge, J. W. *et al.* Long-term effect of gene therapy on Leber's congenital amaurosis. *N Engl J Med* **372**, 1887-1897, doi:10.1056/NEJMoa1414221 (2015).
163 Bainbridge, J. W. *et al.* Effect of gene therapy on visual function in Leber's congenital amaurosis. *N Engl J Med* **358**, 2231-2239, doi:10.1056/NEJMoa0802268 (2008).
164 Torper, O. *et al.* Generation of induced neurons via direct conversion in vivo. *Proc Natl Acad Sci U S A* **110**, 7038-7043, doi:10.1073/pnas.1303829110 (2013).
165 Niu, W. *et al.* In vivo reprogramming of astrocytes to neuroblasts in the adult brain. *Nat Cell Biol* **15**, 1164-1175, doi:10.1038/ncb2843 (2013).
166 Heinrich, C. *et al.* Sox2-mediated conversion of NG2 glia into induced neurons in the injured adult cerebral cortex. *Stem Cell Reports* **3**, 1000-1014, doi:10.1016/j.stemcr.2014.10.007 (2014).
167 Su, Z., Niu, W., Liu, M. L., Zou, Y. & Zhang, C. L. In vivo conversion of astrocytes to neurons in the injured adult spinal cord. *Nat Commun* **5**, 3338, doi:10.1038/ncomms4338 (2014).
168 Rouaux, C. & Arlotta, P. Fezf2 directs the differentiation of corticofugal neurons from striatal progenitors in vivo. *Nat Neurosci* **13**, 1345-1347, doi:10.1038/nn.2658 (2010).
169 Yang, Y. P., Thorel, F., Boyer, D. F., Herrera, P. L. & Wright, C. V. Context-specific alpha- to-beta-cell reprogramming by forced Pdx1 expression. *Genes Dev* **25**, 1680-1685, doi:10.1101/gad.16875711 (2011).
170 Zhou, Q., Brown, J., Kanarek, A., Rajagopal, J. & Melton, D. A. In vivo reprogramming of adult pancreatic exocrine cells to beta-cells. *Nature* **455**, 627-632, doi:10.1038/nature07314 (2008).
171 Al-Hasani, K. *et al.* Adult duct-lining cells can reprogram into beta-like cells able to counter repeated cycles of toxin-induced diabetes. *Dev Cell* **26**, 86-100, doi:10.1016/j.devcel.2013.05.018 (2013).
172 Collombat, P. *et al.* Embryonic endocrine pancreas and mature beta cells acquire alpha and PP cell phenotypes upon Arx misexpression. *J Clin Invest* **117**, 961-970, doi:10.1172/JCI29115 (2007).
173 Ueki, Y. *et al.* P53 is required for the developmental restriction in Muller glial proliferation in mouse retina. *Glia* **60**, 1579-1589, doi:10.1002/glia.22377 (2012).
174 Trapnell, C. *et al.* The dynamics and regulators of cell fate decisions are revealed by pseudotemporal ordering of single cells. *Nat Biotechnol* **32**, 381-386, doi:10.1038/nbt.2859 (2014).
175 Buenrostro, J. D., Giresi, P. G., Zaba, L. C., Chang, H. Y. & Greenleaf, W. J. Transposition of native chromatin for fast and sensitive epigenomic profiling of open chromatin, DNA-binding proteins and nucleosome position. *Nat Methods* **10**, 1213-1218, doi:10.1038/nmeth.2688 (2013).

176 Neph, S. *et al.* BEDOPS: high-performance genomic feature operations. *Bioinformatics* **28**, 1919-1920, doi:10.1093/bioinformatics/bts277 (2012).
177 Valensisi, C., Liao, J. L., Andrus, C., Battle, S. L. & Hawkins, R. D. cChIP-seq: a robust small-scale method for investigation of histone modifications. *BMC Genomics* **16**, 1083, doi:10.1186/s12864-015-2285-7 (2015).
178 Dunn, F. A., Doan, T., Sampath, A. P. & Rieke, F. Controlling the gain of rod-mediated signals in the Mammalian retina. *J Neurosci* **26**, 3959-3970 (2006).
179 Murphy, G. J. & Rieke, F. Network variability limits stimulus-evoked spike timing precision in retinal ganglion cells. *Neuron* **52**, 511-524 (2006).
180 Bishop, D. *et al.* Near-infrared branding efficiently correlates light and electron microscopy. *Nat Methods* **8**, 568-570, doi:10.1038/nmeth.1622 (2011).
181 Della Santina, L. *et al.* Glutamatergic Monopolar Interneurons Provide a Novel Pathway of Excitation in the Mouse Retina. *Curr Biol* **26**, 2070-2077, doi:10.1016/j.cub.2016.06.016 (2016).
182 Kerschensteiner, D., Morgan, J. L., Parker, E. D., Lewis, R. M. & Wong, R. O. Neurotransmission selectively regulates synapse formation in parallel circuits in vivo. *Nature* **460**, 1016-1020, doi:10.1038/nature08236 (2009).